Hong Kong Polytechnic University
Department of Electrical Engineering

POWER SYSTEM STABILITY ENHANCEMENT EMPLOYING CONTROLLERS BASED ON A VERSATILE MODELING

CHUNG CHI YUNG

Thesis submitted for the degree of
Doctor of Philosophy in Engineering

Hong Kong, March 1999

Abstract of thesis entitled 'Power system stability enhancement employing controllers based on a versatile modeling'
submitted by Chung chi yung
for the degree of Doctor of Philosophy
at the Hong Kong Polytechnic University in March 1999

Rapid advances in power electronics have made it both practicable and economic to design powerful thyristor-controlled devices, such as Flexible AC Transmission Systems (FACTS), for stability enhancements. The discrepancies of existing modeling approaches have limited the feasibility of handling these devices or designing its damping controller.

In this thesis, a versatile and generalized approach to model standard power system components is proposed. The more systematic and realistic representation, accompanied by the development of powerful eigenvalue-analysis techniques, facilitates the study of small signal stability (monotonic and oscillatory) of the power systems.

In monotonic stability study, the effect of exciter and governor is critically reviewed based on the exploitation of eigenvalues, modal and sensitivity analyses over a wide range of operating conditions.

In oscillatory stability study, a common FACTS device, the static var compensator (SVC), is used to improve system damping. This study reveals the inadequacy of many conventional methodologies in SVC design since they have ignored (or cannot handle) some important factors such as SVC mode instability and robustness of the power system. Two approaches, combined sensitivities and H_∞ algorithms, are introduced to solve these limitations. Finally, an extended H_∞ algorithm, which is applied to PSS design and successfully solves certain limitations of the existing H_∞ based PSS design, is also presented.

Although these studies are developed on selected controller devices or typical systems for convenience of discussion, extension to more complex systems can be dealt with in a similar way because of the versatility of the proposed modeling methodology.

ACKNOWLEDGMENT

The author wishes to express his sincere gratitude to his supervisors, Dr. C.T. Tse and Prof. A.K. David, for their invaluable advice and guidance.

The academic advice from Dr. A.B. Rad and Mr. K.W. Wang are greatly appreciated.

The financial support provided by the Research Committee of Hong Kong Polytechnic University through the award of scholarships is also gratefully acknowledged.

CONTENTS

LIST OF FIGURES

LIST OF TABLES

NOMENCLATURE

PMT	=	plug-in modeling technique
EXC	=	excitation system
GOV	=	governor system
PSS	=	power system stabilizer
RSC	=	relative sensitivity coefficient
RRSC	=	real part of relative sensitivity coefficient
CSC	=	combined sensitivity coefficient
FACTS	=	flexible AC transmission system
SVC	=	static var compensator
TCSC	=	thyristor controllable series compensator
PS	=	phase shifter
HVDC	=	high voltage direct current
FSFP	=	fixed-structure and fixed-parameter
RHP	=	right-half plane
LHP	=	left-half plane
CI	=	controllability index
OI	=	observability index
RI	=	residue index
COI	=	centre of inertia

LIST OF SYMBOLS

G_d = gain constant

G_c, G_o = critical and operating values of G_d

T_W = controller 'washout' time constants

T_1, T_2 = controller lead, and lag time constants

T = general time constant of any first-order circuit

κ = arbitrary parameter

$\lambda_J = \alpha_J \pm j\omega_J$ = eigenvalue of mode j

$S_{J\kappa}$ = RRSC of mode j with respect to $\kappa \approx \Delta\alpha_J/(\Delta\kappa/\kappa)$

S_{Ig} = RRSC of interarea mode with respect to EXC gain

S_{IG} (S_{SG}) = RRSC of interarea (SVC) mode with respect to G_d at G_o (G_c)

S_{IT} (S_{ST}) = RRSC of interarea (SVC) mode with respect to T

$\Delta\alpha_I$ ($\Delta\alpha_S$) = change in damping constant of interarea (SVC) mode due to change in κ

$\Delta\alpha^o_I$ = overall change in damping constant of interarea mode due to change in both κ and G_o

μ = $-S_{IG}/S_{SG}$ = factor relating the two mode sensitivities

$S^o_{I\kappa}$ = $S_{I\kappa} + \mu S_{S\kappa}$ = CSC of interarea mode with respect to κ, for constant gain margin

ω_I (ω_S) = angular frequency of interarea (SVC) mode

ω_m = geometric mean of ω_I and ω_S

$G\angle\theta$ = stage gain amplitude and phase shift of first-order circuit

g_J (f_J) = change of $G(\theta)$ with respect to T associated with mode j

$\boldsymbol{X}$ = state vector

$\boldsymbol{R}$, $\boldsymbol{Y}$ = input and output vectors

$\boldsymbol{A}$ = system matrix

$\boldsymbol{B}$, $\boldsymbol{C}$, $\boldsymbol{D}$, $\boldsymbol{E}$ = coefficient matrices

U_J, V_J = right and left eigenvectors of A respectively associated with λ_J

X_d, X_q = d– and q–axis synchronous reactances

X_d', X_q' = d–axis and q–axis transient reactances

X_d'', X_q'' = d–axis and q–axis subtransient reactances

X_e = equivalent external impedance

T_{do}', T_{qo}' = d–axis and q-axis transient open-circuit time constants

T_{do}'', T_{qo}'' = d–axis and q–axis subtransient open-circuit time constants

M = machine inertia constant

I_d, I_q = d–axis and q–axis machine currents

V_d, V_q = d–axis and q–axis machine voltages

V_t = terminal voltage

E_{fd} = d–axis field voltage

E_d', E_q' = d–axis and q–axis voltage behind transient reactance

E_d'', E_q'' = d–axis and q–axis voltage behind subtransient reactance

P_e, P_m = machine electrical and mechanical torque (power)

P_a = $P_m - P_e$ = machine accelerating power

f_o = system frequency (Hz)

Ω_o = $2\pi f_o$ = system synchronous speed (radian per sec.)

Ω = rotor speed

Ω_{ref} = reference machine rotor speed

δ = rotor (load) angle

p = differential operator

s = Laplace operator

H_∞ = Hardy space

$\bar{\sigma}(\ )$ = largest singular value

$\|\ \|_\infty$ = ∞ norm

sup = least upper bound

CHAPTER 1

INTRODUCTION

1.1 Classification of stability

Power system stability has been and continues to be a major concern in system operation since it was recognised in 1920 [1]. It may be broadly defined as that property of a power system that enables it to remain in a state of operating equilibrium under normal operating conditions and to retain an acceptable state of equilibrium after being subjected to a disturbance [2]. The stability characteristics of a large electrical power system are too varied to permit a simple classification of all behavior patterns, and it is not possible to separate all analyses into simple categories. Nevertheless, the terms 'large disturbance stability' and 'small disturbance stability' are widely used to classify the stability of a system [3].

1.1.1 Large disturbance stability

Large disturbance (or transient) stability is the ability of the power system to maintain synchronism after subjection to a severe disturbance. The system is designed and operated so as to be stable for a selected set of contingencies. These stability studies are often used to determine machine stability during the initial period of high stress immediately following a nearby fault. If the fault is permanent or sustained, machines may pole slip, i.e. lose synchronism. The large disturbance stability study is a very specific one, from which the engineer concludes that under given system conditions and for a given impact the synchronous machines will or will not remain in synchronism [4]. Stability depends on the magnitude and location of the disturbances. The hazard of this instability is much alleviated by the development of fast-response protective systems, which clear a fault within the shortest possible time.

1.1.2 Small disturbance stability

Small disturbance (or small signal) stability is the ability of the power system to maintain synchronism under small disturbances. For such disturbances, the equations that describe the dynamics of the power system can be linearized for the purpose of analysis. This stability can be divided into two categories [2,5]: monotonic stability and oscillatory stability. To study the system and machine behaviour with regard to these two stability problems, the machine torque is resolved to two components: synchronising torque defined as the accelerating torque component in opposition to the rotor angle variation, and damping torque defined as the accelerating torque component in opposition to the rotor speed variation. Insufficient synchronising torque and damping torque will cause the monotonic and oscillatory instability respectively.

1.1.2.1 Monotonic instability

In early works to study monotonic instability, systems of one or two machines, where generators were viewed as simple voltage sources behind fixed reactances, were commonly used. System stability was assessed by the synchronising coefficient $\Delta P_e/\Delta\delta$ to determine the maximum power transmitted over a long distance. The generator would lose synchronism (or pole slip) if the machine operates beyond a certain limit. Since the machine output power is $P_e = P_{max} \sin \delta$ [6] where P_{max}, δ are the maximum power transfer and the rotor angle, a critical operating condition would correspond to a rotor angle $\delta = 90°$: beyond this a slight δ increase will decrease its output power and will further accelerate the rotor, and eventually will cause pole slipping.

1.1.2.2 Oscillatory instability

Oscillatory stability study is usually associated with power oscillations by one machine against the system (i.e. so-called local mode oscillation) or between groups of machines in different 'areas' (i.e. so-called interarea mode oscillation), or among machine groups of any

combination. This kind of stability behavior constitutes a severe threat to system security and creates serious operating problems. For example, sustained oscillation was reported on the 275kV transmission circuits between Scotland and England for heavy export from Scotland [7], limiting the tieline power flows. Similar oscillation incidents were also recorded in Australia [8] and America [9].

In Hong Kong, this kind of oscillation was first observed in 1977 [10]. The problem was solved at that time by desensitizing the excitation (EXC) responses on the main generation units. During 1984, after the interconnection with South China, severe oscillations (e.g. with swing amplitude of ± 90MW and for as long as 50s) were recorded on a tieline with a nominal transfer of 120MW [11]. This type of tieline oscillations imposes unnecessary limitation on power system operation. In the first case, the oscillation problem was solved by reducing tieline flow and exciter gain on some machines. In the latter case, the problem was overcome by equipping the main generators with power system stabilizers.

1.2 Damping controller devices

The commonest damping controller to suppress low frequency oscillation is the power system stabilizer (PSS) installed at the generator unit. Rapid advances in power electronics have made it both practicable and economic to design powerful thyristor-controlled devices to improve system damping. Some existing devices in [12] are described in this section.

1.2.1 Power system stabilizers (PSS)

A celebrated paper by DeMello and Concordia [13] first presented the idea of PSS tuning through the study of synchronizing and damping torques. The fundamental concept of a PSS is to add supplementary damping to the excitation control by modulating the voltage regulator reference with a stabilizing signal and to provide a component of the electrical torque, which is in phase with shaft speed variations. The implementation details differ depending upon the PSS input signal employed. Several types of stabilizing signal have

been suggested: rotor speed, frequency, power and accelerating power. The pros and cons of using the different signals have been discussed [14-19]. For any input signal, the PSS must be tuned to compensate for the gain and phase characteristic of the excitation system, the generator and the power system [14]. Experience has shown that it is usually possible to eliminate or significantly reduce the incidence of spontaneous oscillations through the use of the PSSs.

1.2.2 Static var compensator (SVC)

An SVC is a variable shunt susceptance used to maintain a constant voltage at its terminals by controlling the reactive power it exchanges with the power system. Voltage regulation is the primary mode of control for most SVCs. However, the application of an SVC to provide additional damping to power swings is of increasing interest. References [20,21] provide important insights into SVC control design concepts for improving system dynamic performance.

The relative merits of a representative set of locally measurable signals for damping control purposes were evaluated in [20]. The signals considered were SVC bus frequency, SVC bus voltage, active power transfer and line current magnitude. The evaluation of the candidate input signals was performed on a two-area system and a three-area system. It was found that the current magnitude is the most robust input signal enabling substantial damping to be achieved with a positive contribution for all operating conditions considered.

1.2.3 Thyristor controlled series compensator (TCSC)

A TCSC is one of the devices proposed within the umbrella of the FACTS concept. It consists of capacitor banks connected in series with transmission lines, where each bank can be bypassed by thyristor-controlled switches. Its use in the power industry is still limited. There is no agreement on the selection of the best TCSC input signal. However, some factors must be considered when selecting an input signal for a power swing damping control function on a TCSC. For example, it must be possible to observe and control the

desired modes. In general, local measurements are preferable rather than remote signals because of reliability and cost issues.

1.2.4 Phase shifter (PS)

A PS is another device proposed in the FACTS concept and it is intended to introduce phase shift between sending end and receiving end voltages. The excitation transformer and the series transformer of the PS are controlled by an arrangement of thyristor switches to modulate the change of voltage phasor. The characteristics of the input signal to be selected for a PS are subject to considerations similar to those discussed for a TCSC. One disadvantage of the PS is that it adds an inductance in series with the transmission line, increasing the circuit reactive power loss as compared to the uncompensated line.

1.2.5 HVDC system

A power network consists essentially of AC transmission lines. However in cases of long distance power transfer, the use of high voltage direct current (HVDC) link is preferred to AC for economic reasons. Apart form this, there are some other special circumstances which also favour the use of HVDC.

A secondary application of HVDC is its ability to aid power oscillation damping by modulating the controls installed at both terminals. Many studies have used the frequency difference between the two interconnected AC systems as the basis for modulation of a DC link [22]. However, the frequency difference signal is reliable only in back-to-back applications because no telemetry of measurement is needed. Good results were achieved in [23] where the rate of change of the parallel AC intertie power was used as the modulation signal for the DC intertie.

1.3 Eigenvalue technique for small disturbance stability

The common approach for transient stability is the step-by-step integration method, dividing the time steps into small intervals (e.g. msec) and using a numerical technique to solve the appropriate equations at each time step. However, these simulation results will provide only a limited insight since repetition is required for all reasonable fault and operating alternatives. The method does not provide a unique generalized stability index leading to a difficulty in identifying measures to ensure sufficient stability margins. Since the spontaneous characteristics of swing oscillations do not depend on the size of disturbances, small disturbance analysis based on the linearised system at the steady-state operating point is a useful role. The eigenvalue analysis of this system will provide many insights of practical value, which are difficult to discern in transient plots.

Many methods have been proposed to represent networks, machines and associated control equipment such as the excitation system (EXC), governor system (GOV) and power system stabilizer (PSS) [24-27] as well as new components such as FACTS devices. New models have been introduced to represent such components [28-30] but have the following weaknesses:

i) limited flexibility because the matrix format and elements have to be reformulated whenever there is any change of the system such as machine equations and control devices

ii) difficult to interface with the other devices

iii) restricted input/output signal selection, e.g. only ΔP_m and ΔV_{ref} as input signals

iv) assumption of infinite busbar, stationary frame or restricted to small systems

v) difficulties in program implementation

vi) limited exploitation of eigenvector analysis because it is very difficult to correlate the state equation with the system parameters in general

1.4 Summary of chapters

The main contributions and important developments of this thesis are given chapter by chapter in the following sequence:

Chapter 2: A highly versatile method, known as the Plug-in Modeling Technique (PMT), suitable for modeling standard power system components is introduced. Component modules can be easily 'plugged' in to form a small perturbation state space model of the entire system irrespective of the size and complexity of the multimachine system. Any variable may then be selected as a control signal. The PMT can overcome the difficulties of some existing approaches as mentioned in Section 1.3. Eigenvector techniques (modal and sensitivity analyses) will then be employed to study the monotonic (Chapter 3) and oscillatory (Chapter 4) stabilities. The modeling method is also suitable for the application of H_∞ methodology in Chapter 5 and 6.

Chapter 3: Based on extensive application of eigenvalues, modal and sensitivity analyses developed, this thesis shows that the monotonic instability is overcome even with a small exciter gain. Therefore, if a controller is designed to enhance system stability associated with the electromechanical effects, damping of oscillatory modes is considered in general stability studies.

Chapter 4: A systematic approach for the design of a common FACTS device, SVC, to eliminate the oscillatory instability is proposed. Modal analysis is used to identify the machine and mode relationships and to show which machines are liable to cause instability. The choices of SVC location and damping signal are based on both modal and sensitivity analyses. As the SVC instability is detected in the design process, the design (structure and setting) is achieved through a combined sensitivity coefficient (CSC) which automatically takes into account the damping of both the interarea and SVC modes. Detailed synthesis of the CSCs shows that a flexible controller design structure should in general have

three lead/lag stages of appropriate time constants. It is also shown that if the SVC mode constraint is ignored, tuning the lead/lag settings for interarea mode damping alone will likely lead to adjustment in the wrong direction.

Chapter 5: A robust H_∞ based SVC is proposed. The controller design is distinguished by that system damping is increased by treating the change of system operating points (e.g. tieline flow) and the dynamics of the SVC mode as low and high frequency model uncertainties respectively. The proposed approach which uses the numerator-denominator uncertainty representation and the partial pole placement technique is able to solve certain limitations of conventional H_∞ design techniques. Case studies confirm that the H_∞ controller is more robust than the CSC controller regarding to the tieline oscillation and the SVC mode instability.

Chapter 6: The H_∞ algorithm in Chapter 5 is also extended to the PSS design. An H_∞ PSS design methodology able to solve certain limitations of other existing H_∞ PSS design techniques is proposed. It is superior to the conventional PSS in terms of the robustness of the closed-loop system on the aspect of model uncertainties.

Chapter 7: The conclusions and recommendations for future work are summarized.

1.5 Publications

1.5.1 Papers accepted

1. C.Y. Chung, C.T. Tse, A.K. David and A.B. Rad, 'Partial pole placement of H_∞ based PSS design using numerator denominator perturbation representation', *IEE Proceedings, Generation, Transmission and Distribution*

2. C. Y. Chung, K.W. Wang and C.T. Tse, 'Selection of the location and damping signal for static var compensator based on modal and sensitivity analyses', *Electric Power System Research*

3. C.Y. Chung, C.T. Tse, A.K. David and A.B. Rad, 'A new H_∞ based PSS design using numerator denominator perturbation representation', *Electric Power System Research*

1.5.2 Papers under review

1. C.Y. Chung, C.T. Tse and A. K. David, 'Monotonic Stability in Single and Multi Machine Systems', *IEE Proceedings, Generation, Transmission and Distribution*

2. C.Y. Chung, C.T. Tse, K.W. Wang, C.K. Cheung and A.K. David, 'Small perturbation stability for modern power systems: Part I: Versatile modeling of system components', *IEEE Transactions on Power Systems*

3. C.Y. Chung, K.W. Wang, C.K. Cheung, C.T. Tse and A. K. David, 'Small perturbation stability for modern power systems: Part II: Systematic approach for static var compensator design', *IEEE Transactions on Power Systems*

4. C.Y. Chung, C.T. Tse and A.K. David, 'Time constant sensitivity syntheses of static var compensator', *IEEE Transactions on Power Systems*

5. K.W. Wang, C.Y. Chung, C.T. Tse and K.M. Tsang, 'Multimachine eigenvalue sensitivities of power system parameters', *IEEE Transactions on Power Systems*

1.5.3 Papers presented at international conferences

1. C.Y. Chung, C.T. Tse and A.K. David, 'New load flow technique based on load transfer and load buses elimination', *Proc. of IEE 4th International Conference on Advances in Power System Control, Operation and Management*, Nov. 1997, Hong Kong, pp. 614-619

2. C.Y. Chung, C.T. Tse, A.B. Rad and A.K. David, 'Analysis of damping effects of an H_∞ based PSS design', *Proc. of Australasian Universities Power Engineering Conference, AUPEC'97*, Sydney, Australia, 1997, pp. 413-418

3. C.Y. Chung, C.K. Cheung, C.T. Tse and A. K. David, 'Machine and load modeling in large scale power industries', *Dynamic modeling control applications for industry workshop, IEEE* industry applications society, April 1998, pp. 7-15

4. C.T. Tse, W.L. Chan and C.Y. Chung, 'Refinement of Concept on Steady State Stability Limit,' *Proc. IEE 417, International Conference on Advances in Power System Control, Operation and Management*, Nov. 1995, pp. 583-589.

5. C.T. Tse, K.L. Chan, S.L. Ho, C.Y. Chung, S.C. Chow and W.Y. Lo, 'Effective loadflow technique with non-constant MVA load for the Hong Kong Mass Transit Railway urban lines power distribution system', *Proc. of IEE 4th International Conference on Advances in Power System Control, Operation and Management*, Nov. 1997, Hong Kong, pp. 753-757

6. K.W. Wang, C.Y. Chung, C.T. Tse and K.M. Tsang, 'Optimum location of power system stabilizers based on probabilistic analysis', *International conference on Power System Technology, POWERCON'98*, August, 1998, Beijing, China, pp.829-833

CHAPTER 2

VERSATILE MODELING OF SYSTEM COMPONENTS

2.1 Introduction

A highly versatile method, known as the Plug-in Modeling Technique (PMT), suitable for modeling standard power system components is introduced. Instead of transforming control blocks to equations, component and network equations are transformed to two types of elementary blocks and these are then amalgamated with the control blocks. Any component such as a static var compensator (SVC), thyristor controllable series compensator (TCSC), phase shifter (PS), high voltage direct current (HVDC) link and its controls, a tieline and a generator with associated control equipment can be modeled as a module and plugged into the network module (Fig. 2.1). Based on a generalized approach proposed in this chapter, the elementary blocks of the entire system can be handled systematically so that the state space equations can be obtained and easily correlated with system parameters. Stability can be examined by time/frequency response, eigenvalue, modal or sensitivity, analyses.

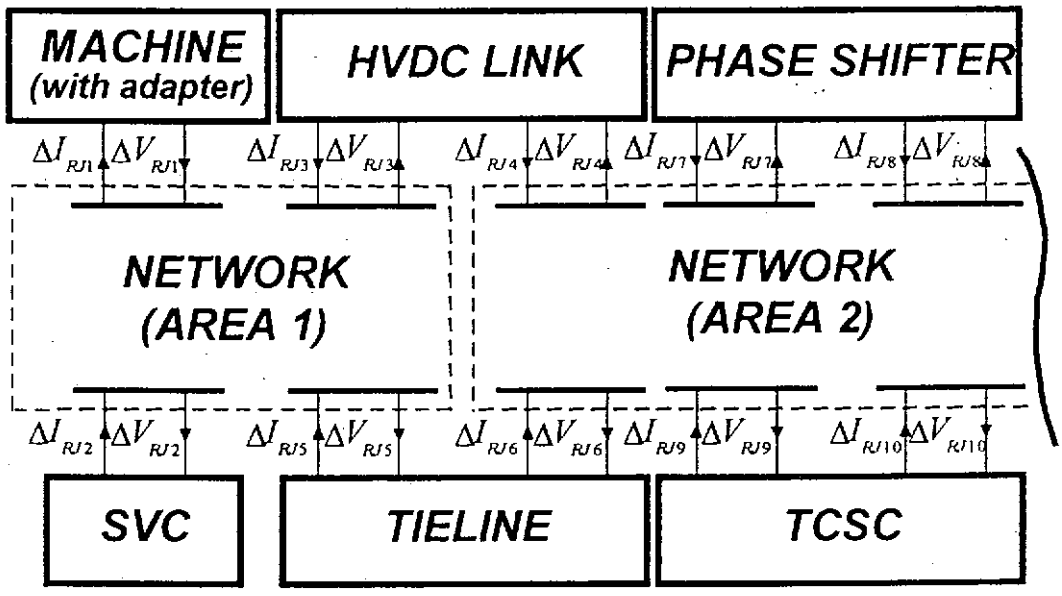

Fig. 2.1 Overall view of PMT connection

2.2 System modeling

2.2.1 Network

In stability studies, the load dynamics may be described by [2]:

$$S = P + jQ = P_0(V/V_0)^a + jQ_0(V/V_0)^b \tag{2.1}$$

Under small perturbation, the load characteristic can be represented by four admittances in (2.2).

$$\begin{bmatrix} \Delta I_R \\ \Delta I_J \end{bmatrix} = \begin{bmatrix} Y_{RR} & Y_{RJ} \\ Y_{JR} & Y_{JJ} \end{bmatrix} \begin{bmatrix} \Delta V_R \\ \Delta V_J \end{bmatrix} \tag{2.2}$$

where [2,31]

$$Y_{RR} = \frac{(a-2)P_0V_{R0}^2}{V_0^4} + \frac{(b-2)Q_0V_{R0}V_{J0}}{V_0^4} + \frac{P_0}{V_0^2}$$

$$Y_{RJ} = \frac{(a-2)P_0V_{R0}V_{J0}}{V_0^4} + \frac{(b-2)Q_0V_{J0}^2}{V_0^4} + \frac{Q_0}{V_0^2}$$

$$Y_{JR} = \frac{(a-2)P_0V_{R0}V_{J0}}{V_0^4} - \frac{(b-2)Q_0V_{R0}^2}{V_0^4} - \frac{Q_0}{V_0^2}$$

$$Y_{JJ} = \frac{(a-2)P_0V_{J0}^2}{V_0^4} - \frac{(b-2)Q_0V_{R0}V_{J0}}{V_0^4} + \frac{P_0}{V_0^2}$$

where subscripts R and J stand for real and imaginary parts in common network frame.

Let busbar injections, voltages and network admittance matrix are related by $\boldsymbol{I} = \boldsymbol{YV}$ where $\boldsymbol{Y}$ is a 2N×2N matrix (N = number of nodes) and currents and voltages are specified as 2N-vectors in the RJ frame.

$$\begin{bmatrix} I_G \\ -I_L \end{bmatrix} = \begin{bmatrix} Y_{GG}'' & Y_{GL} \\ Y_{LG} & Y_{LL} \end{bmatrix} \begin{bmatrix} V_G \\ V_L \end{bmatrix} \tag{2.3}$$

Under small perturbation and with the load represented by (2.2), then

$$\begin{bmatrix} \Delta I_G \\ 0 \end{bmatrix} = \begin{bmatrix} Y_{GG}'' & Y_{GL} \\ Y_{LG} & Y_{LL}' \end{bmatrix} \begin{bmatrix} \Delta V_G \\ \Delta V_L \end{bmatrix} \tag{2.4}$$

and load buses can be eliminated to

$$[\Delta I_G] = [Y_{GG}'][\Delta V_G] \tag{2.5}$$

where

$$Y_{GG}' = Y_{GG}'' - Y_{GL}(Y_{LL}')^{-1} Y_{LG}$$

Now, in (2.5) only the generator buses are retained. If connected buses associated with some system components need to be retained, the equation (2.5) takes the form

$$\begin{bmatrix} \Delta I_G \\ -\Delta I_C \end{bmatrix} = \begin{bmatrix} Y_{GG}''' & Y_{GC} \\ Y_{CG} & Y_{CC}' \end{bmatrix} \begin{bmatrix} \Delta V_G \\ \Delta V_C \end{bmatrix} \tag{2.6}$$

where ΔV_C, ΔI_C are the component voltage and current.

Since all components connected to a common busbar must have the same ΔV_C, for convenience of application (2.6) has to be modified to

$$\begin{bmatrix} \Delta I_G \\ \Delta V_C \end{bmatrix} = \begin{bmatrix} Y_{GG} & C_{GC} \\ C_{CG} & Z_{CC} \end{bmatrix} \begin{bmatrix} \Delta V_G \\ \Delta I_C \end{bmatrix} \tag{2.7}$$

where $Y_{GG} = Y_{GG}''' - Y_{GC}(Y_{CC}')^{-1} Y_{CG}$

$C_{GC} = -Y_{GC}(Y_{CC})^{-1}$

$C_{CG} = -(Y_{CC}')^{-1} Y_{CG}$

and $Z_{CC} = -(Y_{CC}')^{-1}$

The 'output' of network, LHS of (2.7), is the 'input' of components. For instance, if the system consists one machine and one other 'shunt' component as in Fig. 2.2, the equation will be (the 'adapter' will be discussed shortly)

$$\begin{bmatrix} \Delta I_{R1} \\ \Delta I_{J1} \\ \hline \Delta V_{R2} \\ \Delta V_{J2} \end{bmatrix} = \left[\begin{array}{cc:cc} Y11 & Y12 & C13 & C14 \\ Y21 & Y22 & C23 & C24 \\ \hdashline C31 & C32 & Z33 & Z34 \\ C41 & C42 & Z43 & Z44 \end{array}\right] \begin{bmatrix} \Delta V_{R1} \\ \Delta V_{J1} \\ \hline \Delta I_{R2} \\ \Delta I_{J2} \end{bmatrix} \tag{2.8}$$

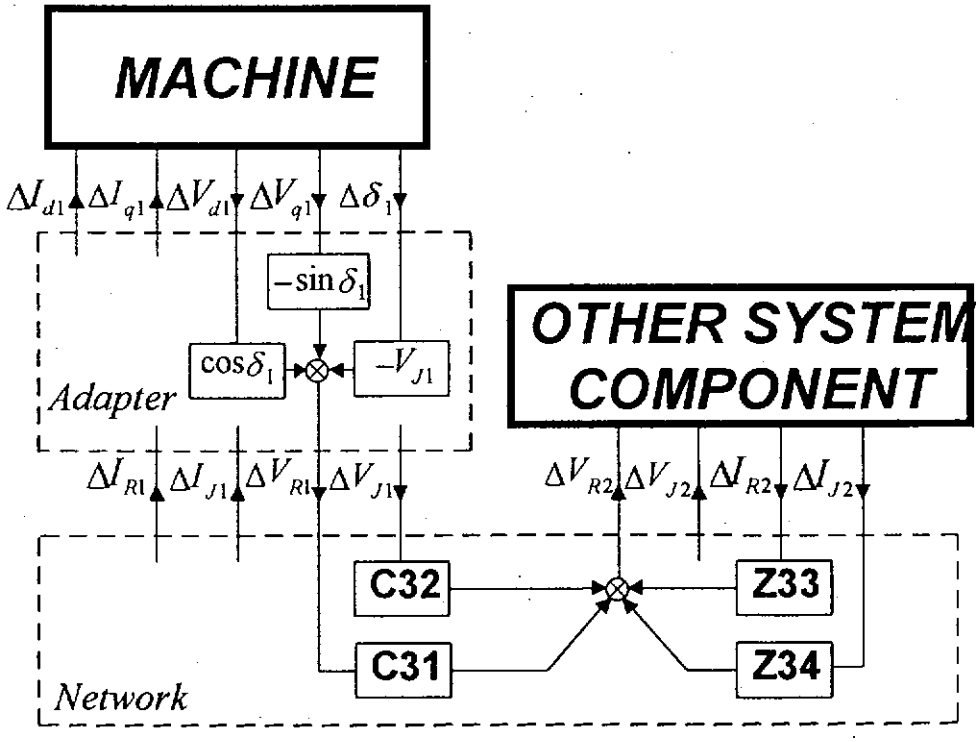

Fig. 2.2 Network representation with one machine and one other shunt component as in (2.8) (only the network connection to ΔV_{R1} and ΔV_{R2} are shown for simplicity)

2.2.2 System components

2.2.2.1 Machines

In Park's two-axis machine model [32], machine behaviour can be described by a set of 3rd-order equations in the machine *dq* frame. For small perturbations, these equations are linearised (Appendix 1) and expressed in the convenient block format which, together with block models of control equipment such as EXC, GOV and PSS (Fig. 2.3), constitute a self-contained individual machine module. Any other order of Park's model (fourth, fifth and sixth) can be used if preferred as shown in Appendix 2. The effect of different load/machine modeling in a typical 7-machine system is analyzed in Appendix 3.

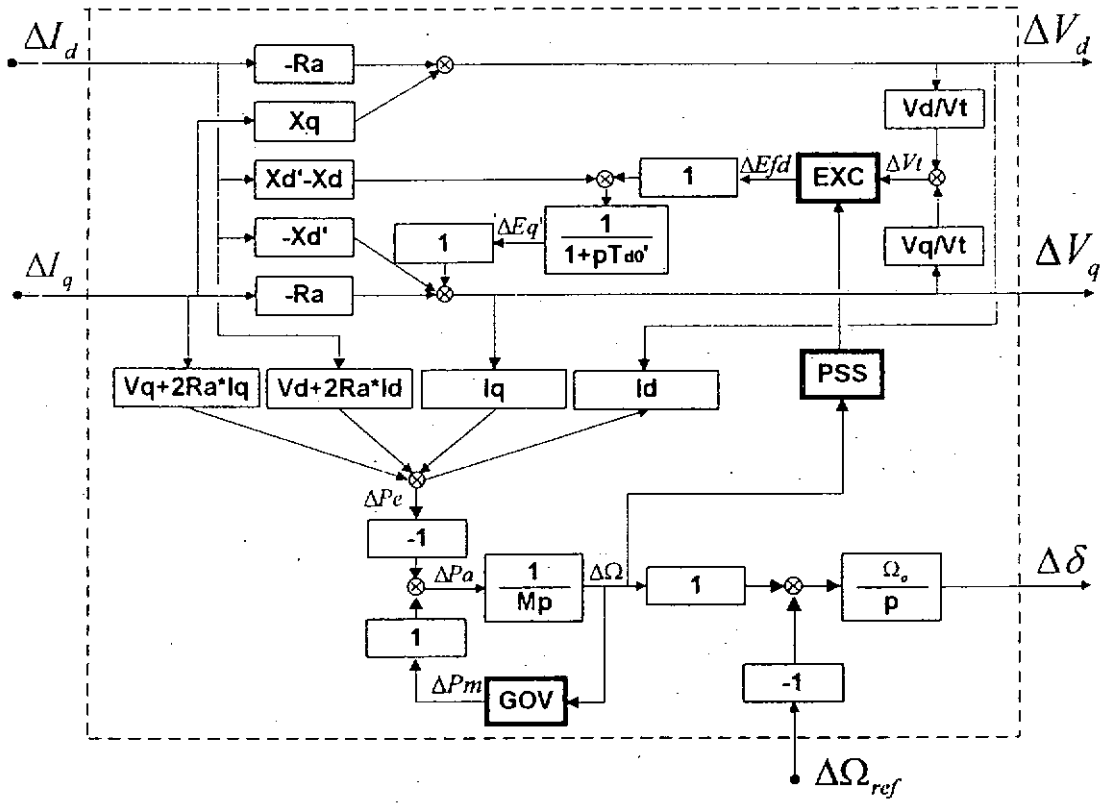

Fig. 2.3 Third order machine module

2.2.2.2 Machine and network frame interface

The generator *dq* frame can be related to the network *RJ* frame by

$$\Delta I_d = \cos\delta\Delta I_R + \sin\delta\Delta I_J + I_q\Delta\delta \tag{2.9a}$$

$$\Delta I_q = -\sin\delta\Delta I_R + \cos\delta\Delta I_J - I_d\Delta\delta \tag{2.9b}$$

$$\Delta V_R = \cos\delta\Delta V_d - \sin\delta\Delta V_q - V_J\Delta\delta \tag{2.9c}$$

$$\Delta V_J = \sin\delta\Delta V_d + \cos\delta\Delta V_q + V_R\Delta\delta \tag{2.9d}$$

where δ is the angle between the *dq* frame and *RJ* frame.

Hence, the machine model can be plugged into the network using the ***adapter*** shown in Fig. 2.2 where equation (2.9c) is depicted in detail.

2.2.2.3 Static var compensator (SVC)

A typical SVC configuration with thyristor controlled reactor and fixed capacitor, connected to a busbar through a step-down transformer, is shown in Fig. 2.4, where X_T is the transformer impedance, B_C and B_L are the susceptance of capacitor and inductor. The SVC equations can be written as

$$X_{SVC} = X_T - \frac{1}{B_C + B_L} \tag{2.10}$$

$$\begin{bmatrix} V_R \\ V_J \end{bmatrix} = X_{SVC}\begin{bmatrix} -I_J \\ I_R \end{bmatrix} \tag{2.11}$$

Substituting (2.10) in (2.11) and using small perturbation theory, (2.12) can be obtained and the SVC block diagram in Fig. 2.5 created. The SVC thyristor controller block in Fig. 2.5 is detailed in Fig. 2.6 where V_{SVC} and I_{SVC} are the magnitudes of voltage and current at the SVC terminal [33] and B_L the controller output.

$$\begin{bmatrix}\Delta I_R \\ \Delta I_J\end{bmatrix} = \frac{1}{X_{SVC}}\left\{\begin{bmatrix}\Delta V_J \\ -\Delta V_R\end{bmatrix} - \frac{1}{(B_C+B_L)^2}\begin{bmatrix}I_R \\ I_J\end{bmatrix}\Delta B_L\right\} \tag{2.12}$$

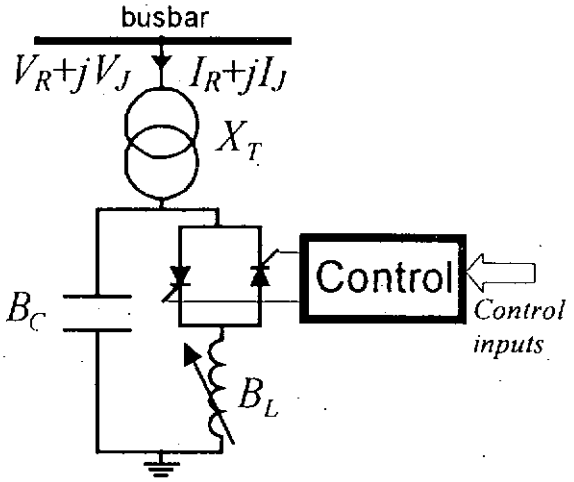

Fig. 2.4 Configuration of SVC

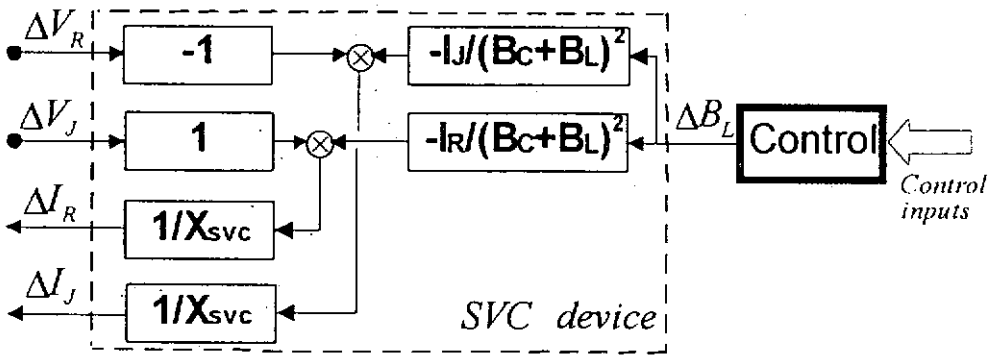

Fig. 2.5 SVC module

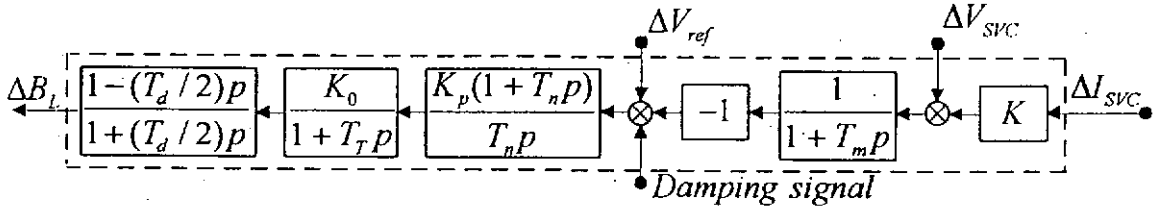

Fig. 2.6 General SVC controller

2.2.2.4 Tieline

Tieline flows are effective damping signals. The equations relating terminal voltages and tieline flows are in (2.13) and depicted in Fig. 2.7.

$$\begin{bmatrix} \Delta I_{R1} \\ \Delta I_{J1} \\ \Delta I_{R2} \\ \Delta I_{J2} \end{bmatrix} = \begin{bmatrix} G_{11} & -B_{11} & G_{12} & -B_{12} \\ B_{11} & G_{11} & B_{12} & G_{12} \\ G_{21} & -B_{21} & G_{22} & -B_{22} \\ B_{21} & G_{21} & B_{22} & G_{22} \end{bmatrix} \begin{bmatrix} \Delta V_{R1} \\ \Delta V_{J1} \\ \Delta V_{R2} \\ \Delta V_{J2} \end{bmatrix} \tag{2.13}$$

i.e. $[\Delta I_{RJ}] = [Y_{TL}][\Delta V_{RJ}]$ (2.14)

Significant tieline signals, if required, can be readily obtained by (2.15-2.19)

$$\Delta P = V_R \Delta I_R + I_R \Delta V_R + V_J \Delta I_J + I_J \Delta V_J \tag{2.15}$$

$$\Delta Q = V_J \Delta I_R - I_J \Delta V_R - V_R \Delta I_J + I_R \Delta V_J \tag{2.16}$$

$$\Delta S = \frac{P}{S} \Delta P + \frac{Q}{S} \Delta Q \tag{2.17}$$

$$\Delta I = \frac{I_R}{I} \Delta I_R + \frac{I_J}{I} \Delta I_J \tag{2.18}$$

$$\Delta V = \frac{V_R}{V} \Delta V_R + \frac{V_J}{V} \Delta V_J \tag{2.19}$$

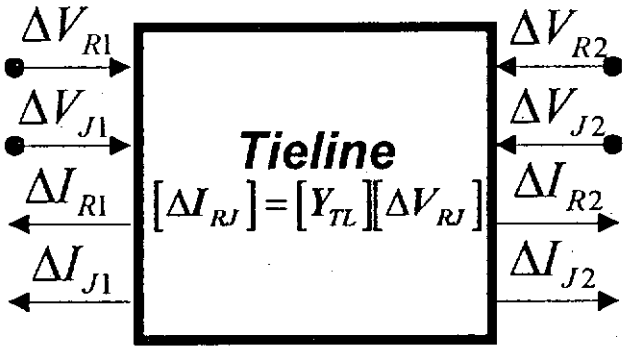

Fig. 2.7 Tieline module

2.2.2.5 Other components

Other components (with ΔV_C as input and ΔI_C as output) can similarly be 'plugged' into the network. The cases of TCSC, PS and HVDC link are shown in Fig. 2.8-2.10, respectively.

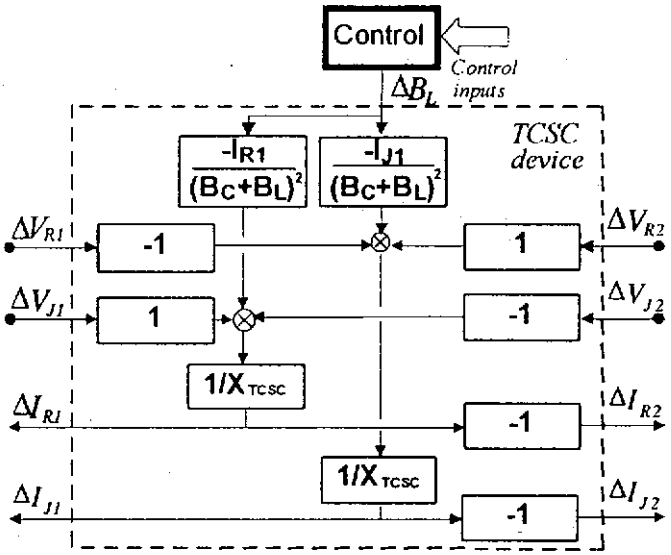

Fig. 2.8 TCSC module

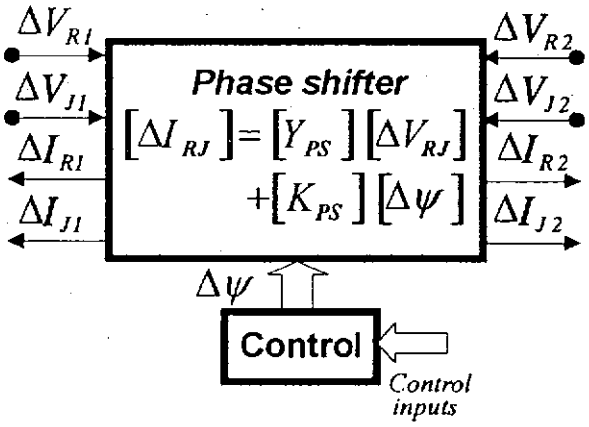

Fig. 2.9 PS module

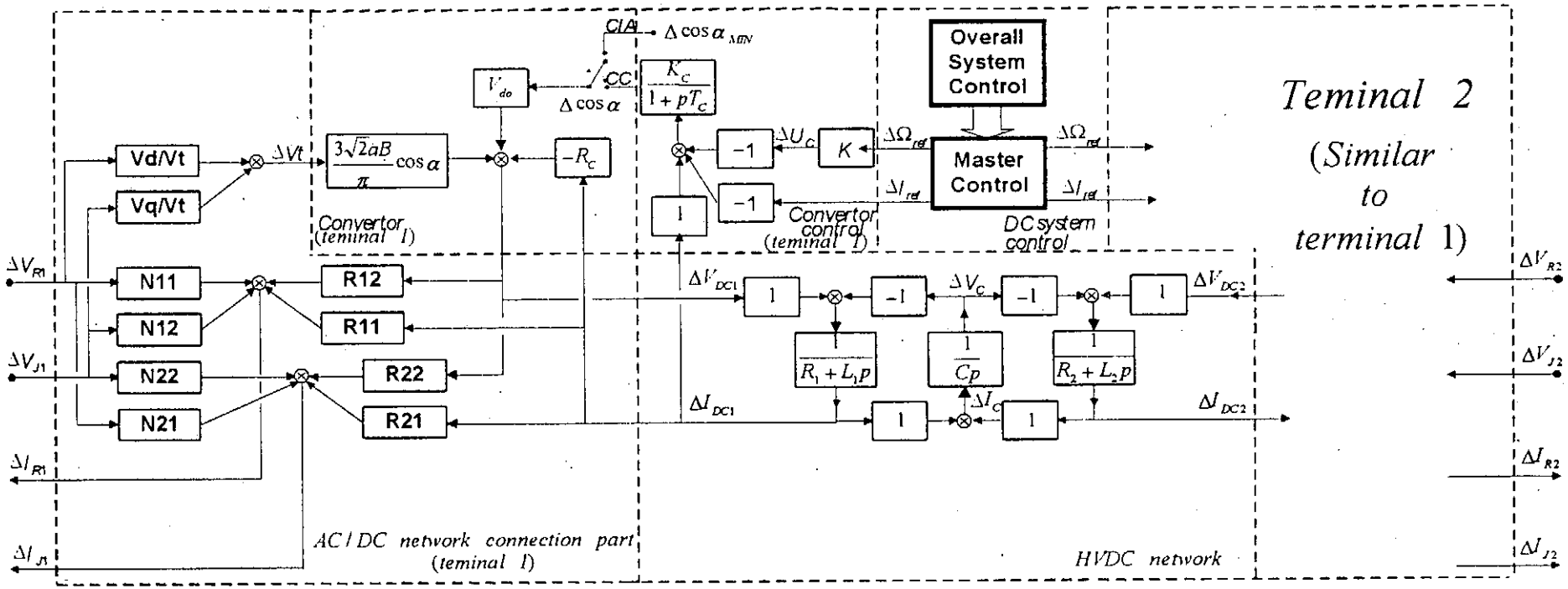

Fig. 2.10 HVDC link module

2.2.3 System formation and analyses

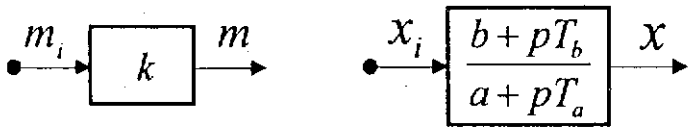

(a) (b)

Fig. 2.11 Elementary transfer blocks

The PMT system consists of only two types of elementary transfer blocks and five types of parameters as shown in Fig. 2.11 where 'm' and 'x' are non-state and state variables respectively. The block structure is so general that the user does not need to be concerned with the matrix format. Existing software such as Matlab [34] can be used and advanced control techniques provided by the toolbox of Matlab can be applied directly.

The state equations (2.20) and (2.21) can be established by means of matrix manipulation (see Appendix 4):

$$\dot{X} = AX + BR + E\dot{R} \tag{2.20}$$

$$Y = CX + DR \tag{2.21}$$

where the eigenvalues of the system matrix A will determine the system stability. The time responses can be calculated from the eigenvalues, eigenvectors, and coefficient matrices B, C, D and E (see Appendix 6). Note that the $E\dot{R}$ term is absent in the usual representation but Appendix 6 shows that its presence would not create any analytical difficulty in stability studies.

The procedure of deriving the state equation and the time response equation, or sensitivity (Appendix 8 and 9) and modal (Appendix 12) analyses is not affected by the size and complexity of the physical system.

2.3 Advantage of the PMT over the conventional modeling technique

2.3.1 Flexibility in modeling

The PMT facilitates the incorporation of EXC and other control equipment to any degree of complexity, including the IEEE models [35] described by nonlinear functions or quadratic/polynomial transfer functions involving complex poles and zeros. These controls can be converted to the elementary block form of Fig. 2.11 as illustrated in Appendix 7.

New devices such as FACTS controllers can also be easily plugged in once their transfer functions can match the network equation (2.7) (i.e. with ΔV_C as input and ΔI_C as output). Furthermore, any modifications of the FACTS devices and/or its controller can be facilitated by changing the related blocks only, without any worries on the change of matrix format/equation.

2.3.2 Freedom to choose input/output signals for controller design

In [27] and [36], the output vectors are restricted to state variables (e.g. $\Delta\Omega$) or their linear combinations, probably because of the difficulty of deriving (2.21) for some non-state variable outputs, e.g. ΔP_e. In the so-called PQR technique [24,25], the output variables are predefined and due to this limitation, it is difficult to take some unusual input/output signals for some desired controller designs. In the PMT, the input/output vectors do not need to be predefined in the program. *Any* locally available variable such as voltage, current, MW, MVAr or MVA can be formed easily, as for example in (2.15) to (2.19), and used as a control signal, or observable output.

2.3.3 Fuller exploitation of eigenvector analyses

The potential of eigenvalue analytical tools (modal and sensitivity analyses) have not been fully exploited in stability studies. The main obstacle is the way in which the system state equations are normally formulated and the difficulty of correlating them with system

parameters. The advantages of the PMT technique are brought out by the relative ease of its integration with many techniques for practical synthesis as described below.

2.3.3.1 Modal analysis

The mode shape is the most common method of the modal analysis. The mode shape for any variable associated with the eigenvalue $\lambda = \alpha + j\omega$ can be determined from CU, where U is the eigenvector and C is the coefficient matrix in (2.21). In references [36,37], modal analysis for non-state variables has not been employed. This may be attributed to the difficulty in establishing C if the y's in Y of (2.21) contain arbitrary non-state variables. However, in the PMT approach, the y's can be chosen as any of the system variables or their combination without restriction because the state equations are built up automatically, irrespective of the system complexity (Appendix 4). For instance, modal analysis has been applied to determine the synchronizing coefficient in Chapter 3 and to study machine torque components in Chapter 4.

In PMT, observability, controllability and residue indices of arbitrary variables can also be obtained (Appendix 12) and have been employed to select the location and damping signals for the SVC in Chapter 4.

2.3.3.2 Sensitivity analysis

Whenever there is an adjustment in a parameter κ, the system matrix A and the eigenvalues will vary accordingly. Hence the sensitivity coefficient can be expressed as [38]:

$$\frac{\partial \lambda}{\partial \kappa} = V^T \frac{\partial A}{\partial \kappa} U \Big/ (V^T U) \tag{2.22}$$

where U (V) is the right (left) eigenvector of A associated with λ, and superscript T denotes transpose. In conventional studies, $\partial\lambda/\partial\kappa$ can be evaluated if κ is an A matrix element. (For instance, κ is a diagonal element of A in the 'participation factor' $\partial\lambda/\partial\kappa$ [37].) Although

references [24-26] stress the advantage of sensitivity analysis, they do not provide a general expression relating the system matrix A and an arbitrary parameter κ to evaluate $\partial A/\partial\kappa$. It seems that there are no existing methods where $\partial A/\partial\kappa$ can be evaluated easily for an arbitrary parameter κ when κ can appear several times in A.

(a) Sensitivity for arbitrary block parameters

In the PMT, matrix A is a function of *all* transfer block parameters so that the final expressions for $\partial\lambda/\partial\kappa$ are only simple algebraic scalar operations. For example in the notation of Fig. 2.11b, $\partial\lambda/\partial b = wz/(hT_a)$, $\partial\lambda/\partial a = -wz/(hT_a)$, $\partial\lambda/\partial T_b = wz\lambda/(hT_a)$ and $\partial\lambda/\partial T_a = -w(zb-ua+\lambda zT_b)/(hT_a^2)$ where u, w, z and h can be derived directly from U and V (Appendix 8). This sensitivity technique has been applied to study the effect of exciter gain on the monotonic limit in Chapter 3 and to design the damping controller of the SVC in Chapter 4.

(b) Sensitivity to arbitrary system parameters

The sensitivity expression for a change in a block parameter is simple and straight forward. However, if a system parameter changes, numerous blocks will be affected. Fortunately, these changes will affect only the zero order blocks (see (A4.3) in Appendix 4). By properly reordering these blocks as:

$$M = [M_1, M_2, M_3] \tag{2.23}$$

where

M_1 = parameters varying with nodal voltages,

M_2 = parameters which are the elements of matrices Y_{GG}, C_{GC}, C_{CG} and Z_{CC} of (2.7),

M_3 = other constant parameters,

it is still possible to obtain $\partial A/\partial \kappa$. The complicated sensitivity expression for system parameters is summarized in Appendix 9 for constant admittance load and third order machine model only. These equations can be directly applied to higher-order machine model, or extended to other system components and load representations, what need to do is only the reordering of zero order blocks and the reconstruction of M_1, M_2 and M_3. The sensitivity $\partial\lambda/\partial\kappa$ for $\kappa = Q_L$ was used to identify the best SVC location in Chapter 4.

2.4 Validity of the PMT program

Validation of the PMT is divided into two stages (see Appendix 10). The first stage is to confirm the validity of the 3rd-order machine model together with the network equation (2.5) (with machine only) by comparing the results of the PMT with the well-known Heffron Phillips (HP) model [6]. The second stage is to validate the network equation (2.7) (with any component) and two component models (SVC and tieline). Validation of other components has not performed due to the lack of convenient and reliable models for comparison. However, it is strongly convinced that whenever equations of *any* component can be accurately addressed and then transformed to a modular format satisfying the network plug-in requirement, this component model should be valid and adequate for PMT, because what the software visualizes is elementary blocks only.

2.5 Summary

A technique of power system modeling for small perturbation studies which can accept any representation of system components together with associated control equipment of any desired degree of complexity has been presented. Modular system components such as machine, SVC, TCSC, PS, HVDC link, tieline and FACTS can be plugged into the network as additional modules. The outstanding feature of the PMT is that the state space equations are available as an explicit function of every parameter and the input and output can be any variable.

CHAPTER 3

MONOTONIC STABILITY IN SINGLE AND MULTI MACHINE SYSTEMS

3.1 Introduction

It has long been recognised that monotonic instability is caused by negative synchronising torque in synchronous machine and that a machine would pole-slip if operated beyond some stability limit. This chapter will focus on the synchronising coefficient ($\Delta P_e/\Delta\delta$). Based on the exploitation of eigenvalues, modal and sensitivity analyses over a wide range of operating conditions in both single and multi machine systems, a fresh interpretation of this coefficient is provided, together with the governor effect and even a slight exciter gain effect.

3.2 Concept refinement of the monotonic stability limit

Machine motion can be described by the following second order swing equation.

$$\frac{M}{\Omega_o} p^2 \Delta\delta = \Delta P_a = \Delta P_m - \Delta P_e \tag{3.1}$$

where p, Δ, Ω_o, M, δ, P_a, P_m and P_e are the differential operator, the increment change, the system synchronous speed, the machine inertia constant and rotor angle and the machine accelerating, mechanical and electrical torque (in power units), respectively.

When the governor effect is ignored ($\Delta P_m = 0$).

$$\Delta\delta = F(p)\Delta P_e \tag{3.2a}$$

where $F(p) = -\Omega_o/Mp^2$. On the other hand, ΔP_e will vary with $\Delta\delta$ and the external system and can be written as

$$\Delta P_e = H(p)\Delta\delta \tag{3.2b}$$

where $H(p)$ represents the effects of the rest of the power system. Fig. 3.1 provides a combined block diagram. λ is a root of the system if it satisfies $-M\lambda^2/\Omega_o = H(\lambda)$. Hence, the relationship of ΔP_e and $\Delta\delta$ can be simply obtained by putting $p = \lambda$ into either $F(p)$ or $H(p)$. From (3.2a), therefore, $\Delta P_e/\Delta\delta = 1/F(\lambda) = -M\lambda^2/\Omega_o$ is always non-positive if λ is real. This contradicts the conventional interpretation that $\Delta P_e/\Delta\delta$ should be positive (negative) for monotonically stable (unstable) systems. In order to investigate this 'contradiction', the $\Delta P_e/\Delta\delta$ relationship has to be explored through $H(p)$, for both single and multi machine systems, taking into account the effect of exciter and governor.

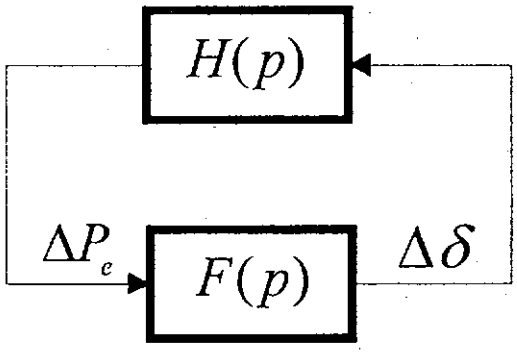

Fig. 3.1 The connection of the swing equation $F(p)$ with the electrical system

3.2.1 Analysis of exciter effect

3.2.1.1 Single machine system

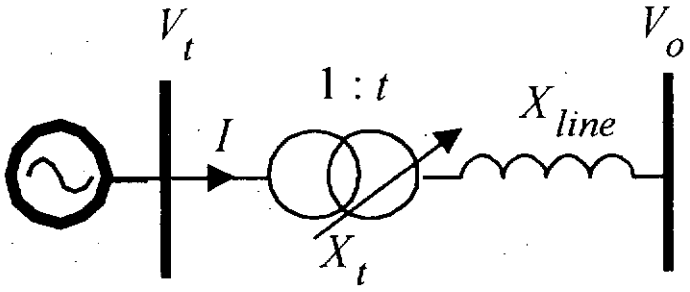

Fig. 3.2 Single machine infinite bus system

A single machine infinite bus power system is shown in Fig. 3.2 where the initial magnitudes of machine terminal voltage (V_t), infinite bus voltage (V_o) are both 1 p.u. and the transformer voltage ratio (t) can be adjusted with loading [39]. The monotonic stability of the Heffron-Phillips (HP) model [6] in Fig. 3.3 will be analysed with respect to different operating conditions. The data of a typical 350 MW generator, exciter and governor are provided in the Appendix 11 (data of machine A_1 of Fig. 3.5).

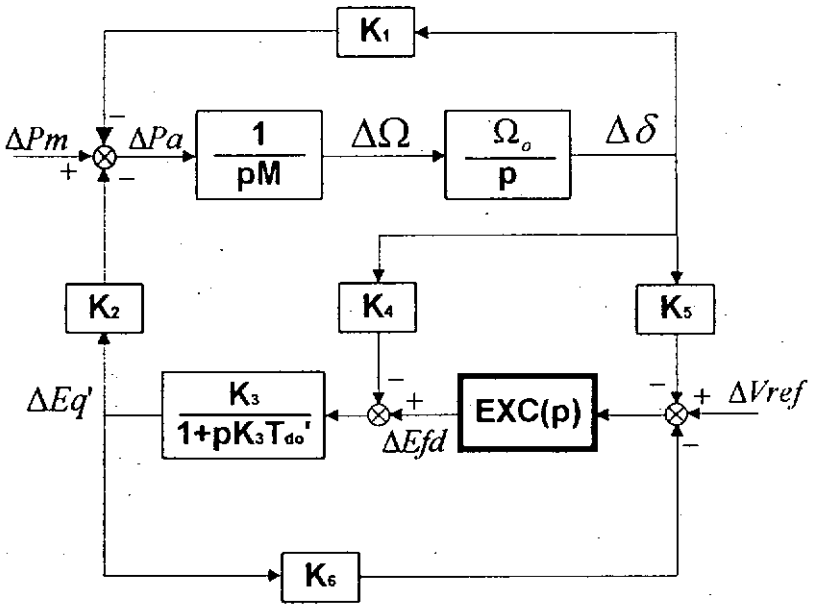

Fig. 3.3 Heffron-Phillips single machine model

(a) Constant flux linkage [1]

If the flux is constant, $\Delta E_q' = 0$, $H(p) = K_1$ and Fig. 3.3 can be reduced to a second order system described by

$$-\frac{M}{\Omega_o} p^2 \Delta\delta = \Delta P_e = H(p)\Delta\delta = K_1 \Delta\delta \tag{3.3}$$

If $K_1 > 0$, the eigenvalues will be imaginary (i.e. $\lambda = \pm j\omega$) and the rotor will oscillate. On the other hand if $K_1 < 0$, the resulting eigenvalues are real (i.e. $\lambda = \pm\alpha$). Analytically, the rotor angle will increase monotonically due to the positive root, and the machine will lose synchronism. If $K_1 = 0$, the system has no feedback and the eigenvalues are zero.

(b) Constant excitation

If the exciter is switched to manual, which is also equivalent to the transfer function of the excitation system $EXC(p) = 0$, then the excitation output $\Delta E_{fd} = 0$ and Fig. 3.3 becomes a third order system. These three roots consist of a pair of complex eigenvalues (usually stable) and a real root. This real eigenvalue will be zero if $H(p) = 0$. The locus of the monotonic limit of $\lambda = 0$ when $EXC(p) = 0$ is shown by the $G = 0$ curve in Fig. 3.4. ($G = EXC(p)\,|_{p=0}$ is the 'DC' gain of the exciter and $EXC(p) = 0$ is equivalent to putting $G = 0$.)

In general,

$$\frac{\Delta P_e}{\Delta\delta} = H(\lambda) = K_1 - \frac{K_2 K_3 K_4}{1 + K_3 T_{do}' \lambda} \tag{3.4}$$

When the machine operates on the limit ($\lambda = 0$), (3.4) can be simplified to

$$\frac{\Delta P_e}{\Delta\delta} = K_1 - K_2 K_3 K_4 \tag{3.5}$$

where all the K constants (except K_3) would vary with the MW and MVAr generation. Table 3.1 is obtained by substituting corresponding λ and K values calculated from the system data in (3.4) and (3.5). It is observed that whilst $K_1 - K_2K_3K_4$ changes sign in the vicinity of the limit [1,2], the sign of $H(\lambda)$ remains unchanged which is the same as for $F(\lambda)$ in Section 3.2.

λ	$H(\lambda)$	$K_1 - K_2K_3K_4$
0^+	< 0	< 0
0	$= 0$	$= 0$
0^-	< 0	> 0

Table 3.1 The sign of $H(\lambda)$ and $K_1 - K_2K_3K_4$ in the vicinity of $\lambda = 0$

(c) Automatic excitation

Normally, a modern machine operates with an automatic excitation control system. The relationship of $\Delta P_e/\Delta\delta$ can be obtained from Fig. 3.3 and the order of the complete system becomes N+3 where N is the order of exciter. $N = 7$ in the present study.

Case 1 : Low exciter gain ($G \leq 5$)

In general,

$$\frac{\Delta P_e}{\Delta\delta} = H(\lambda) = K_1 - \frac{K_2K_3[K_4 + K_5EXC(\lambda)]}{1 + pK_3T_{do}' + K_3K_6EXC(\lambda)} \tag{3.6}$$

When the machine operates on the limit ($\lambda = 0$), (3.6) can be simplified to

$$\frac{\Delta P_e}{\Delta\delta} = K_1 - \frac{K_2K_3(K_4 + K_5G)}{1 + K_3K_6G} \tag{3.7}$$

It is observed that:

(i) the limit of $\lambda = 0$ is *not* affected by *EXC(p)* so long G remains unchanged.

(ii) the other N+2 eigenvalues are affected by *EXC(p)*.

(iii) it can be shown that the sign of (3.7) will change: it is negative (positive) when the machine operates outside (within) the limit, but $H(\lambda)$ of (3.6) remains non-positive, which is similar to the case with a manual exciter (Table 3.1).

(iv) the limit is much enhanced even for a small increase of G from zero (Fig. 3.4).

Case 2 : Normal exciter gain ($G > 5$)

Equation (3.7) still applies but no such limit can be found when the exciter gain exceeds 5 (Fig. 3.4). In other words, pole slip will not occur since a normal exciter gain would be much greater than 5, say 60 in a typical system.

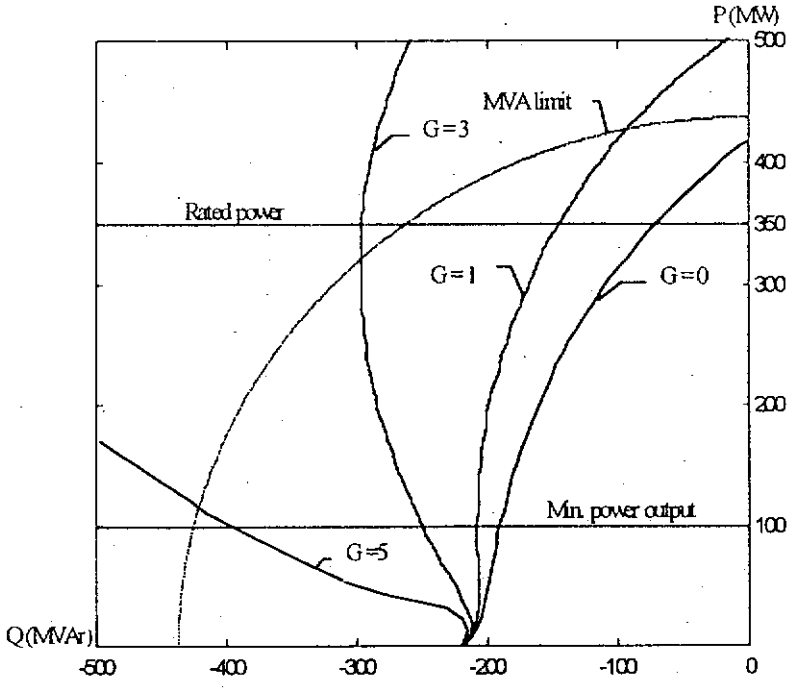

Fig. 3.4 Monotonic stability limits for different EXC gain G (single machine with $X_e = 0.5$ p.u.).

3.2.1.2 Multimachine system

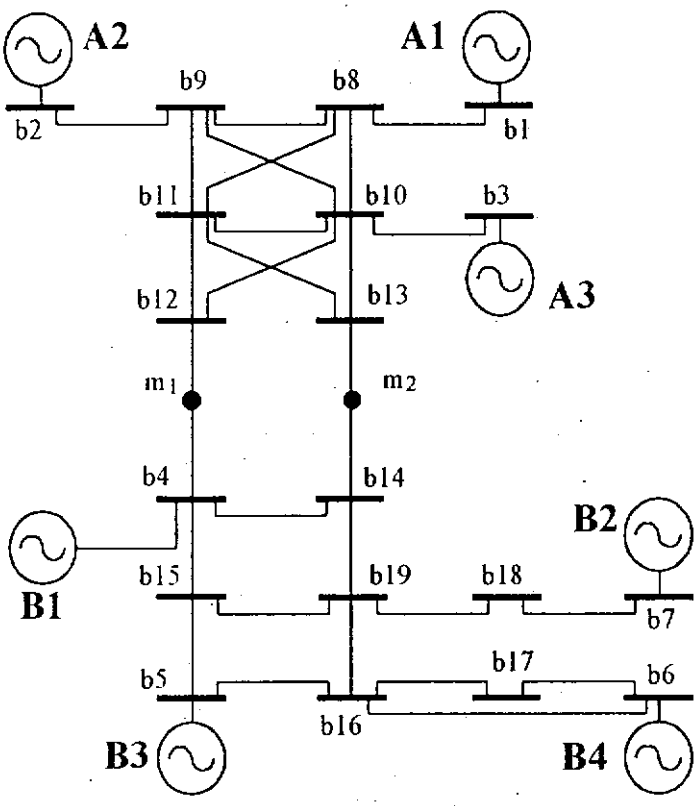

Fig. 3.5 Interconnected seven-machine system

A two area system, areas A and B, connected by tielines and comprising seven machines [40] shown Fig. 3.5, is used in this study. The machine A_1 is the same machine used in single machine case. The block diagrams of the excitation system (EXC) and governor (GOV) for each machine are shown in Fig. 3.6 and 3.7. The loads are represented by constant admittances and all machines by third order models. The system data is shown in Appendix 11. Using the PMT in Chapter 2, the state equation (2.20) and (2.21) and eigenvalues of this system can be obtained and automatically.

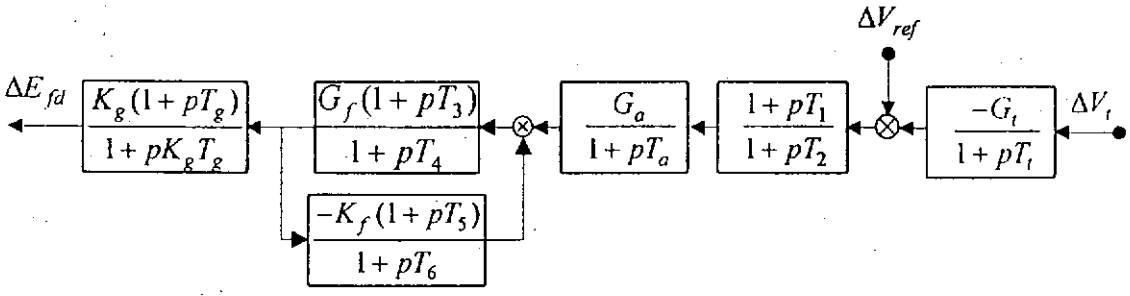

Fig. 3.6(a) Fast acting EXCs of A_1, A_2, A_3 and B_1

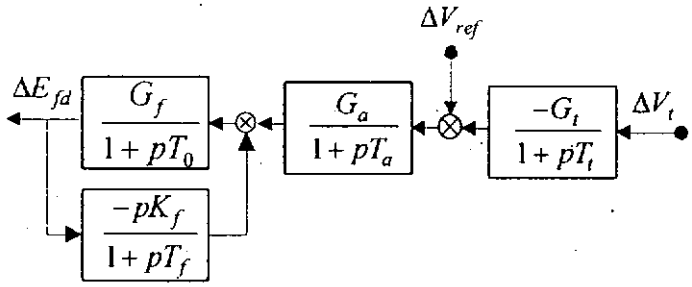

Fig. 3.6(b) Slow acting EXCs of B_2, B_3 and B_4

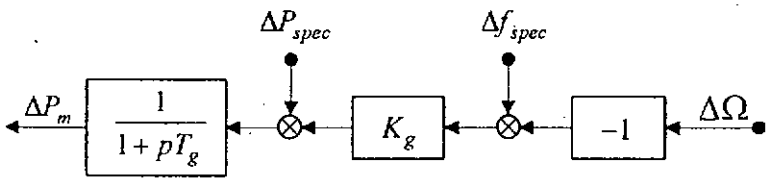

Fig. 3.7 Turbine-governor system (GOV) of all machines

In case of single machine system, the effect of the exciter on monotonic stability can be examined using (3.6). In multimachine systems, however, there is no simple *H(p)* formula to relate ΔP_e and $\Delta\delta$, but the stability limit can still be obtained from eigenvalue searching.

It is found that the 7-machine system will become unstable when the machine A_1 operates with manual exciter in the leading power factor regions outside the curve $G = 0$ in Fig. 3.8. Suppose the manual exciter is then switched to auto by gradually increasing G, the tendency of the limit change with increasing G in Fig. 3.8 also looks similar to that obtained for the single machine system in Fig. 3.8. When $G > 3$, the limit does not exist, hence monotonic instability is unlikely to occur in the multimachine environment. This is an important theoretical insight.

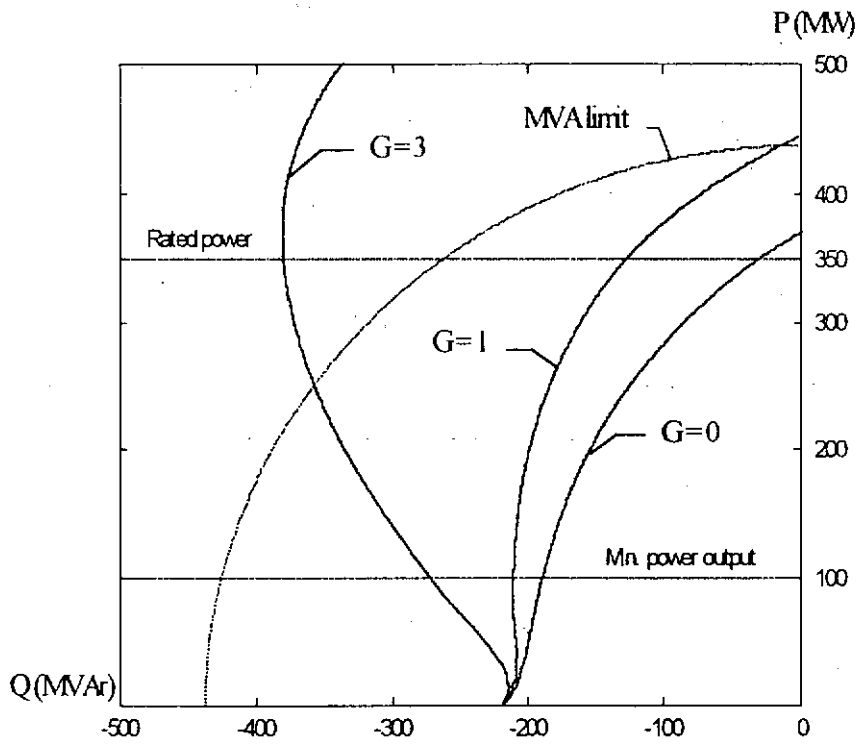

Fig. 3.8 Monotonic stability limits for different EXC gain G of machine A_1 (multimachine)

3.2.1.3 Effect of exciter

Traditionally, it is interpreted that if $\Delta P_e/\Delta\delta$ is positive (negative), the system will be monotonically stable (unstable). In accordance to the $F(p)$ in (3.2a), however, $\Delta P_e/\Delta\delta$ is obviously always negative, irrespective of the stability condition. The relationship between $\Delta P_e/\Delta\delta$ and exciter has been further examined based on $H(p)$ and $\lambda = 0$ loci plotting for different exciter response. The results of both single and multi machine analyses support that the monotonic instability should not occur since all machines are equipped with an auto exciter.

3.2.2 Mode shape analysis of governor effect

3.2.2.1 Mode shape analysis

The modal relationship of any two variables can be obtained by simply putting $p = \lambda$ in the system equations (e.g. $H(p)$). In a complicated system, the relationships of multi variables can only be determined by their mode shapes obtained by CU. The mode shape (in polar form of $\rho\angle\theta$) for any complex λ is a depiction of the phasor relationships between different variables [41]. For instance, the mode shape with respect to all machine output powers will indicate clearly the power relationships with respect to that of the oscillatory (complex) mode: the relative MW swing magnitude represented by the respective ρ values, and the phase relationships indicated by the relative θ values (Chapter 4). In monotonic stability study, the associated eigenvalue is real, hence the mode 'shape' of the variables are only positive or negative numbers, providing the magnitude and sign of relative movements of different variables.

3.2.2.2 Single machine system

If the governor in Appendix 11 (data of machine A_1) is included in the simulation, $\Delta P_m \neq 0$, $\Delta P_a/\Delta\delta = (M\lambda^2)/\Omega_o$ in (3.1) is always non-negative and $\Delta P_e/\Delta\delta$ can only be determined by the mode shapes as shown in Table 3.2 for two operating points. It is observed that

(a) the system is stable at $Q = 0$ but unstable at $Q = -100$,

(b) the real eigenvalue is slightly affected by the governor,

(c) $\Delta P_a/\Delta\delta$ is always positive,

(d) $\Delta P_e/\Delta\delta$ is negative without a governor, but will change sign with λ if a governor is present.

Thus, it can be concluded that the governor effect cannot be ignored if the torque/angle relationship is to be critically examined.

	Without governor		With governor	
Q (MVAr)	-100	0	-100	0
λ	+0.02114	-0.04817	+0.02060	-0.04797
$\Delta\delta$	1	1	1	1
ΔP_a	0.00003	0.00021	0.00035	0.00020
ΔP_m	0	0	-0.05626	0.01372
ΔP_e	-0.00003	-0.00021	-0.05661	0.01352

Table 3.2 Mode shapes of the torque and angle in single machine system

(P = 350MW and G = 0)

	(a) stationary rotating frame				(b) non-stationary rotating frame			
	Without governor		With governor		Without governor		With governor	
Q (MVAr)	-130	0	-130	0	-130	0	-130	0
λ	+0.04596	-0.15708	+0.04554	-0.15658	+0.07165	-0.01451	+0.01806	-0.09246
$\Delta\delta$	1	1	1	1	1	1	1	1
ΔP_a	0.00039	0.00456	0.00038	0.00453	0.16447	-0.04778	0.03902	-0.30740
ΔP_m	0	0	-0.00387	0.01643	0	0	-1.01925	-1.75747
ΔP_e	-0.00039	-0.00456	-0.00425	0.01190	-0.16447	0.04778	-1.05827	-1.45007

Table 3.3 Mode shapes of the torque and angle of machine A_1 in multimachine system

(P = 350MW and G = 0 for machine A_1 and other machines are with governor)

3.2.2.3 Multimachine system

(a) Stationary rotating frame

If the system described in Section 3.2.1.2 is used and if the system rotating frame is assumed stationary, the machine motion equation (3.1) is still valid. The torque/angle relationship for the same 350 MW machine A_1 can be likewise examined by the mode shape of case (a) in Table 3.3. The findings of case (a) in Table 3.3 (multimachine case) are very similar to those of Table 3.2 (single machine case).

(b) Non-stationary rotating frame

In single machine system, the rotating frame of the infinite machine is stationary. However, in multimachine system, the frame is not stationary and a machine has to be synchronised with the system frame. The rotor angle/speed relationship has to be modified by (3.8).

$$\Delta\delta = \frac{\Omega_o[\Delta\Omega - \Delta\Omega_{ref}]}{p} \tag{3.8}$$

where $\Delta\Omega_{ref}$ is the speed of the reference frame and $\Delta\Omega = \Delta P_a/(pM)$. Thus, $\Delta\delta$ can be given by

$$\Delta\delta = \frac{\Omega_o}{Mp^2}\Delta P_a - \frac{\Omega_o}{p}\Delta\Omega_{ref} \tag{3.9}$$

and the sign of $\Delta P_a/\Delta\delta$ is no longer non-negative. The torque/angle relationships are once more evaluated as shown in case (b) of Table 3.3. By comparing with case (a) and (b) in Table 3.3, it is observed that if the rotating frame is considered, there is no deterministic relationship between the torque/angle (either $\Delta P_a/\Delta\delta$ or $\Delta P_e/\Delta\delta$) with respect to eigenvalue sign changes.

(The $\Delta\Omega_{ref}$ of the present study is the centre of inertia (COI) speed which is the weighted average of all machine speeds.)

3.2.2.4 Effect of governor

Governor representation is usually ignored in monotonic stability studies. In this section, the results based on modal analyses concludes that $\Delta P_e/\Delta\delta$ will only change sign with stability if the governor is present and the rotating frame is stationary (for both single and multi machine cases). In a realistic system, however, the frame is non-stationary so that there should be no deterministic relationship between the torque/angle and stability.

3.3 Sensitivity analysis

The study of exciter effect in Section 3.2.1 is based on the locus plotting of $\lambda = 0$ and modal analysis in its vicinity with varying G. The exciter effect can be further examined from the plots of eigenvalue and its sensitivity with respect to G (i.e. $\partial\lambda/\partial G$) of Fig. 3.9 and 3.10 for single machine and Fig. 3.11 and 3.12 for multimachine respectively.

From Fig. 3.9 and 3.11, λ will become more positive (i.e. unstable) when Q decreases, and is very positive when $Q < -300$MVAr. Because of the negative $\partial\lambda/\partial G$ in Fig. 3.10 and 3.12, it may be concluded that λ becomes more negative, or the system tends to be more stable, by the increase of G. The sensitivity is more significant with more positive λ and the improvement is less noticeable when the system is already very stable. This result explains the improvement of stability and the tendency of the limit for increasing G in Fig. 3.4 and 3.8.

3.4 Summary

Synchronising torque/coefficients are often used to determine monotonic stability and the system is conventionally considered to be unstable (stable) if this coefficient is negative (positive). However, based on the torque equations and mode shapes in a single machine system, this coefficient is non-positive, irrespective of the system stability if the governor effect is ignored. With the support of eigenvalue loci and sensitivity analyses under both single and multi machine environment, it is shown that the stability limit is much extended by increasing the exciter gain, and theoretically the limit does not exist for a normal exciter.

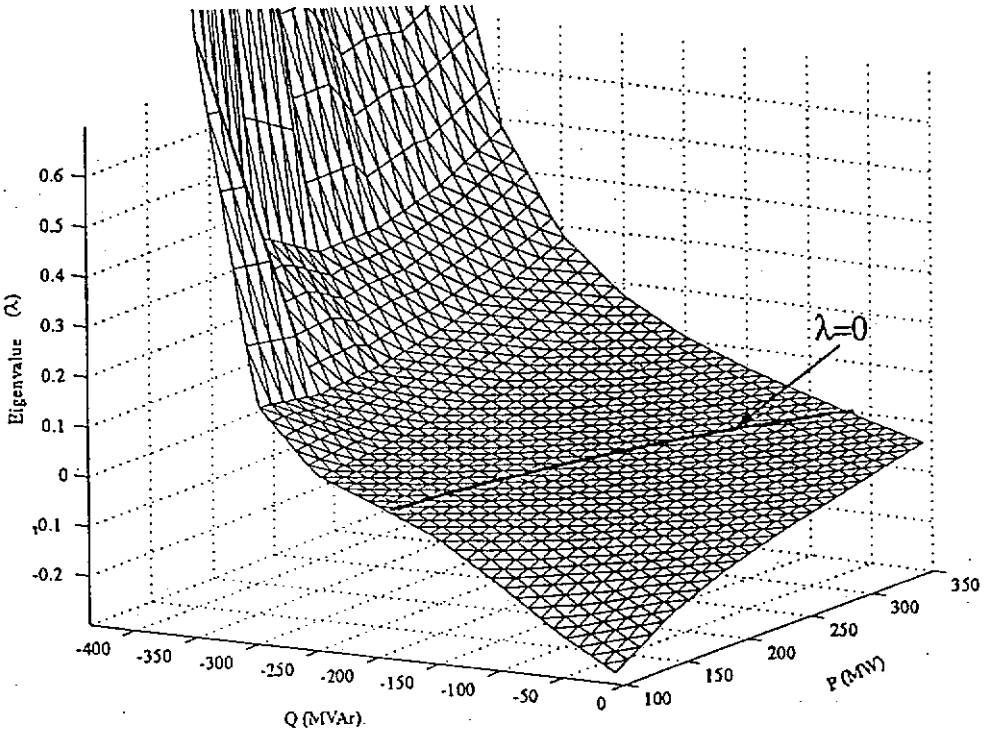

Fig. 3.9 Eigenvalue for different operating points at $G = 0$ (single machine)

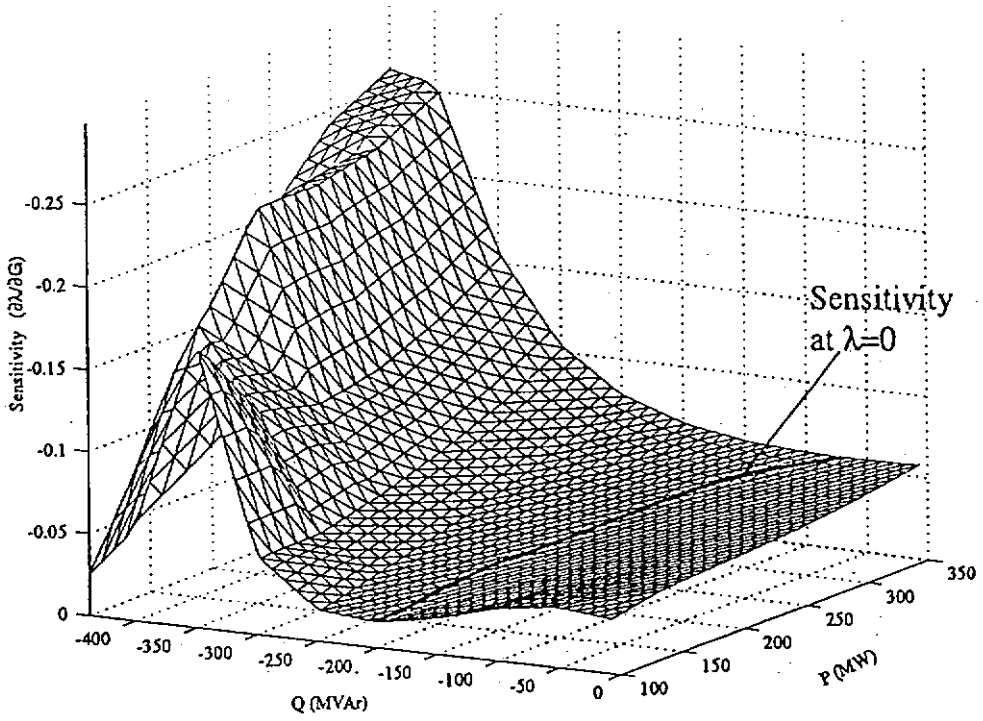

Fig. 3.10 Eigenvalue sensitivity analysis with respect to G
for different operating points at $G = 0$ (single machine)

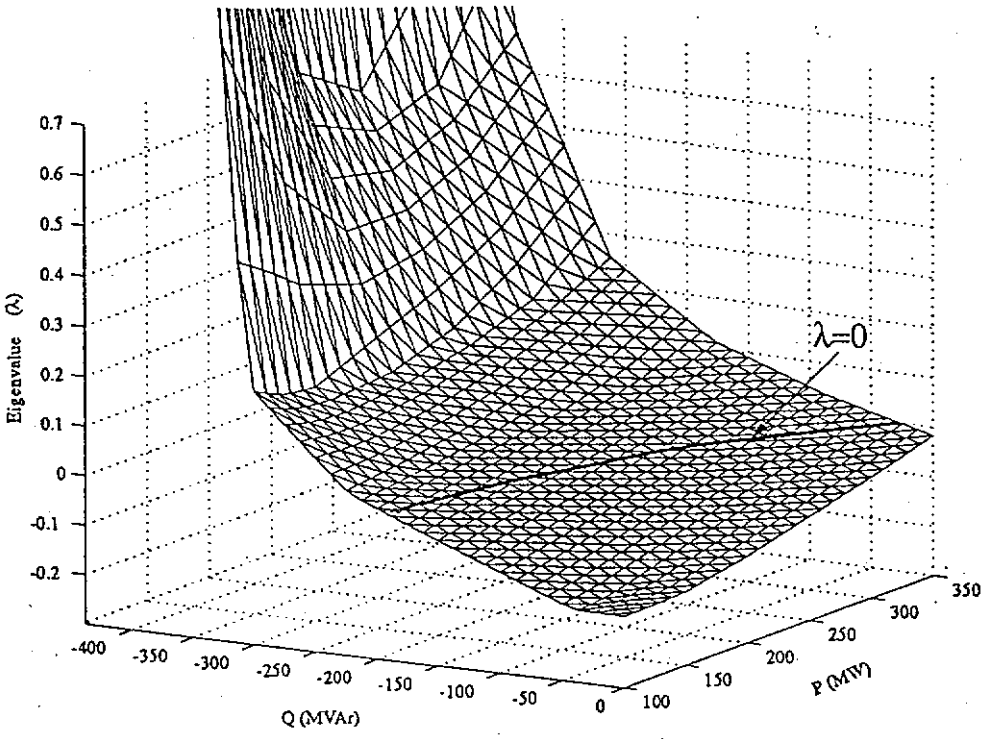

Fig. 3.11 Eigenvalue for different operating points at $G = 0$ (multimachine)

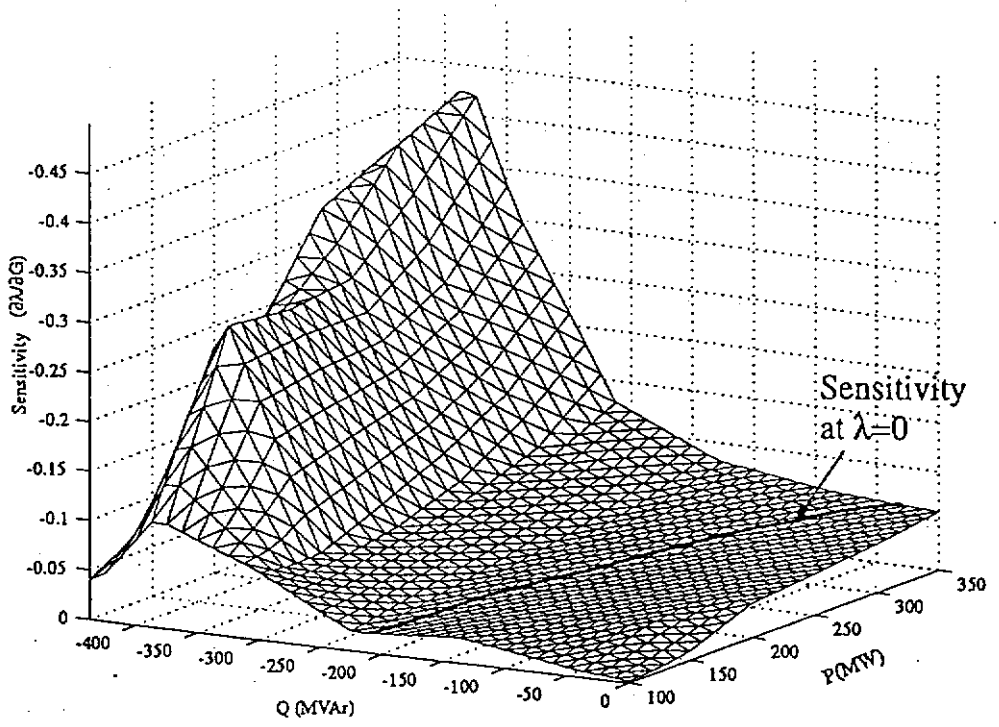

Fig. 3.12 Eigenvalue sensitivity analysis with respect to G
for different operating points at $G = 0$ (multimachine)

CHAPTER 4

STABILITY ENHANCEMENT USING AN SVC CONTROLLER

4.1 Introduction

With the rapid growth of electric power systems and the increasing needs for interconnection between 'areas' of generation, tieline oscillation become a serious hazard because they will impose unnecessary limitations on system operation. Rapid advances in power electronics have made it both practicable and economic to design powerful thyristor-controlled devices and provide other means of system damping enhancement. In this chapter, the commonest FACTS device, static var compensator (SVC), is studied.

The SVC is a shunt compensation device and was first employment by Basin Electric Power Cooperative in 1977 to provide automatic and continuous voltage control on a 115kV network in western Nebraska [43]. The primary application of the SVC is to maintain the busbar voltage at or near a constant value. The SVC is equipped with a voltage regulator that provides synchronizing torque but the damping torque contributions are small [42]. An additional damping controller is necessary for adequate damping. However, when the damping controller gain increases, an unstable mode, the SVC mode, occurs [44].

To improve system damping and provide a safe margin for the SVC, a new and systematic tuning method is proposed in this chapter. Modal analysis is used to identify the machine and mode relationships and to show which machines are more liable to cause instability (Section 4.2). The most effective location and the damping signal for the SVC are carefully selected by means of controllability, observability and residue indices (Section 4.3). Using eigenvalue sensitivity analysis, the correct direction for adjusting the controller settings can

be inferred from the combined sensitivity coefficient (CSC) developed in Section 4.4. Optimization is formulated as the maximization of the damping of the dominant (interarea) mode while maintaining a constant 9.5 dB gain margin for the SVC mode. The controller settings are said to be optimal when the CSC with respect to all the controller parameters are practically zero. Since the CSC approach attempts to look after the damping of both modes simultaneously, the use of a single lead/lag stage (Section 4.4.1) would be too restrictive in the present context. Detailed analysis reveals that a flexible controller structure should, in general, have three lead/lag stages (Section 4.5). It is shown that if the SVC mode constraint is ignored, tuning the lead/lag settings for interarea mode damping alone can actually lead to adjustment in the wrong direction.

4.2 Modal analysis of electromechanical modes

The interconnected system in Fig 3.5, which was used for monotonic stability analysis in Chapter 3, will be considered in this study. In order to have more general simulation results, the loads are represented by voltage dependent exponential models. Realistic values of exponential constants 'a' and 'b' are 1.38 and 3.22, respectively [45,46]. All machines are represented by sixth order models. Since there are seven machines, there will be 7 – 1 = 6 principal modes associated with electromechanical oscillations [47] as shown in Table 4.1 and one of the electromechanical modes ($\lambda = +0.04 \pm j3.42$) is unstable.

Modes	α	ω
1 Inter-area	+0.04	3.42
2 $B_4 \leftrightarrow B_1+B_2+B_3$	–0.41	5.77
3 $B_2 \leftrightarrow B_1+B_3$	–0.49	6.23
4 $B_3 \leftrightarrow B_1+B_2+B_4$	–0.51	6.82
5 $A_3 \leftrightarrow A_1+A_2+B_1$	–1.28	7.64
6 $A_1 \leftrightarrow A_2$	–0.56	8.01

Table 4.1 Electromechanical modes ($\lambda = \alpha \pm j\omega$) of the 7-machines system

Since the electromechanical modes are associated with intermachine power swings, mode shapes of ΔP_e will indicate clearly the intermachine relationships in each mode. The mode shapes, with respect to the seven power outputs (i.e. $y_i = \Delta P_{ei}$, i = 1 to 7) are shown in Fig. 4.1 where the moduli are normalized such that $\sum \Delta P_{ei}^2 = 1$ for every mode (the ΔP_e phasors of very small moduli are not plotted). Mode 1 (unstable) characterized by oscillation between the machines of the two different areas is an interarea mode. Mode 2, 3 and 4 highlight the interaction among the B machines. Mode 5 reveals the interaction between A_3 and the other machines. Mode 6 shows the reaction between A_1 and A_2.

Therefore, system instability is due to mode 1 (interarea), or the so-called tieline oscillation. If an SVC is installed to increase damping, the tieline signal should be used as the damping signal [2,42]. The next section will discuss the selection of the SVC location and the tieline signal for effective damping.

4.3 Selection of the location and damping signal

4.3.1 Selection of the location

4.3.1.1 Modal analysis

An SVC with controller inputs I_{SVC} and V_{SVC} and output B_L has been described in Chapter 2. To increase damping, an additional damping controller ($C(p)$) shown in Fig. 4.2 is required. Even though this damping signal is not yet determined at this stage, it is possible to select the SVC location using the open-loop (i.e. ΔB_L disconnected) controllability index [48], defined by CI = $\left| V_J^T (\boldsymbol{B} + \lambda_J \boldsymbol{E}) \right|$, where superscript T denotes transpose, V_J is the left eigenvector of the jth eigenvalue λ_J and $\boldsymbol{B}$ and $\boldsymbol{E}$ are the coefficient matrices of the state equation (2.20). (see Appendix 12)

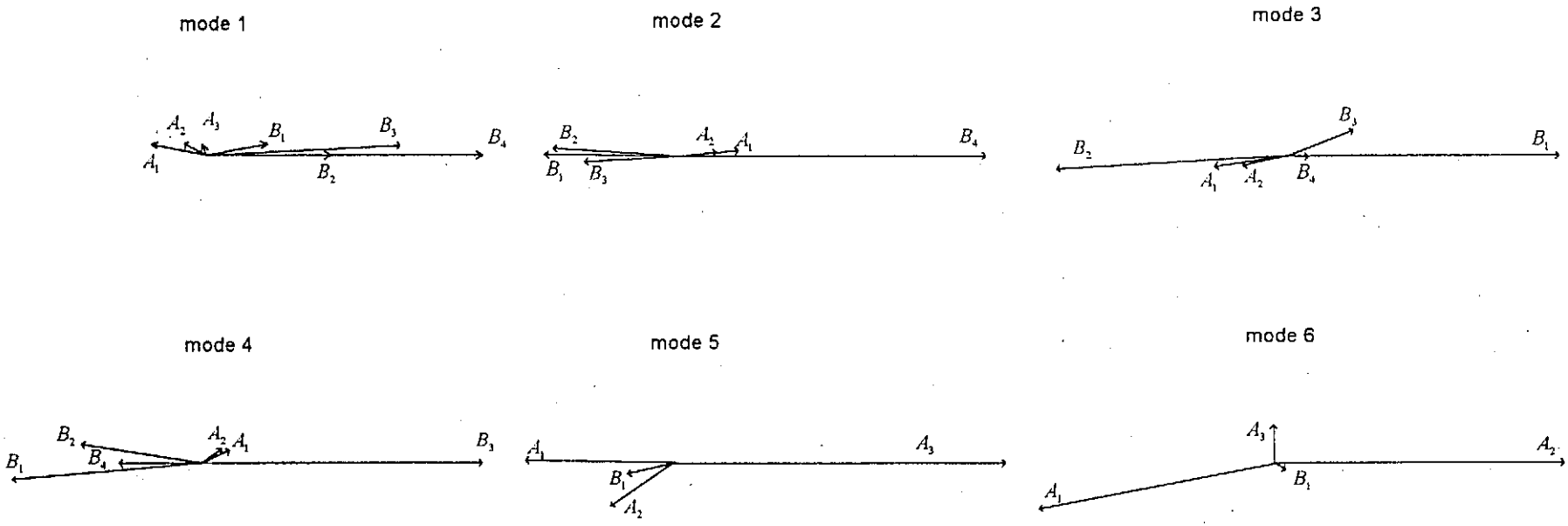

Fig. 4.1 Normalized shapes of electromechanical modes with respect to incremental machine power ΔP_e

Any bus can be considered for SVC installation, however, if tieline flow is employed as the damping signal, the candidate locations should be restricted to 6, namely buses 4, 12, 13 and 14 and midpoints m_1 and m_2 in Fig. 3.5. The CI results in Table 4.2 suggest that buses 12 and 13 are the leading candidates for SVC installation.

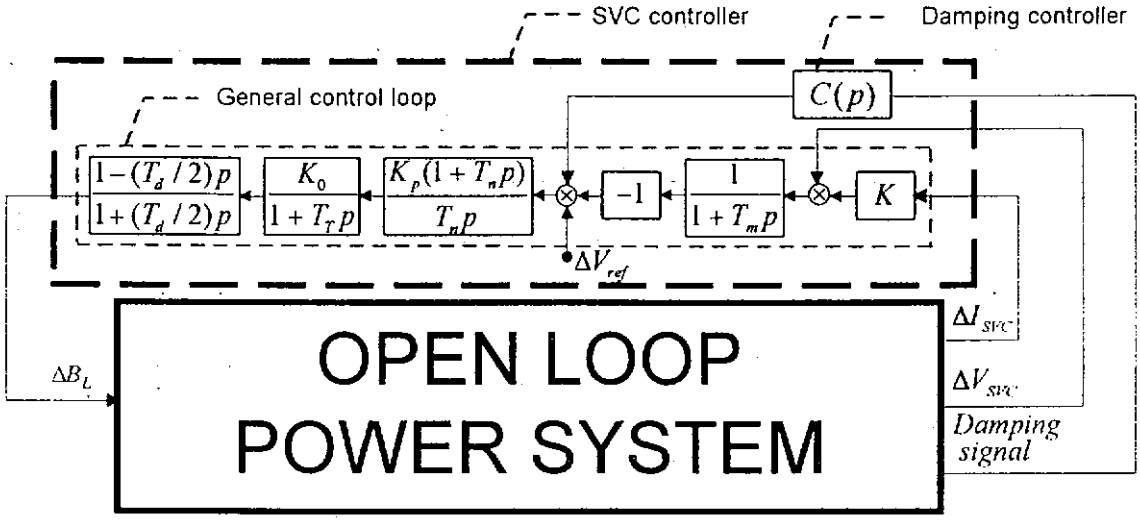

Fig. 4.2 The connection between the controller and the open-loop power system

4.3.1.2 Sensitivity analysis

The CI technique using an open-loop approach assesses the impact of B_L on a particular eigenvalue. Alternatively, since the role of an SVC is to change the bus Q injection, the impact can also be assessed using eigenvalue sensitivity $\partial\lambda/\partial Q$ (Section 2.3.3.2) as shown in Table 4.2. Again, the sensitivity approach supports buses 12 and 13 as effective SVC locations.

Bus	CI	$\partial\lambda/\partial Q$
12	19.846	0.561
m_1	15.647	0.365
4	10.174	0.362
13	18.727	0.569
m_2	16.036	0.379
14	11.805	0.377

Table 4.2 Controllability indices and sensitivity coefficients ($\partial\lambda/\partial Q$) for different locations

4.3.2 Selection of the damping signal

Four locally measurable tieline signals (current flow (I_{TL}), real power (P_{TL}), reactive power (Q_{TL}) and MVA (S_{TL})) can be used as a feedback damping signals and the choice of signal can be guided by the observability index OI = $|CU_J|$ [48], where CU_J is the mode shape of the corresponding damping signals associated with the jth eigenvalue λ_J. The result in Table 4.3 (with respect to only two possible locations) shows that the most effective signal is I_{TL}, and the least effective is Q_{TL}. According to [48], the final choice of location/signal should be determined by the residue index RI = OI*CI. Hence, bus 12 is the best SVC location and current flow the best damping signal.

The choice of location and selection of signal based on open-loop system analysis examines the SVC's impact on the eigenvalue. The next step is to determine the controller structure and the parameter settings such that this impact is directed so as to push the interarea mode eigenvalue to the left half plane of the s-domain in the closed-loop system.

Bus	12		13	
Signal	OI(x10^{-3})	RI	OI(x10^{-3})	RI
I_{TL}	60.240	1.196	48.114	0.901
P_{TL}	51.835	1.029	39.884	0.747
Q_{TL}	25.048	0.497	22.602	0.423
S_{TL}	53.179	1.055	39.492	0.740

Table 4.3 Observability and residue indices for different signals of bus 12 and 13

4.4 Determination of the settings of the damping controller based on sensitivity analysis

The original eigenvalues in Table 4.1 showed that mode 1 (interarea) was unstable. The eigenvalues with an SVC installed at bus 12 are shown in Table 4.4 (see column $G_d = 0$). It is observed that

(a) The additional SVC mode is very stable.

(b) Mode 2 to 6 are almost unchanged.

(c) Mode 1 becomes marginally stable.

In order to provide adequate damping for the mode 1 (interarea), the next step is to effectively design/tune the SVC damping controller.

G_d=	0		G_o=0.073		$2G_o$=0.146		$3G_o$=0.219	
Modes	α	ω	α	ω	α	ω	α	ω
1	−0.09	3.84	−0.19	3.91	−0.28	3.97	−0.36	4.04
2	−0.41	5.82	−0.41	5.83	−0.48	5.86	−0.50	5.89
3	−0.48	6.30	−0.58	6.30	−0.71	6.31	−0.87	6.26
4	−0.51	6.83	−0.53	6.82	−0.54	6.80	−0.53	6.78
5	−1.09	7.69	−1.04	7.68	−0.98	7.69	−0.93	7.71
6	−0.52	8.14	−0.53	8.16	−0.55	8.19	−0.57	8.22
SVC	−1.32	18.61	−0.88	18.63	−0.44	18.67	+0.01	18.72

Table 4.4 Variation of different modes with respect to SVC damping controller gain G_d (Modes 1 to 6 are the same electromechanical modes in Table 4.1)

4.4.1 Damping controller representation

The damping controller with ΔI_{TL} as input and with initially only one lead/lag stage is given in (4.1) and will supplement the setting ΔV_{ref} of the SVC control loop in Fig. 4.2.

$$C(p) = G_d \frac{pT_w}{1+pT_w} \frac{1+pT_1}{1+pT_2} \tag{4.1}$$

where G_d = damping controller gain

T_w = 'washout' time constant

and T_1/T_2 = lead/lag time constants

In normal practice a washout stage is included to suppress the DC offset [2]. A large washout time constant of 7 seconds is selected to ensure that the damping controller will not respond to very low frequency or DC offset; the frequency range of interest does not fall below 0.2 Hz.

4.4.2 Determination of damping controller gain constant G_d

From Table 4.4, although the very stable mode 5 is slightly degraded, the damping of all other modes increases with higher G_d values. However as G_d increases, the SVC mode becomes unstable when G_d reaches a value of 0.219 ($3G_o$). This phenomenon is also common in PSS tuning, where so-called 'local plant mode' instability occurs when the PSS gain increases. To avoid PSS instability, a safe margin (say 9.5 dB = 20 log (3) [49,50]) is applied. In the present context, therefore, G_d value has to be reduced to 1/3 of the critical value G_c if the same 9.5 dB margin as the PSS is adopted. Hence, G_d is set at $G_d = G_o = G_c/3 = 0.219/3 = 0.073$.

4.4.3 Determination of lead/lag time constants

Whenever there is a change in a parameter, the eigenvalue will vary and to determine this effect, the relative sensitivity coefficient (RSC) is defined as RSC = $(\partial\lambda_j/\partial\kappa)\kappa \approx \Delta\lambda_j/(\Delta\kappa/\kappa)$ where κ is any parameter. For a complex eigenvalue, which is of interest for oscillation studies, the real part of the RSC (i.e. RRSC) defined below is especially important:

$$RRSC = S_{j\kappa} = \mathrm{Re}\left\{\frac{\partial\lambda_j}{\partial\kappa}\right\}\kappa \approx \frac{\Delta\alpha_j}{\Delta\kappa/\kappa} \tag{4.2}$$

The main purpose of sensitivity analysis is to make α_j as negative as possible in inherently lightly damped systems so as to increase damping. Since $\Delta\alpha_j = S_{j\kappa}\Delta\kappa/\kappa$, whenever $S_{j\kappa}$ is positive (negative), $\Delta\kappa$ should be made negative (positive) that is κ should decrease (increase) by suitable adjustment to achieve the objective. Hence, whether a lead or lag compensation should be used and the most suitable T values can be decided by sensitivity analysis.

4.4.3.1 Sensitivity analysis of interarea mode

The variation of the sensitivities, RRSC, of the interarea mode (I) with respect to different T values (say, $S_{J\kappa} = S_{IT}$) is shown in Fig. 4.3a. Since the lead and lag compensation effects are always equal and opposite,

$$S_{IT1} = -S_{IT2} \tag{4.3}$$

In Fig. 4.3a, S_{IT1} is negative with respect to different T values and so T_1 should be increased to make α_I more negative. On the other hand, T_2 should be reduced making $T_1 > T_2$ and so a *lead* compensation will be required (if damping out the interarea mode is considered in isolation).

4.4.3.2 Concept of combined sensitivity

However, the design approach described in subsection 4.4.3.1 above is only partially correct as the effect of lead/lag time constant tuning on the critical value G_c of controller gain has been overlooked. Hence, a combined sensitivity concept is now introduced [51].

Fig. 4.4a shows the typical variation of the interarea damping constant α_I, with respect to G_d. Assuming that the damping is improved by increasing a parameter κ to $\kappa + \Delta\kappa$, the original curve (solid line) in Fig. 4.4a will be shifted downwards (dashed line). Therefore, the critical G_c changes and hence the setting $G_o = G_c/3$ will be changed by the controller tuning action described in Section 4.4.2. Let ΔG_c and $\Delta G_o = \Delta G_c/3$ be these changes, respectively. The actual or overall change, due to both the $\Delta\kappa$ and ΔG_o, is given by $\Delta\alpha_I^\circ$, where

$$\Delta\alpha_I^\circ = \Delta\alpha_I + \Delta\alpha_I' \approx \Delta\alpha_I + \frac{\partial\alpha_I}{\partial G_o}\Delta G_o$$

$$= \Delta\alpha_I + \frac{\partial\alpha_I}{\partial G_o/G_o}\frac{\Delta G_o}{G_o} = \Delta\alpha_I + S_{IG}\frac{\Delta G_o}{G_o} \tag{4.4}$$

where S_{IG} = RRSC of the interarea mode, with respect to G_d at G_o.

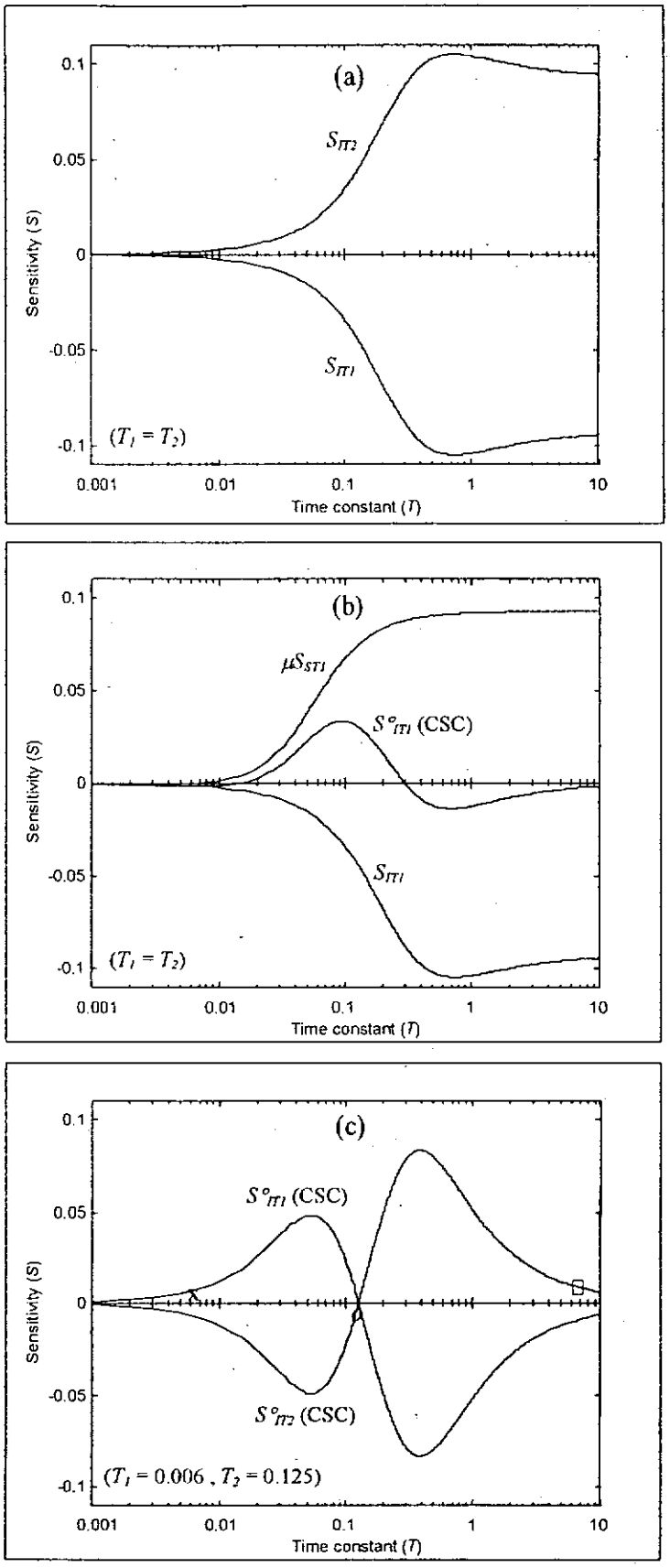

Fig. 4.3 Sensitivities vs. controller lead or lag time constants

An interesting relationship is obtained by expressing $\Delta G_o/G_o$ in terms of the change of SVC mode damping constant α_S. Assuming that zero damping at G_c (Fig. 4.4b) is improved by $\Delta\alpha_S$ due to $\Delta\kappa$, the damping will become zero again at $G_c + \Delta G_c$, thus

$$\Delta\alpha_S \approx -\frac{\partial\alpha_S}{\partial G_c}\Delta G_c = -\frac{\partial\alpha_S}{\partial G_c/G_c}\frac{\Delta G_c}{G_c} = -S_{SG}\frac{\Delta G_c}{G_c} \tag{4.5}$$

where S_{SG} = RRSC of the SVC mode with respect to G_d at G_c.

To keep a constant (9.5 dB) margin, the proportional change in G_o and G_c must be the same, and, using (4.5),

$$\frac{\Delta G_o}{G_o} = \frac{\Delta G_c}{G_c} = -\frac{\Delta\alpha_S}{S_{SG}} \tag{4.6}$$

$\Delta G_o/G_o$ may now be eliminated in (4.4) to give

$$\Delta\alpha_I^{\circ} = \Delta\alpha_I + \mu\Delta\alpha_S \tag{4.7}$$

where

$$\mu = -S_{IG}/S_{SG} \tag{4.8}$$

In the present study, since $S_{IG} < 0$ when $G_d = G_o$ and $S_{SG} > 0$ when $G_d = G_c$, μ is a positive constant, implying, perhaps unexpectedly, that improvement in the SVC mode damping will also enhance the overall damping of the interarea mode, according to (4.7). In the subsequent analysis, sensitivities of the SVC mode need to be included in the design because the tendency towards SVC mode instability at high gain $G_d = G_c$ will restrict the damping controller gain. At low G_d values (relative to G_c), the SVC mode is already very stable (e.g. $\alpha_S = -1.32$ at $G_d = 0$, as shown in Table 4.4), and its variation has insignificant effect on the overall system damping. It is, hence, not necessary at low G_d values to consider SVC mode instability during the damping controller design stage, although the

value of α_S when $G_d = G_o$ will nevertheless be routinely checked after arriving at the ultimate controller settings.

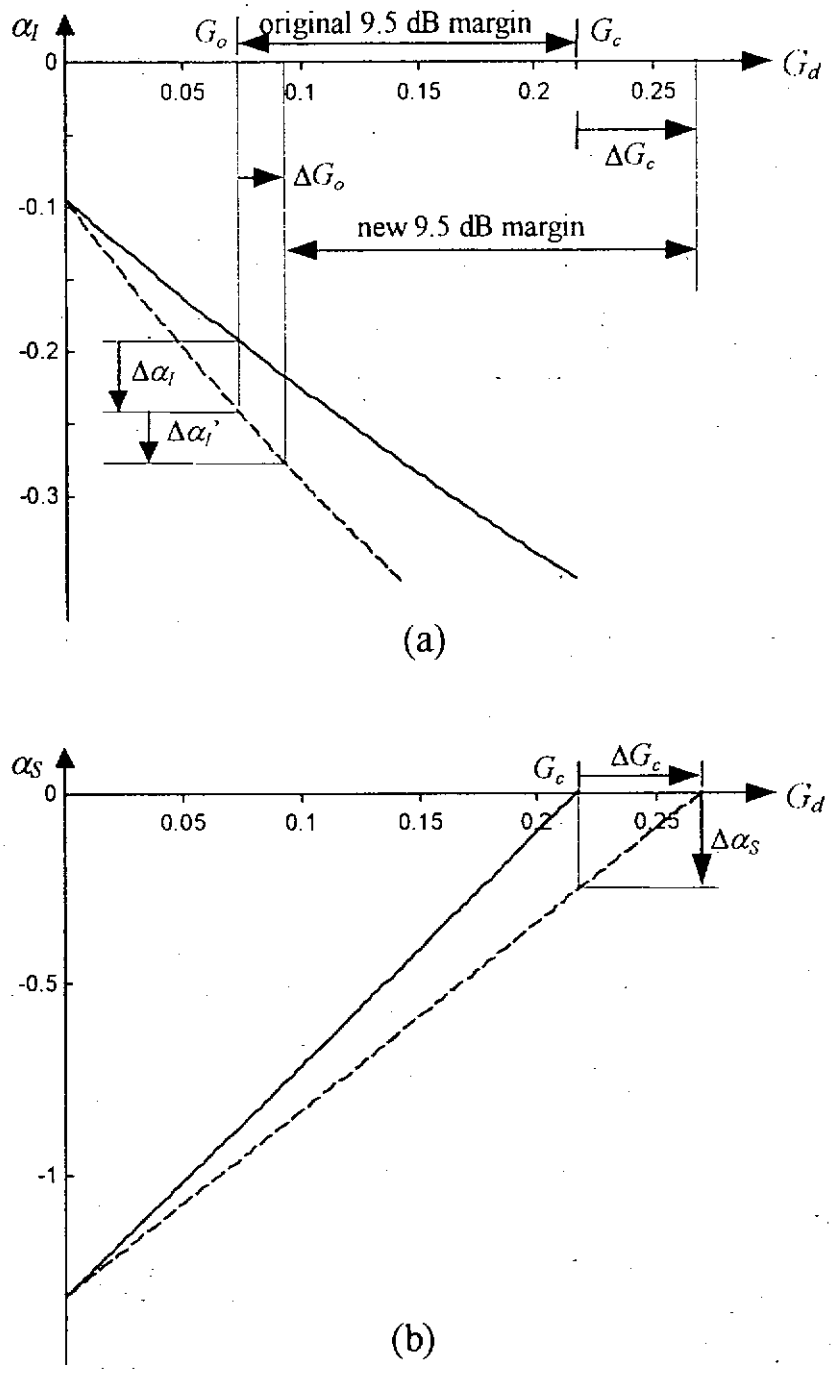

Fig. 4.4 Damping constants vs. controller gain G_d

Finally, dividing (4.7) by $\Delta\kappa/\kappa$, the equation takes the form

$$S^{\circ}_{I\kappa} = S_{I\kappa} + \mu S_{S\kappa} \tag{4.9}$$

where $S^{\circ}_{I\kappa}$ = Combined sensitivity coefficient (CSC) of interarea mode with respect to κ, for constant gain margin

$S_{I\kappa}$ = RRSC of interarea mode, with respect to κ alone

$S_{S\kappa}$ = RRSC of SVC mode with respect to κ

The optimal controller settings in terms of any parameter κ can be determined by making use of the CSC which combines the two mode sensitivities into one by using the factor μ. In this approach, the allowance for a constant gain margin to ensure SVC mode stability is built into the design procedure.

4.4.3.3 Combined sensitivity coefficients with respect to T_1 and T_2, and optimum lead/lag settings (one stage)

The CSCs can be calculated from (4.9) and plotted as functions of T. From (4.3), the sensitivities of T_1 and T_2 are equal and opposite; it is therefore necessary to plot only one of them, say T_1, that is set $\kappa = T_1$ in (4.9). Fig. 4.3b shows the plot of S_{IT1} (same as in Fig. 4.3a), μS_{ST1} has also been computed and plotted and finally by summation S°_{IT1}, the CSC, obtained. Due to the higher sensitivity of S°_{IT1}, $T_1 = T_2 = 0.1$s are chosen as the initial trial values. The optimum setting can be obtained by changing the T values in small steps, in directions suggested by the CSCs of the current settings. The final settings of T_1 and T_2 are 0.006s and 0.125s and the final $G_o = 0.81/3 = 0.27$. This design shifts the interarea mode pole to $-0.27 \pm j4.15$. The corresponding CSCs of T_1 and T_2 in Fig. 4.3c (at points x and o, respectively) are so close to zero and further adjustment would have negligible effect. Note that the final result is an overall *lag* stage in the design circuit and this contradicts the more simplistic observation made in subsection 4.4.3.1 above.

4.4.3.4 Combined sensitivity coefficients with respect to G_d

Putting $\kappa = G_d$ into (4.9), and using (4.8), gives

$$S^{\circ}_{IG} = S_{IG} - (S_{IG}/S_{SG})S_{SG} = 0 \tag{4.10}$$

and the CSC with respect to the controller gain constant G_d is always zero. If one intends to increase the controller gain to enhance damping effects, this will subsequently be nullified by the reduction of the controller gain knob setting required to maintain the gain margin during site test.

4.4.3.5 Combined sensitivity coefficients with respect to 'washout' T_w

The controller washout stage has a transfer function of $pT_w/(1 + pT_w)$ which may be written as $pT_b/(1 + pT_a)$. However, T_b has the same effect as G_d, and T_a is similar to T_2 (lag time constant) alone. Hence

$$S^{\circ}_{ITw} = S^{\circ}_{ITa} + S^{\circ}_{ITb} = S^{\circ}_{IT2} + 0 \tag{4.11}$$

From Fig. 4.3c, the $S^{\circ}_{ITw} = S^{\circ}_{IT2}$ when $T_w = T_2 = 7$s (at point □) is very small at that point. In fact this circuit (characterized by relatively large T) is added for 'washout' purposes.

From the above discussions, it is clear that the only controller parameters of concern in the actual design are the T parameters of the lead/lag stage. Since the CSCs with respect to all controller parameters, i.e. G_d, T_w, T_1 and T_2, are now equal to or approach zero, the settings are considered close to the optimum. Hence, the sensitivity analysis has achieved the objective of maximizing the interarea mode damping while retaining 9.5 dB gain margin to ensure SVC mode stability.

4.4.3.6 Improving damping by additional lead compensation

As seen from Fig. 4.3c, since S°_{TI} at T = 0.4s is quite high, the controller design can be further improved by including one more lead/lag stage and providing possibly some lead compensation. The sensitivity technique is used again in a similar way. The final optimal controller is obtained in (4.12) and the interarea mode eigenvalue is positioned at $-0.41 \pm j4.08$ which meets an acceptable damping ratio (10%) [11] so that no further adjustment is needed. The damping of other modes are checked and there are no undesirable values (Table 4.5).

$$C(p) = 0.0145\frac{7p}{1+7p}\frac{1+0.004p}{1+0.22p}\frac{1+8p}{1+0.257p} \tag{4.12}$$

Modes	α	ω
1	−0.41	4.08
2	−0.47	5.91
3	−1.03	6.59
4	−0.55	6.74
5	−0.89	7.57
6	−0.49	8.25
SVC	−0.98	18.01

Table 4.5 Different system modes when SVC includes damping controller

4.5 Synthesis of lead/lag time constants

Traditionally, a lead/lag circuit is regarded as providing phase compensation for a controller. Thus, a few lead/lag stages would be needed to achieve sufficient phase shifts at the frequency of concern. A different viewpoint will instead be offered as a basis of the SVC damping controller design. From the time constant synthesis, the signs of the sensitivity coefficients can change as shown in Fig. 4.3b and the controller appears to require different degrees of compensation depending on the T ranges, for effective

damping. Although these coefficients are in irregular shape, they are made up of certain characteristic patterns. This knowledge is useful to understand the objectives of the lead/lag stage, the number of lead/lag stages, the tuning direction and settings ranges of the time constants, as explained in this section.

4.5.1 Syntheses of time constant sensitivities for simple lead circuit

Consider a simple lead circuit of transfer function TF = [1 + pT] associated with an arbitrary mode j (with eigenvalue $\lambda_J = \alpha_J \pm j\omega_J$), the circuit gain G or the phase shift θ can be expressed as a function of T and λ_J, according to (A13.2) in Appendix 13, because [1 + $\lambda_J T$] $\equiv G\angle\theta$.

For a cascade circuit of, say, $G_d[1 + pT_a][1 + pT_b]$, the overall gain and phase shift is $G\angle\theta$ = $G_d{*}G_a\angle\theta_a{*}G_b\angle\theta_b$ = $G_dG_aG_b\angle(\theta_a+\theta_b)$. λ_J will vary if circuit gain G is increased to $G(1+\varepsilon)$, i.e. with $G_dG_aG_b$ increased to $G_dG_aG_b(1+\varepsilon)$. It is supposed that the effect on the λ_J variation will be the same if the gain increase is on G_d only, or on G_a only, or on G_b only, so long the fractional changes are of proportional magnitude (that is, $\Delta G_d/G_d$ = $\Delta G_a/G_a$ = $\Delta G_b/G_b = \varepsilon$). Hence,

$$\frac{\partial\lambda_J}{\partial G_d / G_d} = \frac{\partial\lambda_J}{\partial G_a / G_a} = \frac{\partial\lambda_J}{\partial G_b / G_b} \tag{4.13}$$

Hence, for n lead circuits in cascade, the value of $\partial\lambda_J/(\partial G_i/G_i)$ for i = 1, . . n is always equal to $\partial\lambda_J/(\partial G_d/G_d)$, and is independent of the choice of the T's, where $\partial\lambda_J/(\partial G_d/G_d)$ is the relative sensitivity coefficient (RSC) of λ_J with respect to gain constant G_d.

Similarly, it is also supposed that if θ increases to $\theta + \Delta\theta$, the λ_J variation may be the same whether only θ_a or only θ_b increases, i.e. θ = $\theta_a + \theta_b$ is increased to become either (θ_a + $\Delta\theta_a$) + θ_b or θ_a + (θ_b + $\Delta\theta_b$), provided that $\Delta\theta = \Delta\theta_a = \Delta\theta_b$. Again, if this is true, $\partial\lambda_J/\partial\theta_i$ = constant for i = 1, . . n and is again independent of the choice of T's, for n lead circuits in cascade.

The above can be verified by considering the effect of a simple lead circuit $G\angle\theta \equiv [1 + \lambda_J T]$ on the RRSC. As explained in Appendix 13, the sensitivities of mode j with respect to T can be decomposed into two components associated with G and θ, according to (here $S_{J\kappa} = S_{JT}$):

$$S_{JT} = \frac{\partial \alpha_J}{\partial T/T} = \frac{\partial \alpha_J}{\partial G/G}\frac{\partial G/G}{\partial T/T} + \frac{\partial \alpha_J}{\partial \theta}\frac{\partial \theta}{\partial T/T} \tag{4.14}$$

where

(a) $\partial\alpha_J/(\partial G/G) = S_{JG}$ (RRSC with respect to G_d)

(b) $(\partial G/G)/(\partial T/T)$ = change of circuit gain with respect to T

(c) $\partial\alpha_J/\partial\theta$ = sensitivity with respect to phase shift and

(d) $\partial\theta/(\partial T/T)$ = change of phase shift with respect to T

(a) and (c) are independent of T (Appendix 13), whilst (b) = $g_J = g(\alpha_J, \omega_J, T)$ and (d) = f_J, though varying with different T's, are positive and almost 'symmetrical' about $T = 1/\omega_J$ as shown in Fig. 4.5a. Thus, with (4.14) rewritten in the form:

$$S_{JT} = (g_J S_{JG}) + (f_J \frac{\partial \alpha_J}{\partial \theta}) \tag{4.15}$$

it becomes clear that the curve of the RRSC as a function of T consists of two components having the shapes of g and f respectively. $(g_J S_{JG})$ and $(f_J \partial\alpha_J/\partial\theta)$ may be referred to for convenience as the gain and phase shift components of the RRSC.

As seen from Fig. 4.5a, $g_J = f_J = 0.5$ at $T = 1/\omega_J$; $g_J > f_J$ for $T > 1/\omega_J$, and $g_J < f_J$ for $T < 1/\omega_J$. For very low (high) values of T, $|g_J S_{JG}|$ in (4.15) will be smaller (larger) than $|f_J \partial\alpha_J/\partial\theta|$, and there exists a certain T value such that $|g_J S_{JG}| = |f_J \partial\alpha_J/\partial\theta|$. In case of S_{JG} and $\partial\alpha_J/\partial\theta$ are of opposite sign, S_{JT} in (4.15) will have the sign of $\partial\alpha_J/\partial\theta$ at low T's, change sign at a certain value of T, and thereafter have the sign of S_{JG}. Since the peak of f is

only half of that of g, the gain component usually dominates, in particular at high T values. Thus if the lead/lag settings are tuned based on sensitivity plots or on some other methods, improvement of the mode damping is more likely due to the gain effect than the phase effect, even for incorrect phase compensation.

As explained in Appendix 13, the sensitivity plot (with varying T and for $\alpha << \omega$) can be derived from the Bode plot (with varying ω).

4.5.2 Synthesis of interarea mode sensitivities

From Table 4.6 for the interarea mode, both S_{IG} and $\partial\alpha_I/\partial\theta$ are negative and requires the controller gain G and phase shift θ to increase to improve damping ($J = I$ in Table 4.6). $g_I S_{IG}$ and $f_I \partial\alpha_I/\partial\theta$, and their combination S_{IT} are as shown in Fig. 4.6a.

From Fig. 4.6a, the phase component $f_I \partial\alpha_I/\partial\theta$ has a peak at $T = 1/\omega_I$. With reference to the Bode plot of Fig. 4.5c, by choosing $T = 1/\omega_J$, the phase shift θ is maximum at ω_J, and the phase component is therefore most effective at $T = 1/\omega_J$ in Fig. 4.6a. As for the gain component $g_I S_{IG}$, the Bode plot shows that the ΔG at high T value (Fig. 4.5b) is greater than that at low T value (Fig. 4.5c), and thus the gain component would be more effective with high T in Fig. 4.6a.

Since both components are negative, this would imply the parameter T in the lead circuit to be increased. Therefore, on the basis of S_{IT} alone, a *lead* compensation is required to improve the interarea mode damping.

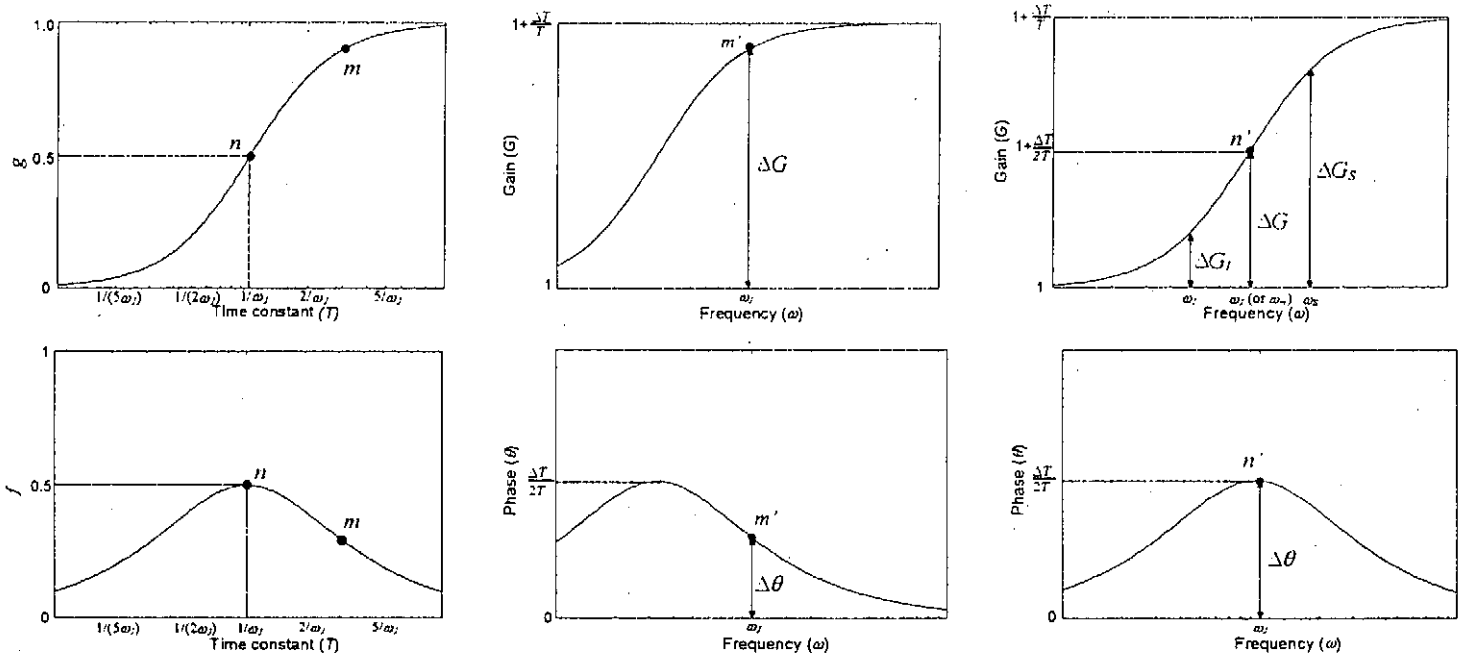

(a) (b) (c)

Fig. 4.5 (a) Sensitivities g and f against T of simple lead circuit $[1 + \lambda T]$, and bode plots of lead circuit $[1 + \lambda(T+\Delta T)]/[1+\lambda T]$ for (b) $T > 1/\omega_J$ and (c) $T = 1/\omega_J$, respectively
(For a lag circuit G and θ look similar but negative, according to Appendix 13)

Mode j	Interarea	SVC *
S_{JG}	–0.0926	0.0926
$\partial\alpha_J/\partial\theta$	-0.0656	–0.0113

Table 4.6 Sensitivities of interarea and SVC modes with respect to controller gain and phase shift

* In accordance with (4.8) and (4.9), the SVC mode sensitivities are scaled by μ (= –(–0.0926)/1.3263 = 0.0698).

4.5.3 Synthesis of SVC mode sensitivities

From Table 4.6, μS_{SG} and $\mu\partial\alpha_S/\partial\theta$ for SVC mode are of opposite sign. ($J = S$ in Table 4.6) To improve the SVC mode damping at $G_d = G_c$ would require the circuit gain G to decrease (since μS_{SG} is positive) or the phase shift θ to increase (since $\mu\partial\alpha_S/\partial\theta$ is negative). Thus, $\mu S_{STI} = \mu g_S S_{SG} + \mu f_S(\partial\alpha_S/\partial\theta)$ would change sign in Fig. 4.6b. At very low T's, the phase component dominates (even though $\partial\alpha_S/\partial\theta$ is relatively small) and S_{STI} is negative (same sign as $\partial\alpha_S/\partial\theta$). (The negative μS_{STI} is too small to be seen from Fig. 4.6b). At high T's, the gain component dominates and S_{STI} is positive (same sign as S_{SG}). Since the gain component is much larger than the phase component, an overall lag compensation is called for (tending to increase the stage gain) improving the SVC mode damping.

4.5.4 Synthesis of combined sensitivities

As shown in Fig. 4.3b, the CSC = S°_{ITI} as a function of T is composed of two curves S_{ITI} and μS_{STI}, and each curve is again made up of two curves (shown in Fig. 4.6a and 4.6b respectively). That is, the CSC is the summation of 4 curves (i-iv), with each curve assuming a standard form of Fig. 4.5b, but having its magnitude scaled by the corresponding sensitivity of Table 4.6. Thus after arrangement of the terms,

$$S^{\circ}_{ITI} = (g_I S_{IG} + \mu g_S S_{SG}) + (f_I \frac{\partial\alpha_I}{\partial\theta} + \mu f_S \frac{\partial\alpha_S}{\partial\theta}) \qquad (4.16)$$

It is noted from Fig. 4.6 that the phase shift component of the CSC defined by ($f_I\partial\alpha_I/\partial\theta + \mu f_S\partial\alpha_S/\partial\theta$) yields two separate plots of almost symmetric curve (ii) and (iv) centered at $T = 1/\omega_I$ and $1/\omega_S$ respectively. According to Fig. 4.5c, θ is maximum at ω_J for $T = 1/\omega_J$, so that the f curves (ii) and (iv) have peaks (i.e. are most effective) at $T = 1/\omega_I$, and $T = 1/\omega_S$, respectively (here $\omega_J = \omega_I$ or ω_S).

On the other hand the gain component of the CSC defined by ($g_I S_{IG} + \mu g_S S_{SG}$) also gives rise to one similar curve (v) by combining curves (i) and (iii) in Fig. 4.6c. This resultant curve is centered at $T = 1/\omega_m$ where $\omega_m^2 = \omega_I\omega_S$. It is positive, implying the need for a lag compensation. With reference to Appendix 14, the lag compensation is to *reduce* the circuit gain at ω_S (ω_I) by ΔG_S (ΔG_I) where $\Delta G_S > \Delta G_I$. Because of subsequent on-site tuning needed to bring about a fixed gain margin at ω_S, there would be a net increase in gain at ω_I amounting to $|\Delta G_S - \Delta G_I|$, tending to improve the interarea mode damping. With similar arguments, the lead compensation required in Section 4.5.2 will reduce the controller gain instead. According to Fig. 4.5c, G has the steepest slope, and hence a maximum difference $\Delta G_S - \Delta G_I$, at ω_m; thus, curve (v) has a peak at $T = 1/\omega_m$. (Here $\omega_J = \omega_m$).

From Fig. 4.6, the two phase components (ii) and (iv) are negative at very low and high T values respectively. However, the gain components curve (v) is positive, resulting that the final CSC curve (a combination of the three) in Fig. 4.3b would have two sign changes. Since the positive peak of (v) dominates in the CSC, a *lag* compensation is preferred. Consideration of the combined sensitivity thus leads to a conclusion contrary to the requirement of a *lead* compensation based on consideration of S_{IT} alone in Section 4.5.2. If the SVC mode instability is not directly taken into account at the design stage, the design may run the risk of applying compensation in the wrong direction.

4.5.5 Desired controller lead/lag composition

To summarize, the overall CSC curve as described by (4.16) may be considered to be composed of curves (iv), (v) and (ii) in Fig. 4.6, and hence is influenced by three peaks at $T = 1/\omega_S$, $1/\omega_m$ and $1/\omega_l$ (in increasing order). Since these are negative, positive and negative peaks respectively in sequence in this case, there will be two sign changes in the overall CSC function. To facilitate flexible adjustments over the full range of T of interest, three lead/lag stages are generally preferred in the controller structure. Their parameters should be capable of adjustment within the ranges suggested by ω_S, ω_m and ω_l.

The present example reveals that in particular situations the adequate number of lead/lag stages needed to obtain an optimum controller design may sometimes be reduced to two, because the peak at ω_S happens to be relatively small, the third stage is not effective and may not be necessary.

4.6 Advantage of eigenvalue sensitivity analysis techniques

The CSC design and the method of synthesis described in this chapter are facilitated by the sensitivity analysis technique developed using the PMT, whereby the CSC with respect to an arbitrary parameter can be evaluated readily irrespective of the size and complexity of the system. This cannot be done by other techniques. Repetitive application of trial-and-error methods may achieve similar objectives but would be time-consuming and impractical to cover the wide parameter ranges of the controller exhaustively. The method is elegant and analytical and can be applied systematically. This sensitivity technique which only requires the eigenvectors of the associated modes provides an accurate and fast solution to the controller optimum design problem.

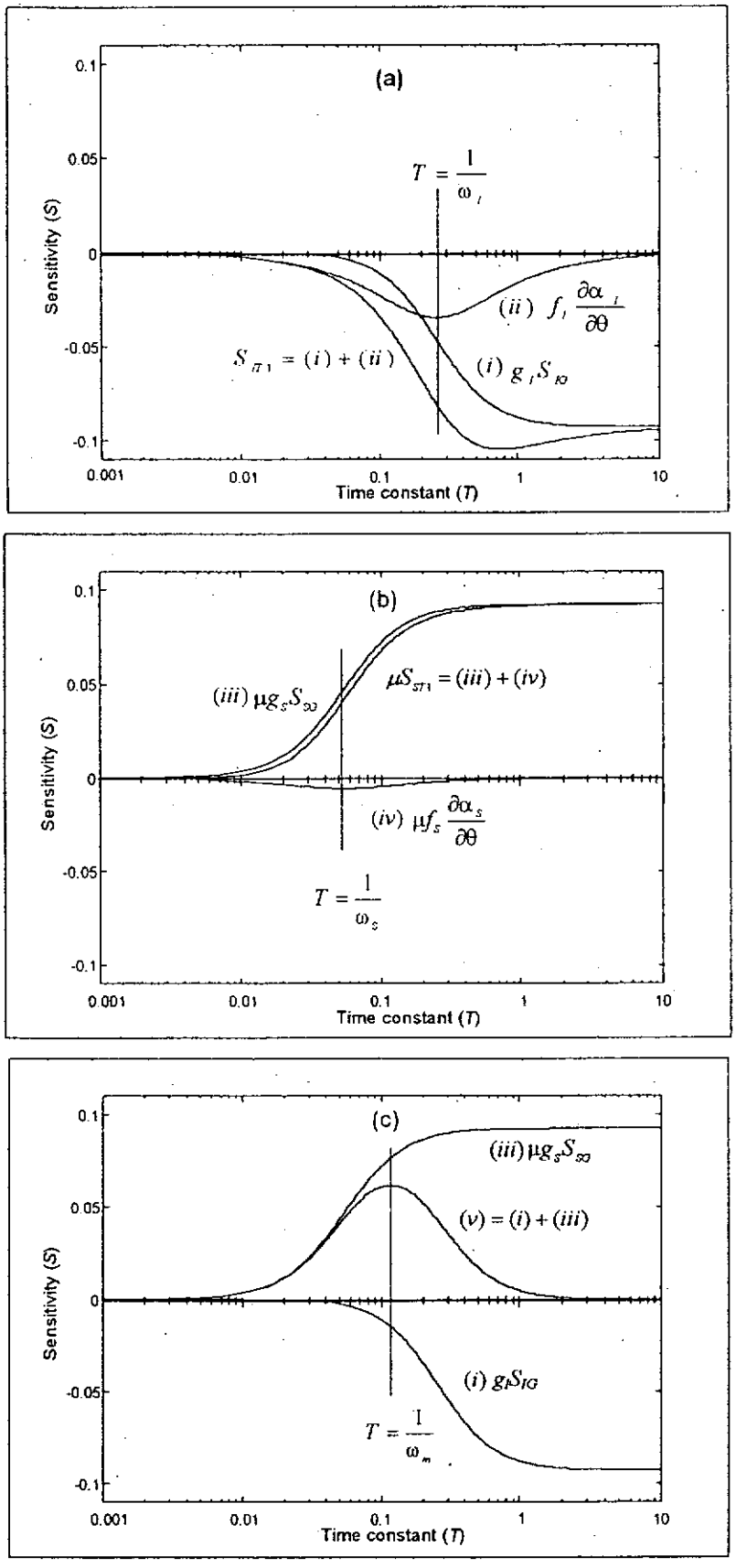

Fig. 4.6 Synthesis of time constant sensitivity coefficients

4.7 Summary

A systematic approach to select the location, damping signal and controller settings for an SVC is proposed. This design is implemented using (a) modal analysis of the machine-mode relationships for selecting the location and damping signal for SVC, and (b) eigenvalue sensitivity analysis to optimize the damping controller parameters. The criterion of optimality is to maximize the interarea mode damping while keeping a constant 9.5 dB gain margin for the SVC mode. Thus, by considering the controller effect on both modes at the same time, a combined sensitivity coefficient (CSC) is calculated, from which the desirable direction of change of each controller setting can be inferred. The controller settings are optimal when the CSCs of all the SVC parameters approach zero over a reasonably wide parameter range. As the CSC of the controller gain is always zero and that of the 'washout' time constant is invariably small, it turns out that the only tunable controller parameters are the time settings of the lead/lag stage. In the course of design optimization, G_d is continuously adjusted to ensure SVC mode stability. The synthesis results show that the controller design may run the risk of wrong compensation if the SVC instability is not considered.

The CSC technique developed is a strong tool for damping controller design while the controller gain increase will create another instability. Thus, the CSC technique can be extended to any FACTS controller design if a safe margin is required to avoid the controller instability.

CHAPTER 5

SVC CONTROL DESIGN BASED ON AN H_∞ ALGORITHM

5.1 Introduction

A combined sensitivity coefficient (CSC) controller based on the sensitivity analysis, which can improve the interarea mode with consideration of SVC mode instability, has been proposed in Chapter 4. However, the main weakness of this classical approach is that the design is based on a single operating point only, without consideration of the robustness of the system and cannot guarantee stability of a highly non-linear system such as a modern power system over a wide range of operating conditions.

Although some robust SVC designs are based on on-line tuning techniques such as adaptive [52], self-tuning [53] and an approach which combines fuzzy control and variable structure techniques [54], power utilities still prefer fixed-structure and fixed-parameter (FSFP) controllers due to limited confidence in on-line tuning schemes [55]. A robust FSFP controller which can enhance system damping over a wide range of operating conditions therefore is desirable.

H_∞ optimal robust control design has recently received increasing attention in power system engineering. The main advantage of this method is that model uncertainties can be accounted for at the design stage. The H_∞ optimization method has been successfully applied to SVC design but was either restricted to a weak radial system which neglected the dynamics of the generator [56] or employed a single-machine infinite bus system [57]. These designs based on the conventional H_∞ algorithm and direct application of these methods to SVC design will create the problems of uncertainty modeling restriction and unobservable modes due to pole-zero cancellation (see Section 5.4).

This chapter will use numerator-denominator perturbation uncertainty modeling and partial pole placement techniques to overcome these limitations (Section 5.5). Based on the 7-machine system in Fig. 3.5, an H_∞ damping controller for an SVC has been successfully designed by treating the dynamics of the SVC mode and noise of the thyristor switching as high frequency model uncertainties, and the change of system operating point as low frequency model uncertainties (Section 5.6). The performance of the H_∞ and the CSC controllers is compared in Section 5.6.5

5.2 Definition of H_∞ norm

The H_∞ norm of a stable transfer matrix *P(s)* is defined as

$$\|P(s)\|_\infty = \sup_{Re(s)>0} \bar{\sigma}[P(s)] = \sup_{\omega \in R} \bar{\sigma}[P(j\omega)] \tag{5.1}$$

where $\bar{\sigma}$ represents the maximum singular value and *sup* denotes the supremum or the least upper bound. Therefore, the H_∞ norm of *P(s)* can be found by first computing the largest singular value of the frequency response matrix *P(jω)* for each frequency, and then taking the maximum of all these largest singular values over frequency.

5.3 Conventional H_∞ mixed sensitivity optimization

Additive and multiplicative uncertainty representations are often used to model perturbed plant in the H_∞ approach. These perturbed plant (*P(s)*) models, with $W_3(s) = 0$ for the additive and $W_2(s) = 0$ for the multiplicative cases, are represented by

$$P(s) = (1 + \Delta_M(s) W_3(s)) P_0(s) + \Delta_A(s) W_2(s) \tag{5.2}$$

where $\Delta_A(s)$, $\Delta_M(s)$ are any frequency dependent functions such that $\|\Delta_A(s)\|_\infty \leq 1$ and $\|\Delta_M(s)\|_\infty \leq 1$, $W_2(s)$ and $W_3(s)$ represent the upper bound of the allowable additive and

multiplicative perturbations and $P_0(s)$ is the nominal plant. This is shown in Fig. 5.1 where ω and $K(s)$ represent a disturbance signal and the controller, respectively.

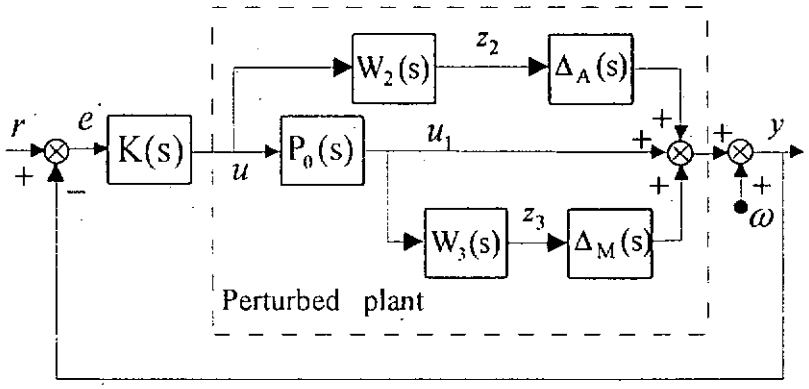

Fig. 5.1 Perturbed plant with additive and multiplicative uncertainty models

The transfer functions from r to e, u and u_1, for $W_3(s) = W_2(s) = 0$, are

$$S(s) = \frac{e}{r} = (1 + P_0(s)K(s))^{-1} \tag{5.3}$$

$$R(s) = \frac{u}{r} = K(s)(1 + P_0(s)K(s))^{-1} = K(s)S(s) \tag{5.4}$$

$$T(s) = \frac{u_1}{r} = P_0(s)K(s)(1 + P_0(s)K(s))^{-1} = 1 - S(s) \tag{5.5}$$

where $S(s)$, $R(s)$ and $T(s)$ are the sensitivity, related additive robustness and complementary sensitivity, of the closed-loop system, respectively.

The main objectives of the H_∞ approach are:

(i) to minimize the effect of disturbance

Disturbances are always concentrated in certain frequency bands. Minimizing the effects of the disturbance ω on the output y is equivalent to minimizing the H_∞ norm of the weighted sensitive function in (5.6).

$$\min\left\|W_1(s)S(s)\right\|_\infty \tag{5.6}$$

where the weighting function $W_1(s)$ is used to define the acceptable magnitude of output error in the presence of disturbances.

(ii) to maintain the stability of the system within the specified perturbations

Based on the small gain theorem [58], robust stability is achieved if and only if the H_∞ norm of the transfer function from ω to z ($z = z_2$ for additive uncertainties and z_3 for multiplicative uncertainties, see Fig. 5.1) is smaller than one, which is equivalent to the H_∞ norm of the transfer function from r to z. The condition for system stabilization in the presence of uncertainties $\Delta_A(s)W_2(s)$ or $\Delta_M(s)W_3(s)$ is, therefore, given by

$$\left\|W_2(s)R(s)\right\|_\infty < 1 \tag{5.7}$$

$$\left\|W_3(s)T(s)\right\|_\infty < 1 \tag{5.8}$$

where the weighting functions $W_2(s)$ and $W_3(s)$ are used to define the maximum perturbation of the nominal plant of additive and multiplicative type, respectively.

From the mixed sensitivity optimization formulation, the optimal H_∞ controller which minimizes the effects of disturbance on the plant output and guarantees the robustness of the plant can be obtained by minimizing J:

$$J = \left\| \begin{matrix} W_1(s)S(s) \\ W_2(s)R(s) \\ W_3(s)T(s) \end{matrix} \right\|_\infty \tag{5.9}$$

The process of J minimization can be achieved by solving two Riccati equations [59,60]. The controller so obtained will have the same order as the augmented plant shown in Fig. 5.2 and can stabilize all perturbed plant represented by (5.2) if the minimal value of $J \leq 1$.

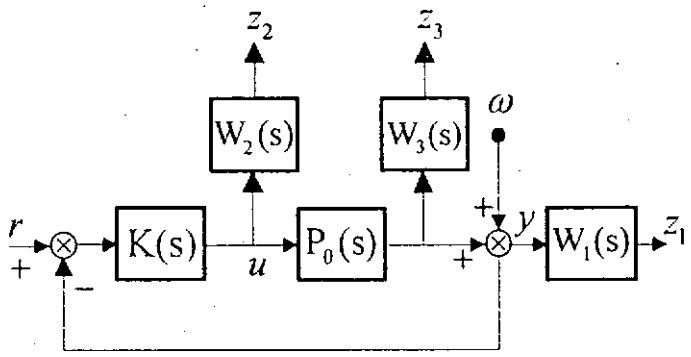

Fig. 5.2 The augmented plant with controller for the conventional H_∞ design method

5.4 Limitations of the conventional H_∞ approach

However, direct application of this method to design a damping controller has the following limitations:

i) Restrictive uncertainty modeling under stable/unstable transition:

The transfer functions $\Delta_A(s)$, $\Delta_M(s)$, $W_2(s)$ and $W_3(s)$ in (5.2) are assumed to be stable. Therefore, the perturbed plant will have the same number of the right-half plane (RHP) poles as the nominal plant. In other words, these models are unable to represent uncertainty when a nominal stable (unstable) plant becomes unstable (stable) after being perturbed [61]. Since stable poles of a power system can become unstable after being perturbed, especially for the oscillatory mode (e.g. interarea mode), this poses a problem.

ii) Unobservable modes due to pole-zero cancellation:

The closed-loop system poles of the designed controller and the nominal plant will include both the poles (stable) and the mirrored left-half plane (LHP) poles (unstable) of the nominal plant. If the nominal plant contains poorly damped modes, the poorly damped modes will be "canceled" by the zeros of the controller and become unobservable for the specified output. Consequently, improvements, if any, due to the controller cannot be recognized. Since the electromechanical mode of the power system

may be close to the imaginary axis, this pole-zero cancellation phenomenon is a serious limitation in damping controller design in the application of this method to power systems.

5.5 Modified H_∞ design methodology

The limitations discussed above can be overcome by the numerator-denominator perturbation representation (Section 5.5.1) and the partial pole placement technique (Section 5.5.2). A single-input single-output model is used for easy explanation but can be extended to multi-input multi-output systems.

5.5.1 Numerator-Denominator perturbation modeling

A plant with the transfer function ($P(s)$) can be written in fractional form as:

$$P(s) = \frac{N(s)}{D(s)} \tag{5.10}$$

The numerator-denominator perturbation model can represent as:

$$P(s) = \frac{N_0(s) + M(s)\Delta_N(s)W_2(s)}{D_0(s) + M(s)\Delta_D(s)W_1(s)} \tag{5.11}$$

where $N_0(s)$ and $D_0(s)$ are the numerator and the denominator of the nominal plant, $M(s)\Delta_N(s)W_2(s)$ and $M(s)\Delta_D(s)W_1(s)$ are the perturbation of the numerator and the denominator (see Fig. 5.3 where $W_1(s)$ and $W_2(s)$ are not to be confused with Fig. 5.2). $M(s)W_2(s)$ and $M(s)W_1(s)$ represent the largest possible perturbations of the numerator and denominator and the magnitude of $\Delta_N(s)$ and $\Delta_D(s)$ should not be greater than one.

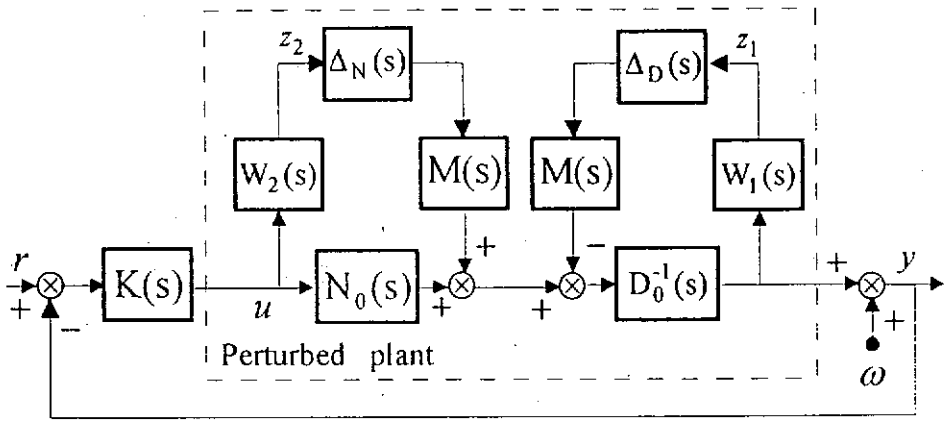

Fig. 5.3 Perturbed plant with numerator-denominator uncertainty model

Define $V(s) = D_0^{-1}(s)M(s)$, then the following inequalities can be obtained.

$$\frac{D(s) - D_0(s)}{D_0(s)} = V(s)\Delta_D(s)W_1(s) \le V(s)W_1(s) \tag{5.12a}$$

$$\frac{N(s) - N_0(s)}{N_0(s)} = \frac{V(s)\Delta_N(s)W_2(s)}{P_0(s)} \le \frac{V(s)W_2(s)}{P_0(s)} \tag{5.12b}$$

$V(s)$, $W_1(s)$ and $W_2(s)$ also represent the weighing functions of the augmented plant in Fig. 5.4 [62]. The use of $V(s)$ (for partial pole placement) becomes clear in Section 5.5.2. Based on this perturbation representation, the optimal H_∞ controller can be obtained by minimizing J:

$$J = \left\| \begin{matrix} W_1(s)S(s)V(s) \\ W_2(s)R(s)V(s) \end{matrix} \right\|_\infty \tag{5.13}$$

Therefore, it can be observed that nominal plant ($P_0(s)$) and perturbed plant ($P(s)$) in (5.11) do not need to have the same number of RHP poles. Hence, the limitation (i) of Section 5.4 is overcome.

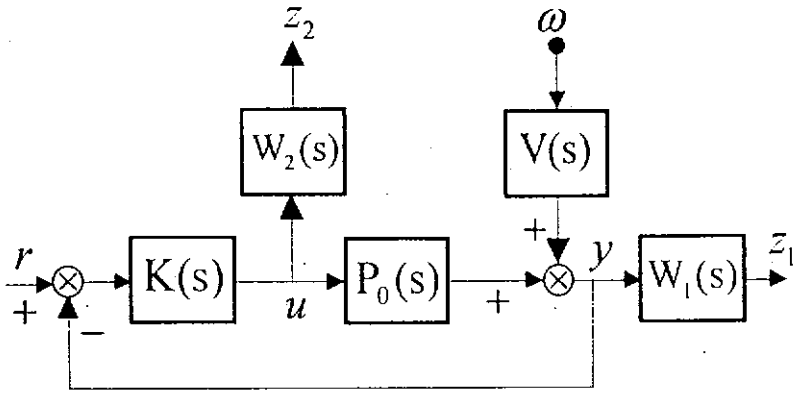

Fig. 5.4 The augmented plant with controller for the proposed H_∞ design method

5.5.2 Partial pole placement technique

From the solution to the mixed sensitivity problem (5.13), the following equalizing property can be obtained [63]:

$$|W_1(j\omega)S(j\omega)V(j\omega)|^2 + |W_2(j\omega)R(j\omega)V(j\omega)|^2 = \beta^2 \tag{5.14}$$

where β is a non-negative constant, implying that

$$\begin{aligned} &W_1(s)W_1(-s)S(s)S(-s)V(s)V(-s) \\ &+W_2(s)W_2(-s)K(s)K(-s)S(s)S(-s)V(s)V(-s) = \beta^2 \end{aligned} \tag{5.15}$$

The plant P, the controller K, the weighting functions W_1, W_2 and V are written in rational forms as

$$P = \frac{N}{D} \qquad W_1 = \frac{A_1}{B_1} \qquad W_2 = \frac{A_2}{B_2} \qquad V = \frac{M}{E} \qquad K = \frac{Y}{X}$$

where all numerators and denominators polynomials are in s-domain.

The sensitivity function S can be expressed as $S=DX/D_{cl}$ where $D_{cl}=DX+NY$ is the closed-loop characteristic polynomial of the feedback system.

By substituting S into (5.15),

$$\frac{D^{\sim}DM^{\sim}M(X^{\sim}XA_1^{\sim}A_1B_2^{\sim}B_2+Y^{\sim}YA_2^{\sim}A_2B_1^{\sim}B_1)}{D_{cl}^{\sim}D_{cl}E^{\sim}EB_1^{\sim}B_1B_2^{\sim}B_2}=\beta^2 \tag{5.16}$$

where if $F(s)$ is any polynomial function, $F^{\sim}$ is defined as $F^{\sim}(s)=F(-s)$.

Because the right hand side in (5.16) is constant, all factors in the numerator of the rational function on the left will cancel the corresponding factors in the denominator. Without loss of generality, M which has LHP roots only, cancels a factor in D_{cl} assuming no cancellations between $M^{\sim}M$ and $E^{\sim}EB_1^{\sim}B_1B_2^{\sim}B_2$. So, choosing M is equivalent to reassigning the open-loop poles (the roots of D) to the locations of the roots of M and this is the concept of partial pole-placement [62]. In particular, if V is not used and there is no cancellations between $D^{\sim}D$ and $B_1^{\sim}B_1B_2^{\sim}B_2$, $D^{\sim}D$ must be canceled by a factor of $D_{cl}^{\sim}D_{cl}$. Therefore, the closed-loop poles (the roots of D_{cl}) will include the stable roots of D and the mirrored LHP poles of the unstable roots of D. This explains why the open-loop poorly damped modes will reappear in the closed-loop system.

5.6 H_∞ based SVC damping controller design

5.6.1 System performance of different tieline flows

It has long been recognized that the most critical (interarea) mode in an interconnected system is due to the heavy tieline flow between areas [4]. In this study, variation of the tieline flow is, therefore, treated as the uncertainty for which a study of the robustness of the system is to be undertaken. The system performance for different tieline flows of the 7-

machine system in Chapter 4 is shown in Table 5.1. (The other electromechanical modes (2-6) in Table 4.4 are found to be quite robust to the tieline flow and are not shown for simplicity). Therefore, the H_∞ controller for an SVC installed at busbar 12 is required to improve the damping robustness of the system for this critical mode and provide a safety margin for the SVC mode similar to the CSC design.

Timeline flow (MW)	100	250	400
Interarea mode (mode 1)	$-0.29 \pm j4.03$	$-0.09 \pm j3.84$	$+0.12 \pm j3.50$
SVC mode	$-1.30 \pm j18.23$	$-1.32 \pm j18.61$	$-1.44 \pm j18.61$

Table 5.1 The interarea and SVC modes of the different open-loop operating conditions

5.6.2 Nominal power plant transfer function

The maximum transfer capacity of the double circuit tieline is 400MVA. The tieline flow of 250MW (same as Chapter 4), is taken as the nominal operating point and other flow conditions are regarded as perturbations of the nominal system. The transfer function of the nominal plant $P(s)$ (from ΔV_{ref} to 'damping signal' (i.e. ΔI_{TL}), see Fig. 4.2) can be obtained by the PMT (where the Laplace operator s now replaces the differential operator p) and the curve fitting method [55] is employed to reduce the plant. Firstly, $P''(s)$ in (5.17) is calculated.

$$P''(s) = EMO(s)P(s) \tag{5.17}$$

where $EMO(s)$ is a second order polynomial with the roots $-0.09 \pm j3.84$. Then the frequency response plot of $P''(s)$ is fitted by a low-order transfer function $P'''(s)$. Finally, the reduced order plant $P'(s)$ can be obtained as:

$$P'(s) = \frac{1}{EMO(s)} P'''(s) \tag{5.18}$$

In the present study, *P'(s)* in (5.19) has a good approximation of the original plant as shown in Fig. 5.5. The deviation due to plant reduction at high frequencies, the SVC mode dynamics and the noise of thyristor switching will be considered as high frequency uncertainties.

$$P'(s) = \frac{-5.734(s^2 + 0.585s + 24.276)(s + 2.234)}{(s^2 + 0.18s + 14.75)(s^2 + 0.96s + 39.88)} \tag{5.19}$$

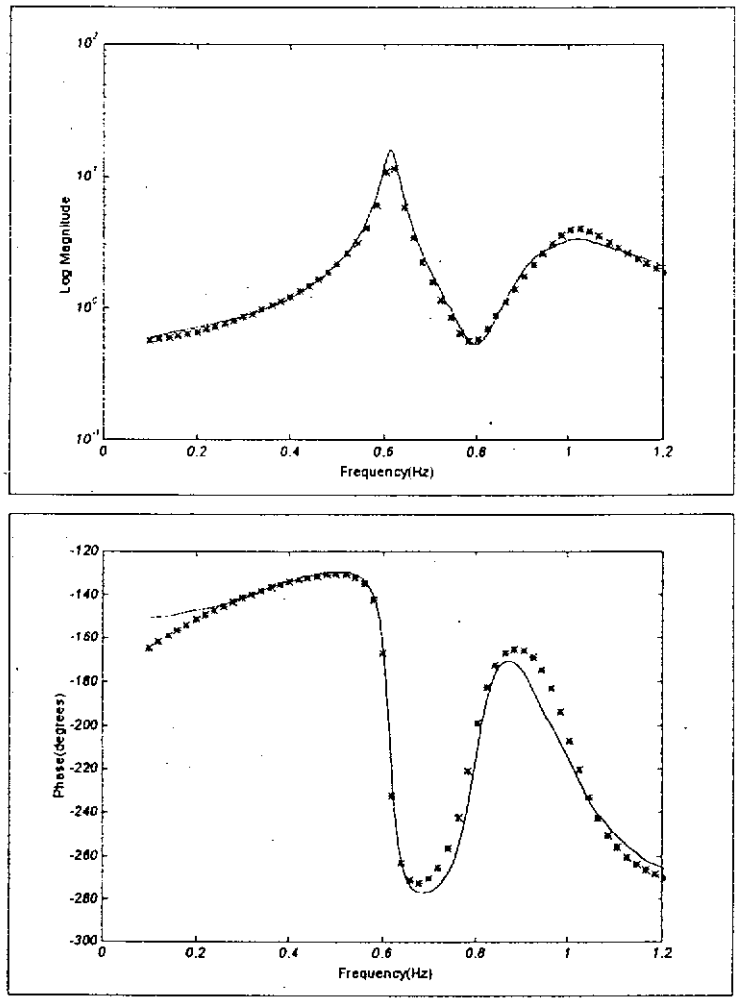

Fig. 5.5 Frequency response of the original plant *P(s)*-(solid line) and reduced plant *P'(s)*-(star line)

5.6.3 Selection of weighting functions

$V(s)$ is used for partial pole placement as mentioned in Section 5.5.2. In order to compare the robust performance of the two controllers, the damping ratio of the interarea mode of the H_∞ controller is set to be the same as that of the CSC controller (i.e. 10%). Therefore, the interarea mode originally at $(-0.09 \pm j3.84)$ should be relocated to $-0.39 \pm j3.84$.

$W_1(s)$ and $W_2(s)$ are chosen to fulfill the inequality of (5.12ab) mentioned before. Since disturbances usually occur in the low frequency range, $S(s)$ will be required to be small in this range. The larger the magnitude of weighting function $W_1(s)$, the smaller the sensitivity of the system to disturbances. So, a low pass filter $W_1(s)$ should be chosen to achieve the required disturbance attenuation. For good robustness against unmodeled dynamics (such as high frequencies noise due to thyristor switching, dynamics of the SVC mode and model deviations arising from plant reduction), $R(s)$ should be small at high frequencies. Therefore, a high pass filter $W_2(s)$ is used to ensure satisfactory performance of the closed-loop system at high frequencies.

The weighting functions $V(s)$, $W_1(s)$ and $W_2(s)$ are finalized to be:

$$V(s) = \frac{(s^2 + 0.78s + 14.90)(s^2 + 1.266s + 40.05)}{(s^2 + 0.18s + 14.75)(s^2 + 0.96s + 39.88)} \tag{5.20}$$

$$W_1(s) = 0.01\frac{s + 400}{s + 4} \tag{5.21}$$

$$W_2(s) = 0.3\frac{(s + 1)(0.01s + 1)}{(1.25s + 1)(0.08s + 1)} \tag{5.22}$$

5.6.4 Controller reduction

The H_∞ algorithm and the selected weighting function result in an 11th-order controller ($K(s)$). Applying the Optimal Hankel norm approximation [64], this high order controller is then reduced to a 5th-order approximation. With the additional washout stage (T_w = 7s), the proposed robust controller ($K'(s)$) is described by:

$$K'(s) = 0.428\frac{7s}{(1+7s)}\ \frac{(1+0.08s)(1+0.047s)(1+0.01s)(1+0.359s)}{(1+0.873s+0.2435s^2)(1+0.172s+0.02993s^2)(1+0.25s)} \qquad (5.23)$$

The frequency response of $K'(s)$ is shown in Fig. 5.6 where the phase deviation at very low frequency is due to the phase-lead property of the washout stage. The interarea mode is relocated from $-0.09 \pm j3.84$ to $-0.40 \pm j3.93$. The difference between the desired assigned location ($-0.39 \pm j3.84$) and actual assigned location ($-0.40 \pm j3.93$) is due to the approximations made in the plant model and the controller design.

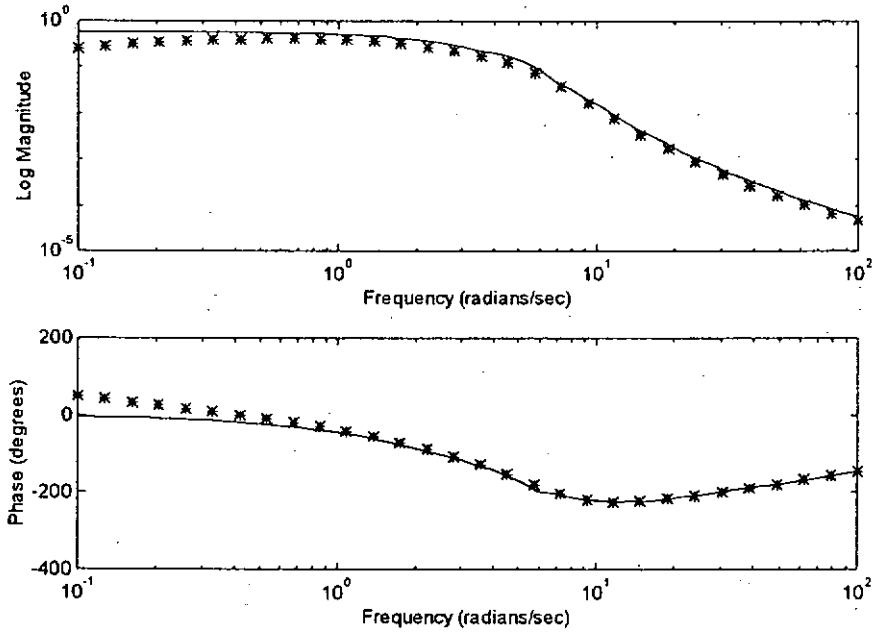

Fig. 5.6 Frequency response of the high order controller $K(s)$-

(solid line) and proposed controller $K'(s)$-(star line)

5.6.5 Controller performance comparison

The robustness of the two damping controllers is compared in Table 5.2 and 5.3. It is observed that both damping controllers will enhance the system damping. However, when the tieline flow is 400MW, the damping ratio for the H_∞ controller is 5.7% ($-0.20 \pm j3.53$) which is higher than 4.6% ($-0.17 \pm j3.71$) for the CSC controller. Moreover, the specified 9.5 dB safe margin at 250MW tieline flow for the CSC controller becomes 8.9dB and 6.7dB for the 100MW and 400MW flow. As for the H_∞ controller, the SVC mode is very robust and stable irrespective of the gain increase and theoretically the safety margin may be regarded as infinite in all the three cases.

	Tieline flow (MW)	100	250	400
H_∞ controller	Interarea mode	$-0.61 \pm j4.14$	$-0.40 \pm j3.93$	$-0.20 \pm j3.53$
	SVC mode	$-1.29 \pm j18.22$	$-1.32 \pm j18.60$	$-1.43 \pm j18.60$
CSC controller	Interarea mode	$-0.66 \pm j4.28$	$-0.41 \pm j4.08$	$-0.17 \pm j3.71$
	SVC mode	$-0.90 \pm j17.75$	$-0.98 \pm j18.01$	$-0.90 \pm j17.55$

Table 5.2 The interarea and SVC modes of the different closed-loop operating conditions

Tieline flow (MW)	100	250	400
H_∞ controller	∞	∞	∞
CSC controller	8.9	9.5	6.7

Table 5.3 Safe dB margin for the SVC mode

5.7 Summary

A new H_∞ based SVC damping controller design methodology is introduced in the present study. The proposed approach which uses the numerator-denominator representation and the partial pole placement technique is able to solve certain limitations of conventional H_∞ design techniques. The performance of the proposed controller is examined by varying tieline flows. It is superior to the CSC damping controller in terms of the robustness of the closed-loop system.

Although this H_∞ technique is applied only to SVC design in this chapter, it is suitable for other power system damping controller design in general. The advantage of this technique will be further discussed with the PSS design exercise in Chapter 6.

CHAPTER 6

PARTIAL POLE PLACEMENT OF H_∞ BASED PSS DESIGN USING NUMERATOR-DENOMINATOR PERTURBATION REPRESENTATION

6.1 Introduction

Recently the H_∞ algorithm has been used to design PSS controllers [55,65,66]. However, the direct application of the conventional H_∞ algorithm to PSS design has certain limitations:

i) certain uncertainty modeling restrictions,

ii) unobservable modes due to pole-zero cancellation,

iii) over-design and hence performance degradation of the controller.

Limitations (i) and (ii) have been solved in [65] but the controller becomes sub-optimal. Limitation (iii) is solved in [55] and [66], however, the uncertainty cannot be handled at the design stage [55] and the resulting non-minimum phase controller is unacceptable for practical applications because of stability problems. Moreover, several internal states of the system need to be used in the design stage which makes it difficult for practical implementation [66]. There is no satisfactory method to solve these limitations simultaneously.

Limitations (i) and (ii) occurred in the SVC design in Chapter 5 as well and were overcome by a method combining the numerator-denominator perturbation uncertainty representation and partial pole placement techniques. By introducing a new weighting function selection method, the method is further modified for the PSS design and solves the limitations (i)-(iii) successfully as explained in this chapter. Based on single and two machine systems, the proposed PSS design is proved to have better performance for a wide range of system

operating conditions than conventional PSS (CPSS) design which uses pole placement techniques [67].

6.2 Proposed approach of weighting function selection

Limitation of over-design and performance degradation of the controller

The main objective of a robust PSS is to provide adequate damping for oscillatory modes at different system operating conditions. Hence the main source of the "uncertainty" arises from the change of system operating conditions. However, in conventional H_∞ designs, the uncertainty model described by (5.2) will cover a wide range of system 'behaviours' having frequency responses, which cannot be achieved for a realistic power system. The mixed sensitivity optimization method is a compromise between the robustness and the performance deterioration. Stabilizing these unrealistic cases will degrade the performance of an actual power system. Furthermore, the conventional H_∞ method may not be able to deal with some practical constraints. For instance, gain restriction at high frequency for a $\Delta\Omega$-input PSS cannot be considered since the torsional mode is not detected in the model.

Referring to the augmented plant in Fig. 5.4, the solution to limitations (i) and (ii) has been discussed in Section 5.5. To overcome the limitation (iii) of the PSS design, a new method to select weighting functions $W_1(s)$ and $W_2(s)$ in Fig. 5.4 is proposed in this section. In this case, the weighting function $V(s)$ is still used for pole placement. $P_0(s)$ would be the nominal transfer function from the PSS output $\Delta Epss$ to the PSS input $\Delta\Omega$, and $K(s)$ is the transfer function of the PSS in Fig. 6.1.

Handling the uncertainty in a correct direction:

Weighting functions are used to guide the H_∞ design method to produce a robust controller that meets the specified performance. The weighting function $W_2(s)$ is used for robustness targeting as mentioned in Chapter 5 but it also acts as a penalty factor of the controller. A

high gain $W_2(s)$ results in low PSS gain. A suitable selection of the phase of $W_2(s)$ will guide the controller to handle the realistic plant and the uncertainty in correct direction. The transfer function from PSS output ($\Delta Epss$) to the component of the electrical torque (ΔPe_p), which can be controlled via excitation modulation, is defined as $GEP(s)$ in Fig. 6.1 [14]. In order to make ΔPe_p in phase with $\Delta\Omega$ and ensure positive damping torque, the PSS should provide a phase-lead so that it can compensate the phase-lag of $GEP(s)$. The phase of $GEP(s)$ can be obtained by the method discussed in Appendix 15. Since the electromechanical mode frequency ranges from 0.7 to 2Hz, $W_2(s)$ should provide sufficient phase-lag to penalize the PSS so that the final PSS design has sufficient phase-lead in this frequency range. However, if the PSS phase-lead is larger than the $GEP(s)$ phase-lag, it will produce, in addition to a damping component of torque, a negative synchronizing torque component [2]. In order to eliminate this desynchronizing effect, an undercompensation of about 10° will be provided in this frequency range. The phase of $W_2(s)$ is hence determined.

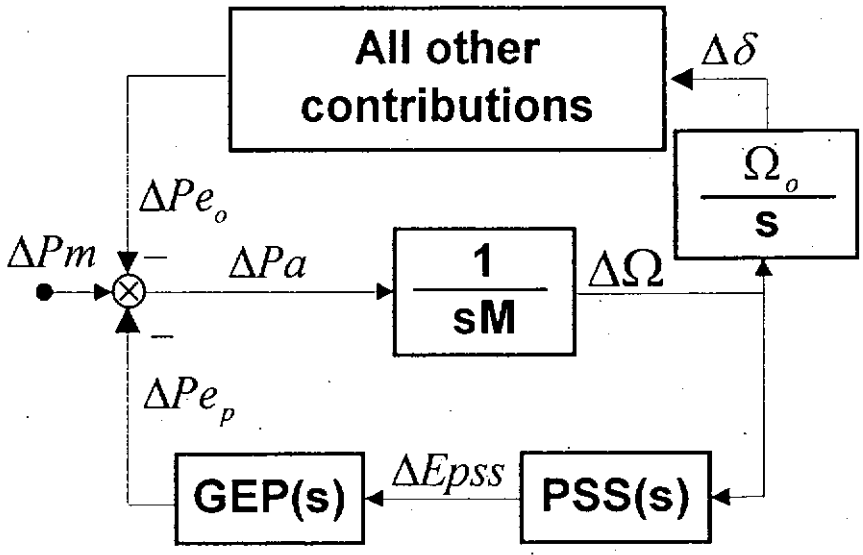

Fig. 6.1 Connection of $GEP(s)$ and PSS with shaft speed input

Handling the size of the uncertainty:

$W_1(s)$ and the gain of $W_2(s)$ are for robust stability. They should be chosen such that (5.12ab) is fulfilled.

Handling the special specification:

In order to prevent the interaction with the torsional mode, the high frequency (say above 7Hz) gain of the PSS can be suppressed by adjusting the high frequency gain of $W_2(s)$.

Because the selected weighing function already guides the controller to the correct direction, the designed controller may be incapable of making the unrealistic case of (5.11) stable and it may have completely different dynamic characteristic for the actual power system. This is the main reason why the penalty factor concept was introduced in [66] and the minimal value of J so obtained was much larger than unity. This fails to fulfill the requirements of the Small Gain Theorem [58] although the system is still stable and provides good performance. The requirement of minimal value of J less than unity is a sufficient condition only.

6.3 H_∞ based PSS design

6.3.1 Single machine infinite busbar system

6.3.1.1 Sixth-order machine system

The H_∞ design technique was first tested on a single machine system. The sixth-order machine model previously used for SVC design is once more used for the PSS design. Instead of plugging into the multimachine module described in (2.7), the machine model (Fig. A2.3) is plugged in an infinite bus network established in Appendix 16. Using the eigenvalue approach with the PMT and the system data provided in Appendix 17, the damping ratio for a wide range of operating conditions (with varying P, Q and X_e) is depicted graphically in Fig. 6.2. The overall performance of the original system (i.e. without PSS) is poor, especially when X_e is high and the load is heavy. A robust PSS (with shaft speed $\Delta\Omega$ as input signal) is therefore introduced to improve damping.

(a)

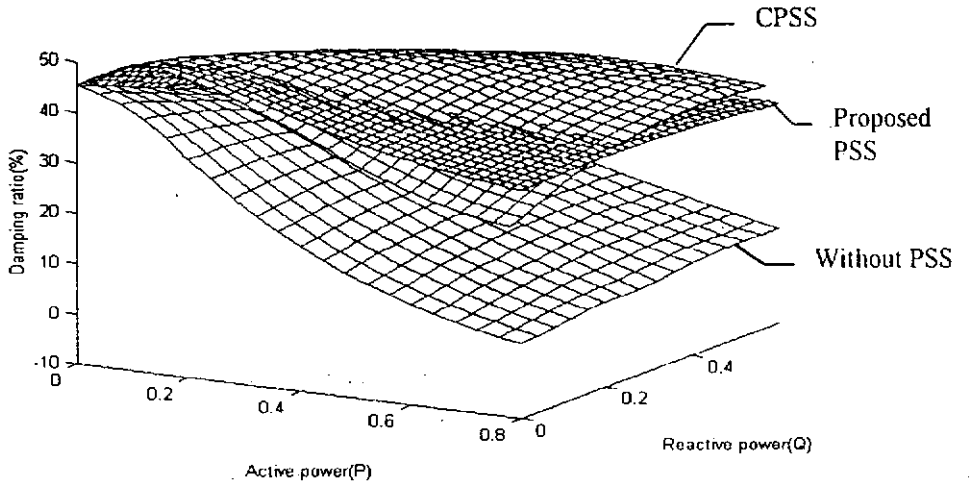

(b)

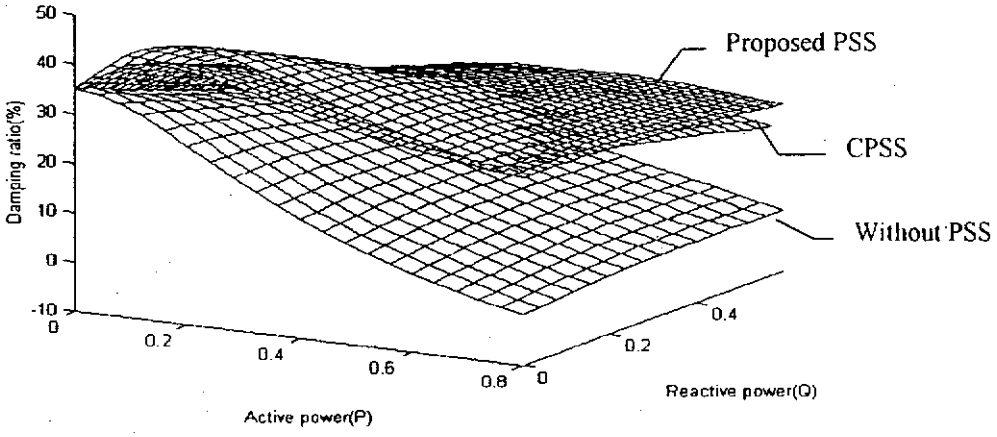

(c)

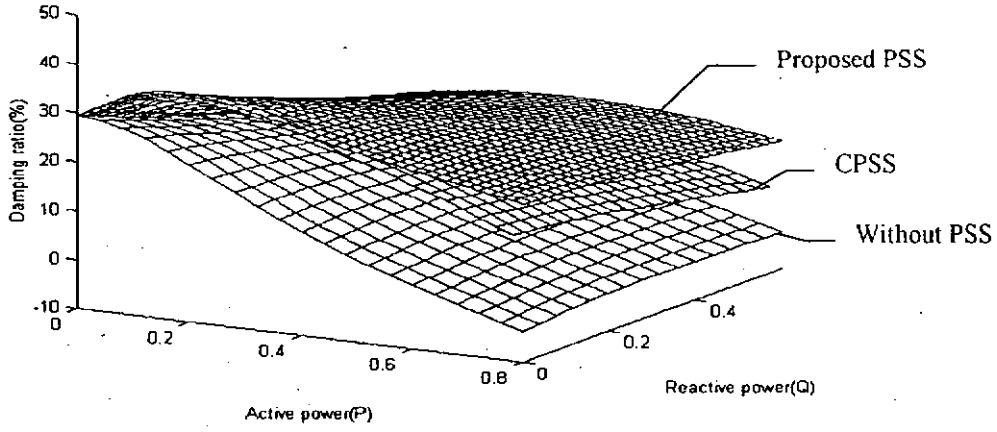

Fig. 6.2 Damping ratio of the electromechanical mode for

(a) $X_e = 0.3$ (b) $X_e = 0.5$ (c) $X_e = 0.7$

6.3.1.2 Nominal power plant transfer function

The nominal operating point is taken as P = 0.8pu, Q = 0.2pu, and X_e = 0.5pu and other operating points are regarded as perturbations of the nominal system. The transfer function of the nominal plant (from $\Delta Epss$ to $\Delta\Omega$) has been obtained as:

$$P(s) = \frac{-1320(s^2 + 21.9s + 122.45)(s+2)s}{(s^2 + 0.24s + 50)(s^2 + 22.89s + 136.28)(s+44.82)(s+22.13)(s+3.6)(s+1.8)} \quad (6.1)$$

The eigenvalues of the nominal system are shown in Table 6.1a. By the pole-zero cancellation, the plant can be reduced to $P'(s)$ in (6.2). The frequency response of the original plant and the reduced plant are similar as shown in Fig. 6.3.

$$P'(s) = \frac{-1320s}{(s^2 + 0.24s + 50)(s+44.82)(s+22.13)(s+3.6)} \quad (6.2)$$

(a) Open-loop system	(b) Closed-loop system
$-0.12 \pm j7.07$	$-2.02 \pm j7.04$
$-11.44 \pm j2.31$	$-11.57 \pm j2.23$
-1.8	$-17.08 \pm j15.14$
-3.6	$-48.42 \pm j27.64$
-22.13	-0.144
-44.82	-1.75
	-3.66
	-96.68

Table 6.1 Eigenvalues of the open-loop and closed-loop systems

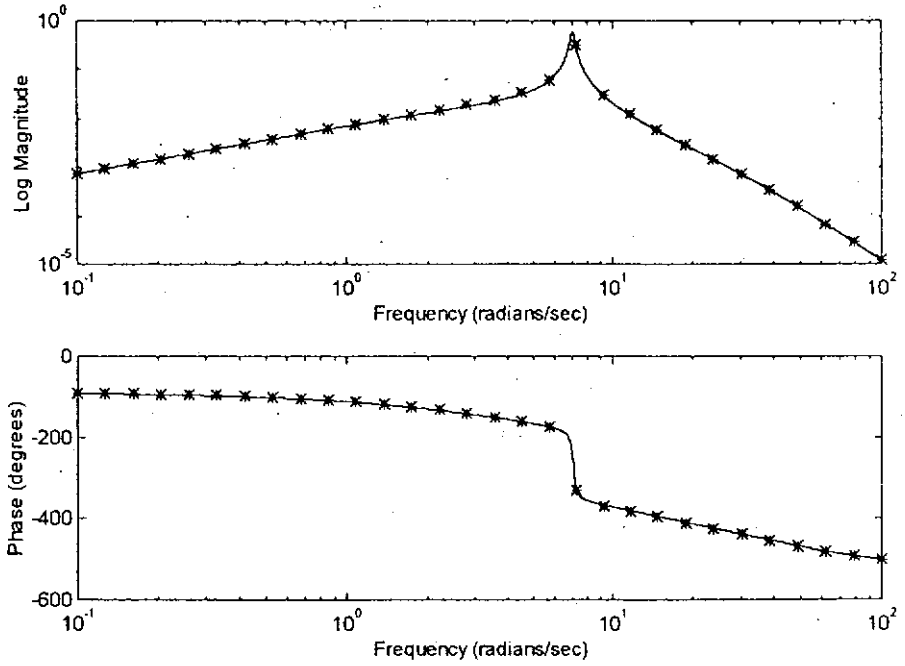

Fig. 6.3 Frequency response of the original plant *P(s)*-(solid line) and reduced plant *P'(s)*-(star line)

6.3.1.3 Selection of weighting functions

The *V(s)* function introduced in Section 5.5.2 is used for partial pole placement. Choosing 30% as the desired damping ratio, the electromechanical mode ($-0.12 \pm j7.07$) is relocated to $-2.22 \pm j7.07$. This can be achieved by selecting *V(s)* as

$$V(s) = \frac{(s^2 + 4.44s + 54.91)}{(s^2 + 0.24s + 50)} \tag{6.3}$$

Based on Fig. 6.4, it can be shown that $W_2(s)$ has to be a double phase-lag transfer function for sufficient compensation. However, to avoid torsional interaction and to fulfill the previously mentioned inequalities of (5.12ab), the weighting functions $W_1(s)$ and $W_2(s)$ as discussed in Section 6.2 would be

$$W_1(s) = 0.01\frac{s+400}{s+4} \tag{6.4}$$

$$W_2(s) = 0.1\frac{(0.015s+1)^2}{(0.15s+1)^2} \tag{6.5}$$

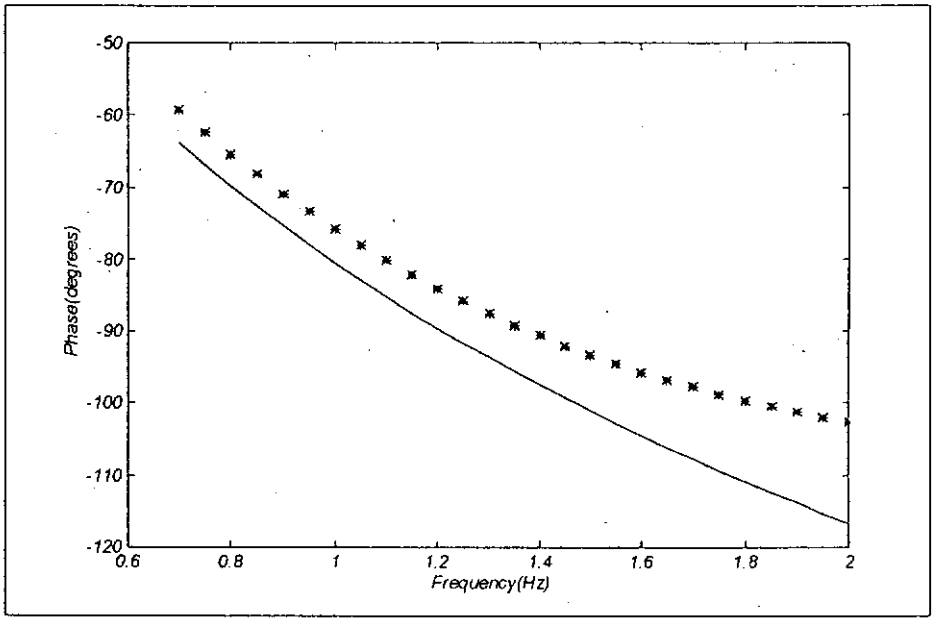

Fig. 6.4 Phase characteristic of *GEP(s)*-(solid line)and $W_2(s)$-(star line)

6.3.1.4 Controller reduction

Based on the H_∞ algorithm and using the above weighting function, the controller (*K(s)*) would be of 10th-order. Applying the Optimal Hankel norm approximation [64], this high order controller is then reduced to a 3rd-order approximation. Finally, the proposed robust controller (*K'(s)*) is described by:

$$K'(s) = -8.258\frac{7s}{(1+7s)}\ \frac{(1+0.0853s)(1+0.3023s)}{(1+0.0382s+0.0005396s^2)(1+0.0106s)} \tag{6.6}$$

where the washout stage with T_w = 7s is added to avoid DC offsets. The frequency response of *K'(s)* is shown in Fig. 6.5 where the phase deviation at very low frequencies is due to the phase-lead property of the washout stage. The closed-loop system poles of the power system and the proposed controller are shown in Table 6.1b. The electromechanical

mode is relocated from $-0.12 \pm j7.07$ to $-2.02 \pm j7.04$. The difference between the desired assigned location ($-2.22 \pm j7.07$) and actual assigned location ($-2.02 \pm j7.04$) is due to the approximations made in the plant model and the controller design.

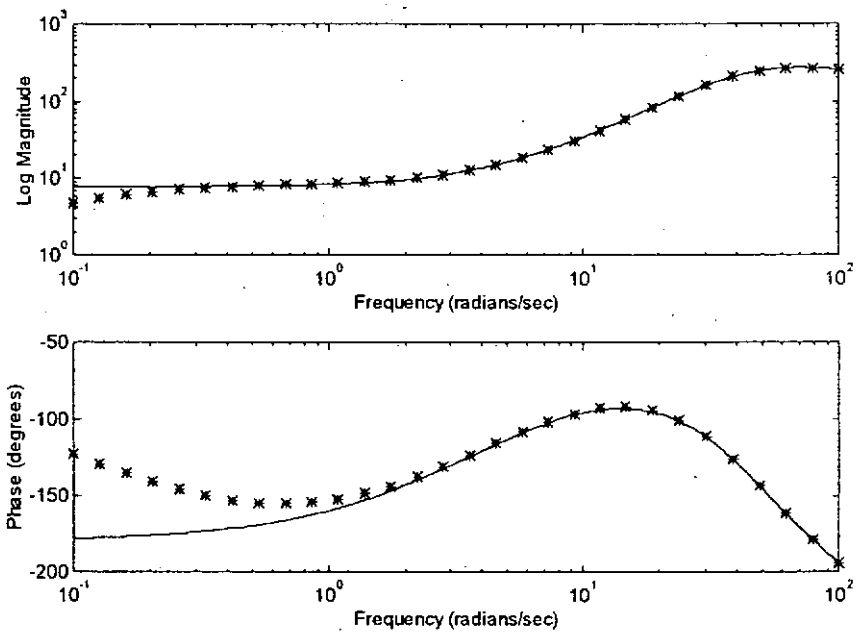

Fig. 6.5 Frequency response of the high order controller *K(s)*-(solid line) and proposed controller *K'(s)*-(star line)

6.3.1.5 PSS performance comparison

The robustness of this PSS is compared with a conventional PSS (CPSS) designed using pole assignment [67]. From Fig. 6.2, it is observed that both PSSs will enhance the system damping, in particular at heavy load when the original system was poorly damped or unstable. (The effect is not so obvious at light load when the system is already quite stable). However, at heavy loading conditions in the vicinity of $P_{rated} = 0.8$pu, $Q_{rated} = 0.6$pu for $X_e = 0.7$pu, the damping ratio for the CPSS case cannot reach the so-called acceptable level of 10% [11], whilst it is almost 20% for the proposed PSS. Indeed, the system damping ratio with the proposed PSS is well above 20% for most operating points.

6.3.2 Two machine system

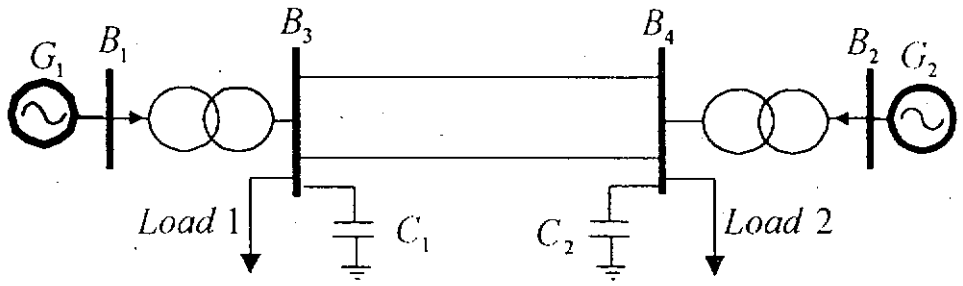

Fig. 6.6 System configuration

The PMT approach is next used to establish the two-machine and double circuit system in Fig. 6.6. The system data is provided in Appendix 19. It is assumed that the daily MW demand of Load 1 and 2 vary according to Fig. 6.7 and the MVAr demands are charactised by $Q_1 = (1+2*P_1)/4$ and $Q_2 = (1+2*P_2)/5$ [68]. The sharing of generation is allocated such that the tieline flow is 300MW, 250MW and 200MW during the peak, off-peak and light load of Load 2 respectively. Eigenvalues are computed and the damping ratio of the critical mode (interarea) is shown in Fig. 6.8. It is observed the damping ratio of the original system is low, and is even negative at heavy load at noon time.

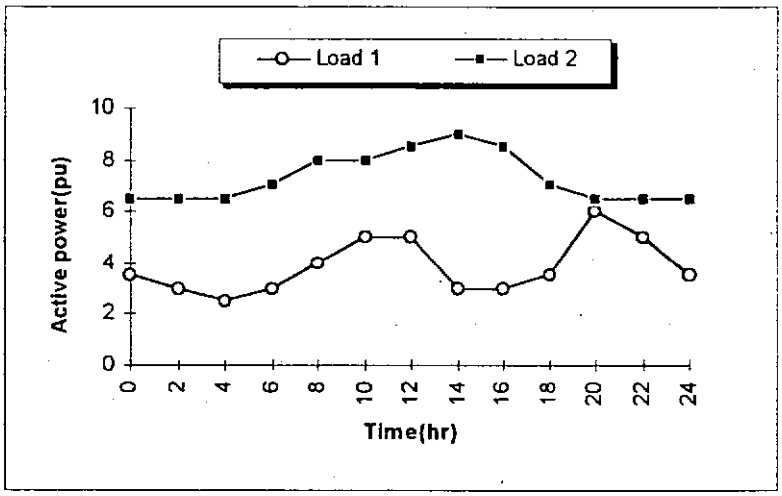

Fig. 6.7 Daily load demand curves

To improve system damping, the robust PSS to be installed at G_1 is designed by using techniques of the weighting function selection and controller reduction (similar to the

single-machine case) where the plant condition at zero hour was used as the nominal condition and the conditions at other hours are regarded as perturbations of the nominal plant. Again, the effectiveness of the two aforesaid PSSs are compared in Fig 6.8. It is noticed that although both PSSs enhance the system damping throughout the whole day, the damping ratio of the CPSS could not attain the 20% level when the load becomes heavy. It is also found that the damping ratio of the proposed PSS can be maintained above 20% under poorly damped conditions. This diagram, of course, is unable to represent the other advantages (i)-(iii) as discussed before.

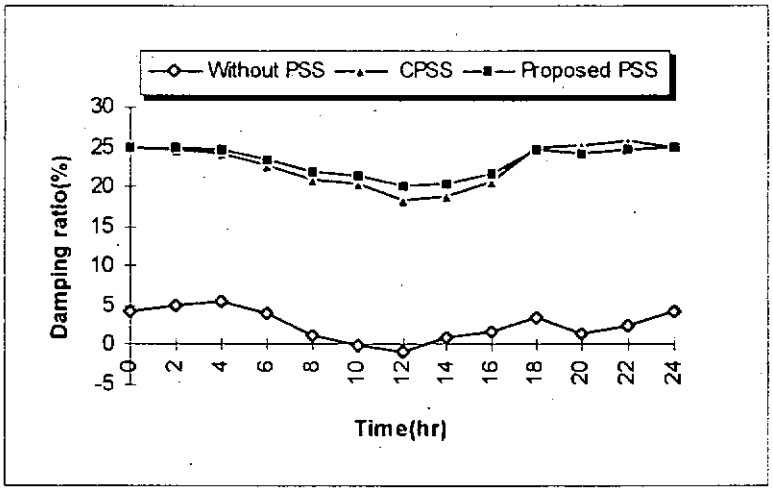

Fig. 6.8 Daily curve of the damping ratio

6.4 Summary

A new H_∞ design methodology is introduced in this chapter which is able to solve certain limitations of existing H_∞ PSS design techniques. The robust PSS is successfully designed by treating the change of system operating conditions as model uncertainty. System damping with the proposed controller is enhanced precisely at the conditions when such enhancement is useful. It is superior to the conventional PSS in terms of the robustness of the closed-loop system in respect of model uncertainties. This methodology can guarantee the stability of the closed-loop system with predefined uncertainties such as load variation and tieline flow variation. The design procedure has been fully discussed with a single machine case, and the technique is also illustrated for a two-machine system.

CHAPTER 7

CONCLUSIONS AND RECOMMENDATIONS

7.1 Conclusions

Power system instability imposes limitations on power system operation. The aim of this thesis is to advance the understanding of, and alleviate the stability problem in, multimachine systems.

A power system modeling method (Plug-in Modeling Technique) for small perturbation studies, which can accept any representation of system components together with associated control equipment of any desired degree of complexity, has been presented. Modular system components such as machine, SVC, TCSC, PS, HVDC link and tieline can be plugged into the network as additional modules. Instead of transforming control blocks to equations, component and network equations are transformed to two types of elementary blocks and these are then amalgamated with the control blocks. Based on this generalized approach, these elementary blocks of the entire system can be handled systematically, irrespective of the size and complexity of the multimachine system, so that the state space equations can be obtained and easily correlated with system parameters. This is an important contribution because the state space equations are available as an explicit function of every parameter, and the input and output signals can be any system variable. With the relative ease of integration with the eigenvector techniques, the multimachine analytical program developed is distinguished by the following features:

a) it can perform modal analysis on any variable,
b) eigenvalue sensitivity coefficients with respect to all block/system parameter can be directly obtained.

Based on extensive application of eigenvalues, modal and sensitivity analyses under both single and multi machine environment, a significant conclusion is that the stability limit is much extended by increasing the exciter gain, and theoretically the limit does not exist even for a small exciter gain. Therefore, this thesis will concentrate on oscillatory stability.

Tieline oscillation is an important and common problem as it restricts the power transfer between interconnected systems. Installing a damping controller to an SVC and using the tieflow as stabilizing signal have been accepted as an effective means to enhance interarea mode damping for power systems. However, the choice of controller gain is restricted by SVC mode oscillation. Although the SVC instability has been recognized by some researchers [44], it seems that the SVC constraint has so far not been quantitatively considered at the design stage. Based on the fuller exploitation of the eigenvector technique by the PMT, an improved design of the controller is attempted using

a) modal analysis investigation of the machine-mode relationship to show which machines are more liable to cause instability,
b) both modal and sensitivity analyses for selecting SVC location and damping signal,
c) sensitivity analysis to optimize controller parameters.

The criterion of optimality is to maximize the interarea mode damping while keeping a constant 9.5 dB gain margin for the SVC mode. Thus, by considering the controller effect on both modes at the same time, a combined sensitivity coefficient (CSC) is calculated, from which the desirable direction of change of each controller setting could be inferred. The setting is said to be optimal when the CSC with respect to all damping controller parameters approaches zero.

As the CSC of the controller gain constant is always zero and that of the 'washout' time constant is invariably small, it turns out that the only tunable controller parameters are the lead/lag time constants. Detailed synthesis of the CSCs shows that, the lead/lag design has to fulfill three objectives: to provide correct phase compensation for the interarea mode and the SVC mode, and to increase the controller gain by making use of different characteristics at the two mode frequencies. Hence, it is an important insight to conclude that a flexible

controller design structure should in general have three lead/lag stages of appropriated time constants. It is also shown that if the SVC mode constraint is ignored, tuning the lead/lag settings for interarea mode damping alone can actually lead to adjustment in the wrong direction.

However, the CSC approach can achieve the optimum design at one operating point only, similar to all classical methods, without consideration of the robustness the system. In order to enhance system stability over a wide range of operating conditions, an H_∞ based SVC is developed to increase the damping of the interarea mode. The numerator-denominator uncertainty representation and the partial pole placement technique are employed to solve the limitations of the conventional H_∞ design. The change of system operating conditions (e.g. tieline flow) and the dynamics of the SVC mode are treated as low and high frequency model uncertainties respectively, which are accounted for at the design stage. Case studies confirm that the H_∞ controller is more robust than the CSC controller regarding to the tieline oscillation and the SVC mode instability.

By extending this H_∞ algorithm to PSS design with a new weighting function selection method, an H_∞ PSS design methodology able to solve certain limitations of existing H_∞ PSS design techniques is proposed. The robust PSS is successfully designed by treating the change of system operating conditions as model uncertainty. System damping with the proposed controller is enhanced precisely at the conditions when such enhancement is useful. It is superior to the conventional PSS in terms of the robustness of the closed-loop system in respect of model uncertainties. This methodology can guarantee the stability of the closed-loop system with predefined uncertainties such as load variation and tieline flow variation. This is an important and new extension of H_∞ PSS designs.

Although these studies are confined to some typical systems for convenience of discussion, more complex systems can be dealt with in a similar way because of the versatility of the PMT.

7.2 Recommendations for future work

1 H_∞ algorithm has been applied to PSS design in single and two machine systems with consideration of the robustness of the load and tieline flow variations. In a multimachine system, the system operation variations become more complicated such as load characteristics and line/generator outages and are beyond the scope of the present research study. Examination of this more important and interesting aspect in the power stability studies should be continued.

2 The discussion in this thesis is confined to the case of installing a single controller in systems distinguished by one lightly damped (interarea mode). Attention should be given to developing multi-controller design methodologies as applied to general multi-area interconnected systems.

3 Voltage dependent load model has been used in the PMT. In order to have a more accurate simulation results, the load model could be elaborated to cater for frequency dependent characteristics and motor loads.

4 In this thesis, the location and damping signal of FACTS devices are selected by modal analysis for one operating point only. However, due to the increase of system stress, unusual load types and load distribution, the non-linearities of the system behaviour is more significant. The change of system operating points may affect the effectiveness of the selected location and damping signal. The selection of robust damping signals and location for different FACTS applications is an open research area.

REFERENCES

[1] C.P. Steinmetz, 'Power Control and Stability of Electric Generating Stations', *AIEE Trans.*, vol XXXIX, Part II, 1920, pp. 1215-1223

[2] P. Kundur, 'Power System Stability and Control', EPRI series, McGraw-Hill, Inc.

[3] P. Kundur, G.J. Rogers, D.Y. Wong, L. Wang and M.G. Lauby, 'A comprehensive computer program package for small signal stability analysis of power systems', *IEEE. Trans.*, 1990, PWRS-5, pp. 1076-1083

[4] P.M. Anderson and A.A. Fouad, 'Power system control and stability', Galgotia publications

[5] Task Force on Terms & Definitions: System Dynamic Performance Subcommittee, 'Proposed Terms & Definitions for Power System Stability', *IEEE Trans.* 1982, PAS-101, pp. 1894-1898

[6] W.G. Heffron and R.A. Phillips, "Effect of a Modern Amplidyne Voltage Regulator on Under- excited Operation of Large Turbine Generators", *AIEE*, 1952, Vol. 71, pp. 692-697

[7] W. Fairney and A. Myles, 'Low frequency oscillations on the 275kV interconnectors between Scotland and England', International Conference on Large High Voltage Electric Systems, paper 31-08, 1982 session, September

[8] R.L. Bolden, P.J. Wallage and A.W. Grainger, 'Considerations in the improvement of system damping on the South East Australian interconnected system', CIGRE, 1982, paper 31-05

[9] E.L. Busby, J.D. Hurley, F.W. Keay and C. Raczkowski, 'Dynamic stability improvement at Monticello station – analyical and field tests', *IEEE Trans.*, PAS-98, 1979, pp. 889-899

[10] C.K. Law, C.T. Tse and Y.B. Lee, 'Dynamic stability of the China Light and Power System', paper 4-06, *4th Conference on Electric Power Supply Industry*, Bangkok, 1982

[11] G.J. Lou, X.H. Xu, S.Q. Long and Q.C. Li, 'Low frequency oscillations on the interconnectors between Hong Kong and Guagndong', *Proc. of the Chinese Society of Electrical Engineering*, Vol. 6, Jan, 1998, pp. 29-35

[12] G.N. Taranto, 'Robust control design for power system damping controllers with application to FACTS devices', PhD thesis, Rensselaer Polytechnic Institute, December 1994

[13] P. DeMello and C. Concordia, 'Concepts of Synchronous Machine Stability as Affected by Excitation Control', *IEEE Trans.*, 1969, PAS-88, pp. 316-329

[14] E.V. Larsen and D.A. Swann, 'Applying power system stabilizers', *IEEE Trans.*, PAS-100, 1981, pp. 3017-3046

[15] A.T. Wilson, G.D. White, G.M. Breuer and R.L. Bolden, 'Investigation and control of the damping of power system oscillations', IFAC symposium 1997, Melbourne

[16] F.P. DeMello, L.N. Hannett and J.M. Undrill, "Practical approaches to supplementary stabilizing from accelerating power', *IEEE Trans*, PAS-97, 1987, pp. 1515-1522

[17] P. Kundur, D.L. Lee and H.M. Zein El-Din, "Power system stabiliziers for thermal units: Analytical techniques and on-site validation', *IEEE Trans*, PAS-1, 1981, pp. 81-95

[18] M. Klein, G.J. Rogers, S. Moorty and P. Kundur, "Analytical invertigation of factors influencing power system stabilizers performance', *IEEE Trans*, EC-3, 1992, pp. 382-390

[19] P. Kundur, M. Klein, G.J. Rogers and M.s. Zywno, "Application of power system stabilizers for enhancement of overall system stability', *IEEE Trans*, PWRS-2, 1989, pp. 614-626

[20] E.V. Larsen and J.H. Chow, 'SVC control concepts for system dynamic performance,' IEEE Tutorial Course: Applications of static var systems for system dynamic performance, paper 87 TH01875-5-PWR, pp. 36-53, 1987

[21] N. Martins and L.T.G. Lima, 'Determination of suitable locations for power system stabilizers and static var compensators for damping electromechanical oscillations in large scale power systems,' *IEEE Trans.*, PWRS-5, 1990, pp. 1455-1468

[22] H.A. Peterson and P.C. Krause, 'Damping of power swings in a Parallel AC and DC system,' *IEEE Trans.*, PAS-85, 1966, pp. 1231-1239

[23] R.L. Cresap and W.A. Mittelstadt, 'Small-signal modulation of the Pacific HVDC intertie,' *IEEE Trans.*, PAS-95, 1976, pp. 536-541

[24] R.T. Alden and H.M. Zein El-din, 'Multimachine dynamic stability simulations', *IEEE Trans.*, 1976, PAS-95, pp. 1529-1534

[25] Z. Erazaz and N.K. Sinha, 'Dynamic stability evaluation for multimachine system: an efficient eigenvalue approach', *IEE Proc. D. Control Theory & Appl.*, 1981, Vol. 128, No. 6, pp. 268-274

[26] G. Gross, C.F. Imparato and P.M. Look, 'A tool for the comprehensive analysis of power system dynamic stability', *IEEE Trans.*, 1982, PAS-101, pp. 226-234

[27] C.M. Lim and S. Elangovan, 'Design of stabilisers in multimachine power systems', *IEE Proc. C., Gen. Trans. & Distrib.*, 1985, Vol. 132, No. 3, pp. 146-153

[28] C.H. Cheng and Y.Y. Hsu, 'Damping of generator oscillations using an adaptive static var compensator', *IEEE Trans.*, 1992, PWRS-7, pp. 718-724

[29] K.S. Smith, L. Ran and J. Penman, 'Dynamic modeling of a unified power flow controller', *IEE Proc. C., Gen: Trans. Distrib.*, 1997, Vol. 144, No. 1, pp. 7-12

[30] H. Chen and G. Andersson, 'A versatile approach for the control of FACTS equipment in multimachine power systems', *Electrical Power & Energy Systems*, 1995, Vol. 17, No. 3, pp. 215-221

[31] C.T. Tse, K.L. Chan, S.L. Ho, C.Y. Chung, S.C. Chow and W.Y. Lo, 'Effective loadflow technique with non-constant MVA load for the Hong Kong Mass Transit Railway urban lines power distribution system', *Proc. of IEE 4th International Conference on Advances in Power System Control, Operation and Management*, Nov. 1997, Hong Kong, pp. 753-757

[32] R.H. Park, 'Two reaction theory of synchronous machines-Part I', *Trans., AIEE*, 1929, Vol 48, pp. 716-727 ; 'Part II' *Trans., AIEE*, Vol. 52, pp. 352-354

[33] IEEE Working Group, 'Static VAR compensator models for power flow and dynamic performance simulation', *IEEE Trans.*, 1994, PWRS-9, pp. 229-240

[34] The Math Works Inc. 'User's guide for Simulink/Matlab'

[35] IEEE Committee Report, 'Excitation system models for power system stability studies', *IEEE Trans.*, 1981, PAS-100, pp. 494-509

[36] J.E. Vanness, 'Improving reduced dynamic models of power systems', 1997, *PICA Conference Proceedings*, pp. 155-157

[37] Y.Y. Hsu and C.L. Chen, 'Identification of optimum location for stabiliser applications using participation factors', *IEE Proc. C, Gen. Trans. & Distrib.*, 1985, Vol. 134, No. 3, pp. 238-244

[38] J.E. Vanness, J.M. Boyle and F.P. Imad, 'Sensitivities of large, multiple-loop control systems', *IEEE Trans.*, 1965, AC-10, pp. 308-315.

[39] C.T. Tse, W.L. Chan and C.Y. Chung, 'Refinement of Concept on Steady State Stability Limit,' *Proc. IEE 417, International Conference on Advances in Power System Control, Operation and Management*, Nov. 1995, pp. 583-589.

[40] C.Y. Chung, K.W. Wang, C.T. Tse, C.K. Cheung and A.K. David, 'Machine and load modeling in large scale power industries', *Dynamic modeling control applications for industry workshop*, *IEEE* industry applications society, April 1998, pp. 7-15

[41] C.T. Tse and S.K. Tso, 'Refinement of Conventional PSS Design in Multimachine System by Modal Analysis', *IEEE Trans.*, 1993, PWRS-8, pp. 598-605.

[42] S.E.M. de Oliveira, 'Synchronizing and damping torque coefficients and power system steady-state stability as affected by static var compensators', *IEEE Trans.*, 1994, PWRS-9, pp.109-119

[43] R.L. Hauth, I. Humann and R.J. Newell, 'Application of a static var system to regulate system voltage in western Nebraska', *IEEE Trans.*, 1978, PAS-97, pp.1955-1964

[44] A.J.P. Ramos and H. Tyll, 'Dynamic performance of a radial weak power system with multiple static var compensators', *IEEE Trans.*, 1989, PWRS-4, pp. 1316-1325

[45] M.E. El-Hawary and L.G. Dias, 'Bus sensitivity to model parameters load-flow studies', *IEE Proc. C, Gen. Trans. Distrib.*, 1987, Vol. 134, No. 1, pp. 302-305

[46] C.Y. Chung, C.T. Tse and A.K. David, 'New load flow technique based on load transfer and load buses elimination', *Proc. of IEE 4th International Conference on Advances in Power System Control, Operation and Management*, Nov. 1997, Hong Kong, pp. 614-619

[47] F.P. DeMello, P.J. Nolan, T.F. Laskowski and J.M. Undrill, 'Coordinated application of stabilizer in multimachine power systems', *IEEE Trans.*, 1980, PAS-99, pp. 892-901

[48] B. Porter, 'Modal control theory and applications', Taylor and Francis Ltd, 1972

[49] Western systems coordinating council test procedures task force: 'Test procedure for power system stabilizers', July, 1976

[50] R.G. Farmer and B.L. Agrawal, 'State-of-the-art technique for power system stabilizer tuning', *IEEE Trans.*, 1983, PAS-102, pp. 699-707

[51] C.T. Tse, and S.K. Tso, 'Design optimisation of power system stabilisers based on modal and eigenvalue-sensitivity analyses', *IEE Proc. C, Gen. Trans. Distrib.*, 1988, Vol. 135, No. 5, pp. 406-415

[52] J.R. Simth, D.A. Pierre, D.A. Rudbery, I. Sadighi and A.P. Johnson, 'An enhanced LQ adaptive VAR unit controller for power system damping', *IEEE Trans.*, 1989, PWRS-4, pp. 443-451

[53] W. Li, 'A comparative study of damping schemes on damping generator oscillations', *IEEE Trans.*, 1993, PWRS-8, pp. 613-619

[54] P.K. Dash, S. Mishra and A.C. Liew, 'Fuzzy-logic-based VAR stabiliser for power system control', *IEE Proc. C., Gen. Trans. & Distrib.*, 1995, Vol 142, No. 3, pp. 618-624

[55] Yang, T.C., 'Applying H_∞ optimization method to power system stabilizer design, Part I and II', *Electrical Power & Energy Systems*, 1997, Vol.19, No. 1, pp.29-43

[56] M. Parniani and M.R. Iravani, 'Optimal robust control design of static VAR compensators', *IEE Proc. C., Gen. Trans. & Distrib.*, 1998 Vol 145 No. 3, pp. 301-307

[57] W. Li and H.T. Ming, 'Design of a H_∞ static var controller for the damping of generator oscillations', *International conference on Power System Technology, POWERCON'98*, August, 1998, Beijing, China, pp.785-789

[58] C.A. Desoer and M. Vidyasagar, 'Feedback systems: Input-Output properties', Academic Press, New York

[59] B.A. Francis, 'A course in H_∞ control theory', Lecture notes in Control and Information Sciences, Springer-Verlag, 1987

[60] R.Y. Chiang and M.G. Safonov, 'Robust Control Toolbox', Matlab User's Guide, 1981

[61] D.W.C. Ho, J. Lam and T.W.K. Chan, 'Mixed H_∞ optimization with model-matching', *IEE Proc. Control Theory Appl*, Vol.141, No. 5, 1994, pp.329-340

[62] H. Kwakernaak, 'Robust control and H_∞ optimization', Automatica, 1993, 29(2), 255-273

[63] H. Kwakernaak, 'Minimax frequency domain performance and robustness optimization of linear feedback systems', *IEEE Trans. Aut. Control*, AC-30, pp.994-1004

[64] K. Glover, 'All optimal Hankel norm approximation of linear multivariable systems and their L^∞-Error bounds', *Int. J. Control*, 1984, Vol. 39, pp. 1145-1193

[65] K.A. Folly, Y. Naoto and S. Hiroshi, 'Design of H_∞-PSS using numerator-denominator uncertainty representation', *IEEE Trans.* on Energy Conversion, 1996, Vol.19, No. 1, pp.29-43

[66] J.H. Chow, J.P. Harris, M.A. Kale, H.A. Othman, J.J. Sanchez-Gasca, and G.E. Terwilliger, 'Robust control design of power system stabilizers using multivariable frequency domain techniques', *Proc. 29th IEEE Conf. on Decision and control*, December 1990

[67] S. Bahram, 'Control system design using Matlab', Prentice Hall 1993

[68] K.W. Wang, C.T. Tse, K.M. Tsang, 'Algorithm for Power System Dynamic Stability Studies Taking Account the Variation of Load Power', *Proc. of IEE 4th International Conference on Advances in Power System Control, Operation and Management*, Nov. 1997, Hong Kong, pp.445-450

[69] R.A. Decarlo and R. Saeks, 'Interconnected dynamical systems', Marcel Dekker, New York, 1981, pp. 53-60

[70] B.C. Kuo, 'Automatic control systems', Prentice Hall, 1976, pp. 102-104

APPENDIX 1

THIRD ORDER MACHINE EQUATION

The 3rd-order machine equations in Park's *dq* frame [32] are

$$pE_q' = [E_{fd} - (X_d - X_d')I_d - E_q']/T_{do}' \quad \text{(A1.1a)}$$

$$p\delta/\Omega_0 = \Omega - \Omega_{ref} \quad \text{(A1.1b)}$$

$$p\Omega = [P_m - P_e]/M \quad \text{(A1.1c)}$$

$$V_t^2 = V_d^2 + V_q^2 \quad \text{(A1.1d)}$$

$$V_d = -R_a I_d + X_q I_q \quad \text{(A1.1e)}$$

$$V_q = E_q' - X_d' I_d - R_a I_q \quad \text{(A1.1f)}$$

$$P_e = V_q I_q + V_d I_d + (I_d^2 + I_q^2)R_a \quad \text{(A1.1g)}$$

and in small perturbation form,

$$\Delta E_q' = [\Delta E_{fd} - (X_d - X_d')\Delta I_d]/(1 + pT_{do}') \quad \text{(A1.2a)}$$

$$\Delta\delta = \Omega_0[\Delta\Omega - \Delta\Omega_{ref}]/p \quad \text{(A1.2b)}$$

$$\Delta\Omega = (\Delta P_m - \Delta P_e)/pM \quad \text{(A1.2c)}$$

$$\Delta V_t = V_d\Delta V_d/V_t + V_q\Delta V_q/V_t \quad \text{(A1.2d)}$$

$$\Delta V_d = -R_a\Delta I_d + X_q\Delta I_q \quad \text{(A1.2e)}$$

$$\Delta V_q = \Delta E_q' - X_d'\Delta I_d - R_a\Delta I_q \quad \text{(A1.2f)}$$

$$\Delta P_e = (V_q + 2R_a I_q)\Delta I_q + I_q\Delta V_q + (V_d + 2R_a I_d)\Delta I_d + I_d\Delta V_d \quad \text{(A1.2g)}$$

APPENDIX 2

BLOCK DIAGRAM OF DIFFERENT ORDER MACHINES

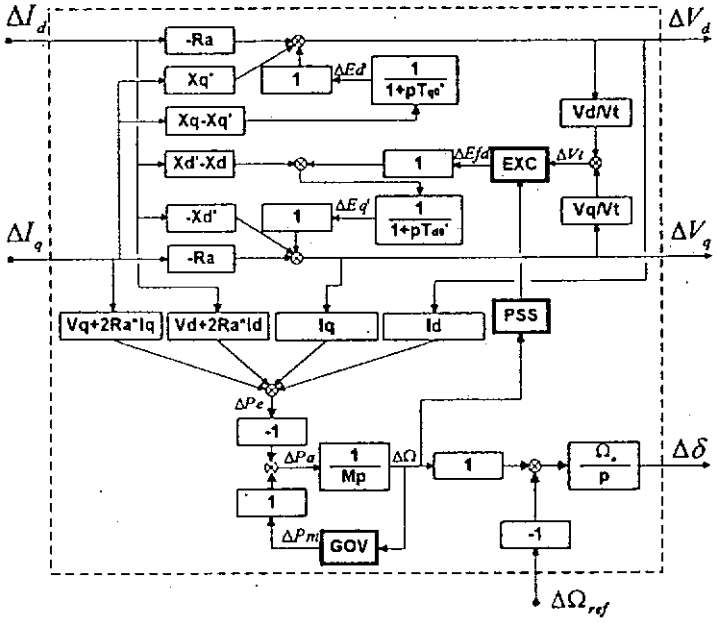

Fig. A2.1 Fourth order machine module

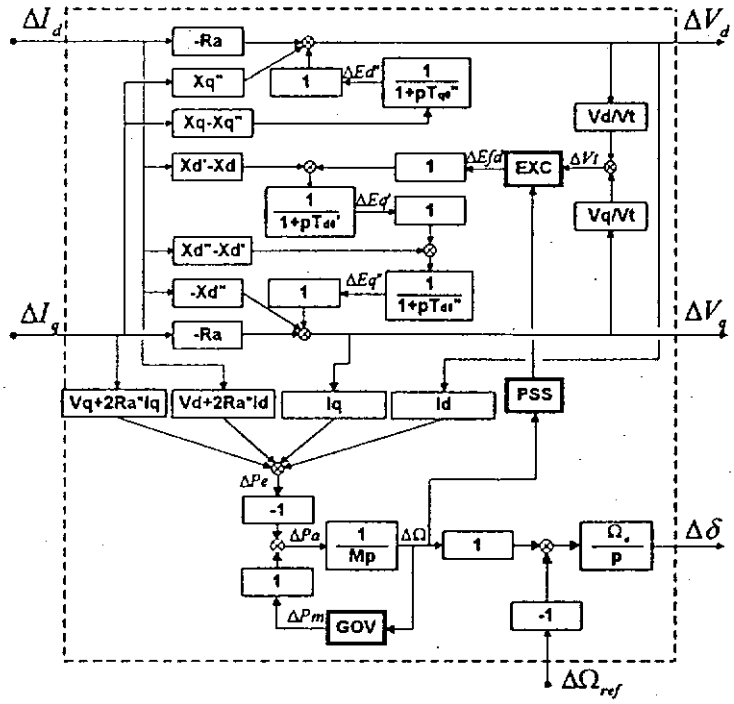

Fig. A2.2 Fifth order machine module

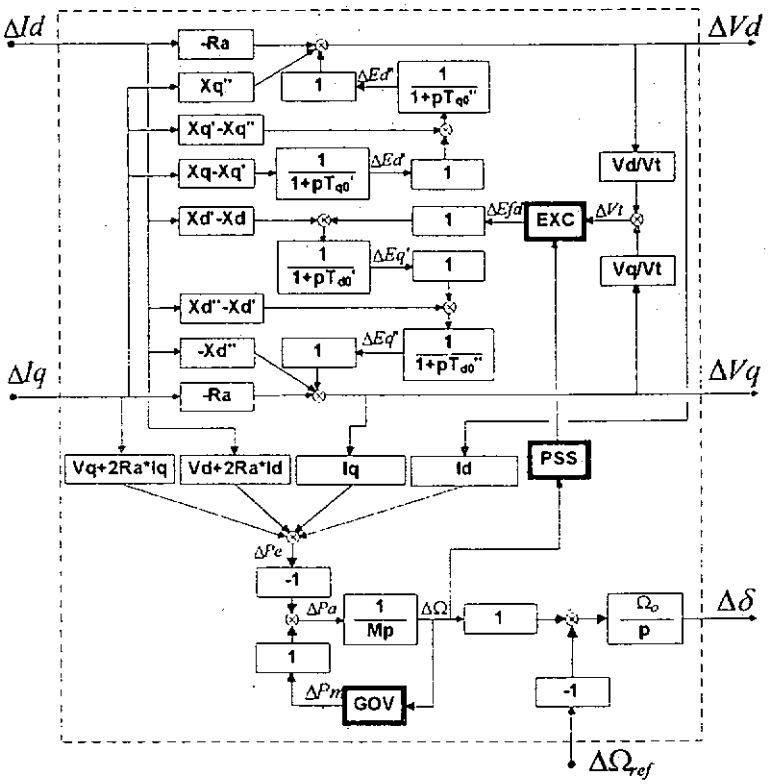

Fig. A2.3 Sixth order machine module

APPENDIX 3

EFECT OF LOAD AND MACHINE MODELING

When machines and loads are represented by a third order model and constant admittances, the eigenvalues of the six electromechanical modes for the 7-machine system (Fig. 3.5) have been calculated and given in Table A3.1.

Modes	α	ω
1	+0.18	3.60
2	−0.09	5.37
3	+0.04	5.76
4	−0.27	5.88
5	−0.24	6.09
6	−0.27	7.48

Table A3.1 Electromechanical modes ($\lambda = \alpha \pm j\omega$) for 3rd-order machine and constant admittance load models

Load is regarded as constant admittance with (a,b) of equation (2.1) = (2,2) in the table. Alternative load models are constant current for (a,b) = (1,1), or constant MVA for (a,b) = (0,0). In the present studies, the boundary of (a,b) variation is restricted to (0,0) (0,2) (2,0) and (2,2) in the illustrations of Fig. A3.1.

For the mode 1 (interarea), the eigenvalue will change from $+0.18 \pm j3.60$ to $+0.12 \pm j3.17$ if the constant admittance load is replaced by constant MVA load. When different machine model is used, the eigenvalue will be different. For instance, using order six for the machine and (a,b) = (2,0) for load, the unstable eigenvalue will become stable. As for the other modes, the effect of machine model variation is more significant than that of the load. As a conclusion, appropriate load/machine modeling is vital to reliable and accurate stability studies.

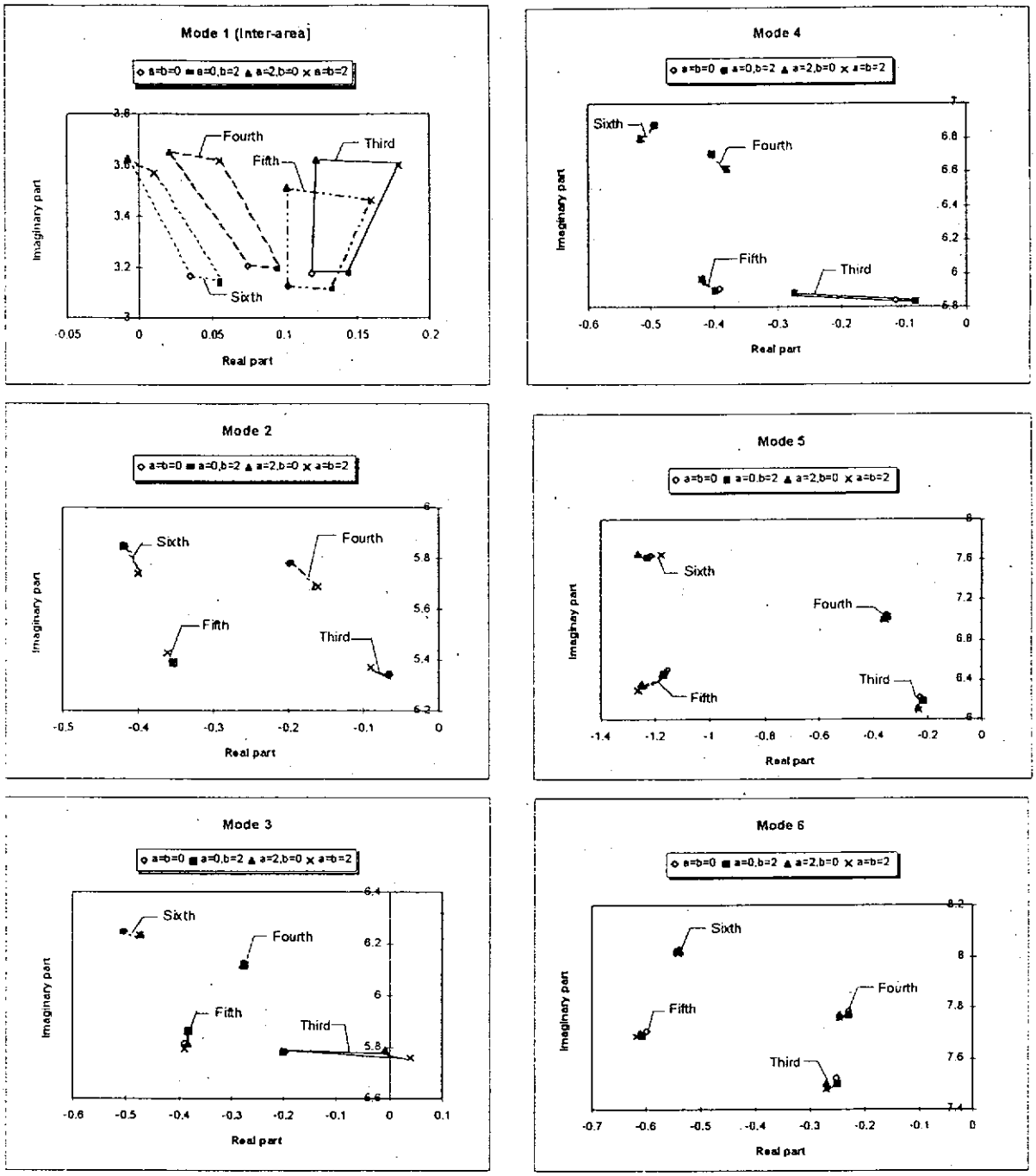

Fig. A3.1 The effect of a and b values (see equation (2.1)) and machine model orders of different electromechanical modes (Different axis-scales have been used for different modes)

APPENDIX 4

FORMATION OF STATE SPACE EQUATION

In the PMT, there are two types of blocks as shown in Fig. 2.11. An example of connection of a four-block system is shown in Fig. A5.1 of Appendix 5. Generalizing this to all the system blocks, a connection or L-matrix can be constructed as:

$$\begin{bmatrix} X_i \\ Y \\ M_i \end{bmatrix} = \begin{bmatrix} L_1 & L_2 & L_3 \\ L_4 & L_5 & L_6 \\ L_7' & L_8' & L_9' \end{bmatrix} \begin{bmatrix} X \\ R \\ M \end{bmatrix} \tag{A4.1a}$$

(A4.1b)

(A4.1c)

where $\boldsymbol{X}_i$, $\boldsymbol{X}$, $\boldsymbol{M}_i$ and $\boldsymbol{M}$ are vectors collecting all the x_i, x, m_i and m variables of Fig. 2.11, and $\boldsymbol{R}$ and $\boldsymbol{Y}$ are the input and output vectors. As the equation of the nth zero order block is $m_n = k_n m_{i_n}$, the matrix equation for *all* zero order blocks will be

$$\boldsymbol{M} = \boldsymbol{K}\boldsymbol{M}_i \tag{A4.2}$$

where $\boldsymbol{K} = < k_n > \tag{A4.3}$

= diagonal matrix of k_n, n = 1,2,....

Similarly, the equation of the first order block is

$$x_n = x_{i_n}\left(b_n + pT_{b_n}\right)/\left(a_n + pT_{a_n}\right) \tag{A4.4}$$

Expanding (A4.4), the equation for all the first order blocks is

$$\dot{\boldsymbol{X}} = -\boldsymbol{K}_a\boldsymbol{X} + \boldsymbol{K}_b\boldsymbol{X}_i + \boldsymbol{K}_t\dot{\boldsymbol{X}}_i \tag{A4.5}$$

where $\boldsymbol{K}_a = < k_{a_n} > = < a_n/T_{a_n} > \tag{A4.6a}$

$\boldsymbol{K}_b = < k_{b_n} > = < b_n/T_{a_n} > \tag{A4.6b}$

and $\boldsymbol{K}_t = < k_{t_n} > = < T_{b_n}/T_{a_n} > \tag{A4.6c}$

are diagonal matrices (n = 1,2,...).

The state space equation can be constructed from (A4.1), (A4.2) and (A4.3) by eliminating M_i, M and X_i from (A4.1). Therefore,

$$Y = CX + DR \tag{2.21}$$

where $C = L_4 + L_6HL_7$

$D = L_5 + L_6HL_8$

$H = (I - L_9)^{-1}$

I = identity matrix

and $L_i = KL_i'$ for i = 7,8 and 9.

$$\dot{X} = AX + BR + E\dot{R} \tag{2.20}$$

where $A = S(K_bF - K_a)$ (A4.7)

$B = SK_bG$

$E = SK_iG$

$S = (I - K_iF)^{-1}$ (A4.8)

$F = L_1 + L_3HL_7$ (A4.9)

and $G = L_2 + L_3HL_8$

APPENDIX 5

FORMATION OF THE L-MATRIX

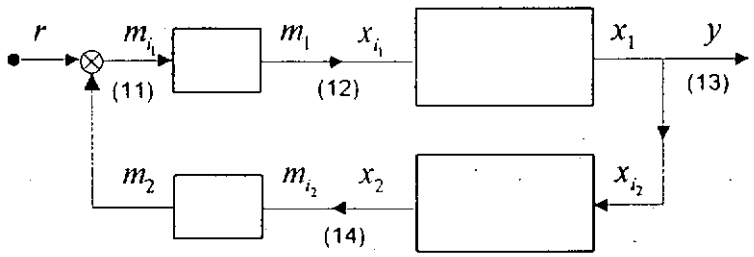

Fig. A5.1 Example of a 4-block system

With reference to the simple example of a four-block system shown in Fig. A5.1, and by comparing the corresponding node numbers of the LHS and RHS vectors ('1' if equal otherwise '0'), the sparse connection-matrix equation is

$$
\begin{array}{c}
\\
(12)\\(13)\\(13)\\(11)\\(14)
\end{array}
\begin{bmatrix} x_{i_1} \\ x_{i_2} \\ y \\ m_{i_1} \\ m_{i_2} \end{bmatrix}
=
\begin{array}{c}
\begin{matrix} (13) & (14) & (11) & (12) & (11) \end{matrix} \\
\begin{bmatrix} & & & 1 & \\ 1 & & & & \\ 1 & & & & \\ & & 1 & & 1 \\ & 1 & & & \end{bmatrix}
\end{array}
\begin{array}{l}
\begin{bmatrix} x_1 \\ x_2 \\ r \\ m_1 \\ m_2 \end{bmatrix}
\begin{matrix} (13) \\ (14) \\ (11) \\ (12) \\ (11) \end{matrix}
\end{array}
$$

Since the input data are a sequence of blocks (i.e. branches) rather than nodal information, this technique is much simpler and faster than the indirect method of using incidence matrices [69].

APPENDIX 6

TIME RESPONSE ANALYTICAL SOLUTION

The response of (2.20) is [70]:

$$X(t) = \Phi(t)X(0+) + \int_0^t \Phi(\tau)BR(t-\tau)d\tau \qquad \text{for } t > \tau > 0$$

where $\Phi(t) = P\exp(\Lambda t)Q$

$$P = [U_1, U_2, \ldots], \quad U_J = \text{eigenvector} \tag{A6.1a}$$

$$Q = P^{-1} \tag{A6.1b}$$

and Λ = diagonal matrix of eigenvalues.

Integrating (2.20) with respect to time t,

$$\int_{0-}^{0+} \frac{dX}{dt}dt = \int_{0-}^{0+} (AX + BR)dt + \int_{0-}^{0+} E\frac{dR}{dt}dt$$

$$\int_{t=0-}^{t=0+} dX = E\int_{t=0-}^{t=0+} dR$$

For small perturbation analysis, $X(0-) = 0$ and $R(0-) = 0$, and for an input step function of magnitude R, there results

$$X(0+) = ER(0+) = ER$$

and $R(t-\tau) = R \qquad \text{for } t > \tau > 0$

Thus, $X(t) = P\exp(\Lambda t)QER + \int_0^t P\exp(\Lambda\tau)QBRd\tau$

$$X(t) = P\exp(\Lambda t)QER + P[\exp(\Lambda t) - I]\Lambda^{-1}QBR \tag{A6.2a}$$

and $Y(t) = CX(t) + DR$ (A6.2b)

APPENDIX 7

REPRESENTATION OF COMPLICATED TRANSFER FUNCTIONS

Nonlinear function under small perturbations, or 'quadratic' transfer functions, may be included as elementary blocks in Fig. 2.11. This appendix illustrates how some typical cases shown in Fig. A7.1 are processed.

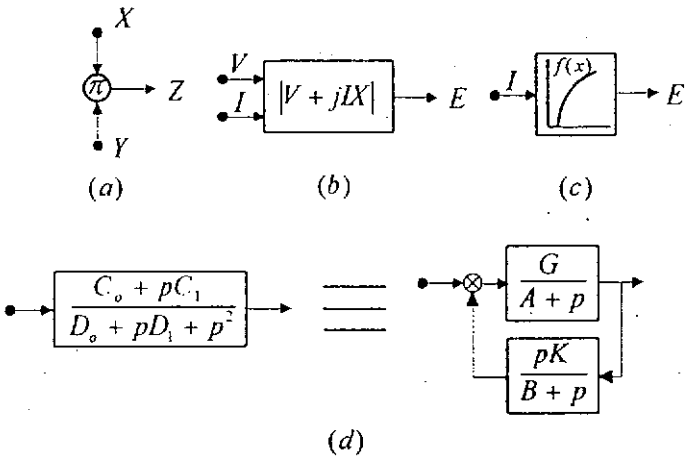

Fig. A7.1 Examples of 'non-elementary' transfer functions

Case a: $Z = XY$

$$\Delta Z = Y\Delta X + X\Delta Y$$

Case b: $E = |V + jIX|$

$$E^2 = V^2 + I^2X^2$$

$$\Delta E = (V/E)\Delta V + (X^2I/E)\Delta I$$

Similarly $I = |I_d + jI_q|$

$$\Delta I = (I_d/I)\Delta I_d + (I_q/I)\Delta I_q$$

Case c: $E = f(I)$

$$\Delta E = m\Delta I$$

where m = slope $(\partial E/\partial I)$ at the operating point.

Case d: A 'quadratic' transfer function may be represented by two elementary blocks. The two block diagrams are identical so long as

$$G = C_1$$

$$A = D_0 C_1 / C_0$$

$$K = C_0 / C_1^2 + D_0 / C_0 - D_1 / C_1$$

$$B = C_0 / C_1$$

In the limiting case where $C_0 = 0$, $C_1 = 0$, or if the numerator polynomial is also quadratic, it is still possible to express the original second order block as a combination of elementary blocks by more elaborate circuit block manipulation. Any high order polynomial can be also represented by elementary blocks since it is a combination of quadratic and first order.

APPENDIX 8

EVALUATION OF SENSITIVITY COEFFICIENTS FOR ARBITRARY BLOCK PARAMETERS

From (A4.7) and (A4.8), system matrix A is a function of K_b, K_a and K_t. Hence, for $\kappa = k_b$, k_a or k_t in the nth block as defined in (A4.6), $\partial A/\partial \kappa$ can be expressed as follows:

$$\frac{\partial A}{\partial k_b} = S\frac{\partial K_b}{\partial k_b}F \tag{A8.1a}$$

$$\frac{\partial A}{\partial k_a} = -S\frac{\partial K_a}{\partial k_a} \tag{A8.1b}$$

or
$$\frac{\partial A}{\partial k_t} = \frac{\partial S}{\partial k_t}(K_bF - K_a) = -S\frac{\partial (I - K_tF)}{\partial k_t}S(K_bF - K_a)$$

$$= S\frac{\partial K_t}{\partial k_t}FS(K_bF - K_a) = S\frac{\partial K_t}{\partial k_t}FA \tag{A8.1c}$$

where $\partial K/\partial k$ ($\partial K_b/\partial k_b$, $\partial K_a/\partial k_a$ and $\partial K_c/\partial k_c$) will have only one non-zero element of unity value (the nth diagonal element). Therefore, if $W^T = (w_1, w_2,...)$ and $Z^T = (z_1, z_2,...)$ are two arbitrary vectors, the product of $W^T(\partial K/\partial k)Z = w_n z_n$ will be as simple as the product of two scalars. Because of this feature, $\partial \lambda/\partial \kappa$ can be evaluated very easily as shown below.

Define the scalar

$$h = V^T U = (v_1, v_2, \ldots)(u_1, u_2, \ldots)^T$$

and the vectors

$$W^T = V^T S = (w_1, w_2, \ldots) \tag{A8.2a}$$

$$Z = FU = (z_1, z_2, \ldots)^T \tag{A8.2b}$$

where S and F are already available in (A4.8) and (A4.9), respectively, when forming the state space equation.

Substituting (A8.1) in (2.22),

$$\frac{\partial \lambda}{\partial k_b} = \frac{\boldsymbol{V}^T \boldsymbol{S} \dfrac{\partial \boldsymbol{K}_b}{\partial k_b} \boldsymbol{F}\boldsymbol{U}}{\boldsymbol{V}^T \boldsymbol{U}} = \frac{\boldsymbol{W}^T \dfrac{\partial \boldsymbol{K}_b}{\partial k_b} \boldsymbol{Z}}{\boldsymbol{V}^T \boldsymbol{U}} = \frac{w_n z_n}{h} \tag{A8.3a}$$

$$\frac{\partial \lambda}{\partial k_a} = \frac{-\boldsymbol{V}^T \boldsymbol{S} \dfrac{\partial \boldsymbol{K}_a}{\partial k_a} \boldsymbol{U}}{\boldsymbol{V}^T \boldsymbol{U}} = -\frac{w_n u_n}{h} \tag{A8.3b}$$

or $$\frac{\partial \lambda}{\partial k_t} = \frac{\boldsymbol{V}^T \boldsymbol{S} \dfrac{\partial \boldsymbol{K}_t}{\partial k_t} \boldsymbol{F}\boldsymbol{A}\boldsymbol{U}}{\boldsymbol{V}^T \boldsymbol{U}} = \frac{\boldsymbol{V}^T \boldsymbol{S} \dfrac{\partial \boldsymbol{K}_t}{\partial k_t} \boldsymbol{F}\boldsymbol{U}\lambda}{\boldsymbol{V}^T \boldsymbol{U}} = \frac{w_n z_n \lambda}{h} \tag{A8.3c}$$

Hence for $\kappa = b$, a, T_b, or T_a, $\partial\lambda/\partial\kappa$ becomes, using (A4.6),

$$\frac{\partial \lambda}{\partial b} = \frac{\partial \lambda}{\partial k_b} \frac{\partial k_b}{\partial b} = \frac{\partial \lambda}{\partial k_b} \frac{1}{T_a} = \frac{w_n z_n}{h T_a} \tag{A8.4a}$$

$$\frac{\partial \lambda}{\partial a} = \frac{-w_n u_n}{h T_a} \tag{A8.4b}$$

$$\frac{\partial \lambda}{\partial T_b} = \frac{w_n z_n \lambda}{h T_a} \tag{A8.4c}$$

or $$\frac{\partial \lambda}{\partial T_a} = \frac{\partial \lambda}{\partial k_b} \frac{\partial k_b}{\partial T_a} + \frac{\partial \lambda}{\partial k_a} \frac{\partial k_a}{\partial T_a} + \frac{\partial \lambda}{\partial k_t} \frac{\partial k_t}{\partial T_a}$$

$$= -\left(\frac{\partial \lambda}{\partial k_b} b + \frac{\partial \lambda}{\partial k_a} a + \frac{\partial \lambda}{\partial k_t} T_b\right) / T_a^2$$

$$= -w_n (z_n b - u_n a + \lambda z_n T_b) / (h T_a^2) \tag{A8.4d}$$

Consequently, the sensitivities of λ, with respect to the nth block, are obtained by picking up the nth elements from the vectors $\boldsymbol{U}$, $\boldsymbol{W}$ and $\boldsymbol{Z}$ and then performing a simple algebraic operation with some other scalars according to (A8.4), where $\boldsymbol{W}$ and $\boldsymbol{Z}$ can be derived from $\boldsymbol{V}$ and $\boldsymbol{U}$ in (A8.2). Therefore the sensitivity with respect to all block parameters can be evaluated once these vectors are formed.

APPENDIX 9

EVALUATION OF SENSITIVITY COEFFICIENTS FOR ARBITRARY SYSTEM PARAMETERS

With diagonal matrix $\boldsymbol{K}$ of (A4.3) collecting all the parameters of zero order blocks, parameters associated with system operating condition are all included in $\boldsymbol{K}$. From (A4.4), (A4.5), and (A4.6), $\partial \boldsymbol{A}/\partial\kappa$ can be expressed as

$$\frac{\partial \boldsymbol{A}}{\partial \kappa} = \frac{\partial[\boldsymbol{S}(\boldsymbol{K}_b\boldsymbol{F} - \boldsymbol{K}_a)]}{\partial \kappa} = \boldsymbol{S}\left(\boldsymbol{K}_t \frac{\partial \boldsymbol{F}}{\partial \kappa}\boldsymbol{A} + \boldsymbol{K}_b \frac{\partial \boldsymbol{F}}{\partial \kappa}\right) \tag{A9.1a}$$

$$\frac{\partial \boldsymbol{F}}{\partial \kappa} = \frac{\partial\left(\boldsymbol{L}_1 + \boldsymbol{L}_3\boldsymbol{H}\boldsymbol{L}_7\right)}{\partial \kappa} = \boldsymbol{L}_3\boldsymbol{H}\frac{\partial \boldsymbol{K}}{\partial \kappa}\left(\boldsymbol{L}_9{}'\boldsymbol{H} + \boldsymbol{I}\right)\boldsymbol{L}_7{}' \tag{A9.1b}$$

Investigating the elements of $\boldsymbol{K}$ associated with system operating condition, some of them are the simple functions of variables associated with generator buses, which are collected in $\boldsymbol{M}_1$ of (2.23) or $\boldsymbol{M}_{1(i)}$ of (A9.2) corresponding to i-th machine.

$$\boldsymbol{M}_{1(i)} = \left[\, I_{di}, I_{qi}, V_{di}, V_{qi}, V_{ti}, \cos\delta_i, \sin\delta_i \right] \tag{A9.2}$$

The others describing network equation are collected in $\boldsymbol{M}_2$ of (2.23). With $\partial \boldsymbol{K}/\partial\kappa$ constructed from the partial derivatives of elements of $\boldsymbol{M}_1$ and $\boldsymbol{M}_2$, $\partial\lambda/\partial\kappa$ for κ = (system parameter) therefore can be evaluated from (2.22) and (A9.1).

A9.1 Derivatives of $\boldsymbol{M}_{1(i)}$ to j-th nodal voltages ($V_{Rj} + jV_{Jj}$)

Firstly, assuming that the nodal voltages and generator currents are defined in rectangular coordinates. E_{Qi} can also be expressed referencing network frame as:

$$\begin{aligned} &E_{QRi} + jE_{QJi} = \left(V_{Ri} + jV_{Ji}\right) + \left(I_{Ri} + jI_{Ji}\right)\left(R_{ai} + jX_{qi}\right), \\ &E_{QRi} = V_{Ri} + I_{Ri}R_{ai} - I_{Ji}X_{qi}, \\ &E_{QJi} = V_{Ji} + I_{Ri}X_{qi} + I_{Ji}R_{ai} \end{aligned} \tag{A9.3}$$

$$E_{Qi}^2 = E_{QRi}^2 + E_{QJi}^2,$$

$$E_{QRi} = -E_{Qi}\sin\delta_i,\ E_{QJi} = E_{Qi}\cos\delta_i \tag{A9.4}$$

From the nodal voltage equation of overall network $\boldsymbol{I} = \boldsymbol{YV}$, coordinates transformation (2.9) and,

$$V_{ti}^2 = V_{Ri}^2 + V_{Ji}^2 \tag{A9.5}$$

the partial derivatives can be expressed as follows by using a constant C_0 with $C_0 = 1$ for $i = j$ and $C_0 = 0$ for $i \neq j$. Subscript '$(.)j$' stands for 'Rj' or 'Jj'.

$$\frac{\partial I_{Ri}}{\partial V_{Rj}} = \frac{\partial I_{Ji}}{\partial V_{Jj}} = G_{ij} \tag{A9.6a}$$

$$\frac{\partial I_{Ri}}{\partial V_{Jj}} = -\frac{\partial I_{Ji}}{\partial V_{Rj}} = -B_{ij} \tag{A9.6b}$$

$$\frac{\partial E_{QRi}}{\partial V_{Rj}} = \frac{\partial E_{QJi}}{\partial V_{Jj}} = C_0 + R_{ai}\frac{\partial I_{Ri}}{\partial V_{Rj}} - X_{qi}\frac{\partial I_{Ji}}{\partial V_{Rj}} \tag{A9.7a}$$

$$\frac{\partial E_{QRi}}{\partial V_{Jj}} = -\frac{\partial E_{QJi}}{\partial V_{Rj}} = R_{ai}\frac{\partial I_{Ri}}{\partial V_{Jj}} - X_{qi}\frac{\partial I_{Ji}}{\partial V_{Jj}} \tag{A9.7b}$$

$$\frac{\partial E_{Qi}}{\partial V_{(.)j}} = -\frac{\partial E_{QRi}}{\partial V_{(.)j}}\sin\delta_i + \frac{\partial E_{QJi}}{\partial V_{(.)j}}\cos\delta_i \tag{A9.7c}$$

$$\frac{\partial \sin\delta_i}{\partial V_{(.)j}} = \frac{-1}{E_{Qi}}\left(\frac{\partial E_{QRi}}{\partial V_{(.)j}} + \frac{\partial E_{Qi}}{\partial V_{(.)j}}\sin\delta_i\right),$$

$$\frac{\partial \cos\delta_i}{\partial V_{(.)j}} = \frac{1}{E_{Qi}}\left(\frac{\partial E_{QJi}}{\partial V_{(.)j}} - \frac{\partial E_{Qi}}{\partial V_{(.)j}}\cos\delta_i\right) \tag{A9.8}$$

$$\frac{\partial I_{di}}{\partial V_{(.)j}} = \frac{\partial I_{Ri}}{\partial V_{(.)j}}\cos\delta_i + \frac{\partial I_{Ji}}{\partial V_{(.)j}}\sin\delta_i + I_{Ri}\frac{\partial\cos\delta_i}{\partial V_{(.)j}} + I_{Ji}\frac{\partial\sin\delta_i}{\partial V_{(.)j}},$$

$$\frac{\partial I_{qi}}{\partial V_{(.)j}} = -\frac{\partial I_{Ri}}{\partial V_{(.)j}}\sin\delta_i + \frac{\partial I_{Ji}}{\partial V_{(.)j}}\cos\delta_i - I_{Ri}\frac{\partial\sin\delta_i}{\partial V_{(.)j}} + I_{Ji}\frac{\partial\cos\delta_i}{\partial V_{(.)j}} \tag{A9.9}$$

$$\frac{\partial V_{di}}{\partial V_{Rj}} = C_0\cos\delta_i + V_{Ri}\frac{\partial\cos\delta_i}{\partial V_{Rj}} + V_{Ji}\frac{\partial\sin\delta_i}{\partial V_{Rj}},$$

$$\frac{\partial V_{di}}{\partial V_{Jj}} = C_0 \sin\delta_i + V_{Ri}\frac{\partial \cos\delta_i}{\partial V_{Jj}} + V_{Ji}\frac{\partial \sin\delta_i}{\partial V_{Jj}},$$

$$\frac{\partial V_{qi}}{\partial V_{Rj}} = -C_0 \sin\delta_i - V_{Ri}\frac{\partial \sin\delta_i}{\partial V_{Rj}} + V_{Ji}\frac{\partial \cos\delta_i}{\partial V_{Rj}},$$

$$\frac{\partial V_{qi}}{\partial V_{Jj}} = C_0 \cos\delta_i - V_{Ri}\frac{\partial \sin\delta_i}{\partial V_{Jj}} + V_{Ji}\frac{\partial \cos\delta_i}{\partial V_{Jj}} \qquad \text{(A9.10)}$$

$$\frac{\partial V_{ti}}{\partial V_{Rj}} = C_0\frac{V_{Ri}}{V_{ti}},\ \frac{\partial V_{ti}}{\partial V_{Jj}} = C_0\frac{V_{Ji}}{V_{ti}} \qquad \text{(A9.11)}$$

A9.2 Derivatives of M_2 to nodal voltages ($V_{Rj} + jV_{Jj}$)

M_2 of (2.23) will be consisted of the elements of $\boldsymbol{Y}_{GG}'$ alone when the machine is considered only. When static loads are represented by equivalent shunt admittances and added to the corresponding diagonal elements of $\boldsymbol{Y}_{LL}'$ of (2.4), only the equivalent admittances are affected by nodal voltages. Thus,

$$\frac{\partial \boldsymbol{Y}_{GG}'}{\partial V_{(.)j}} = \frac{\partial}{\partial V_{(.)j}}[\boldsymbol{Y}_{GG} - \boldsymbol{Y}_{GL}(\boldsymbol{Y}_{LL}')^{-1}\boldsymbol{Y}_{LG}]$$

$$= \boldsymbol{Y}_{GL}\boldsymbol{Y}_{LL}^{-1}\frac{\partial \boldsymbol{Y}_{LL}'}{\partial V_{(.)j}}\boldsymbol{Y}_{LL}^{-1}\boldsymbol{Y}_{LG} \qquad \text{(A9.12)}$$

When the deviation of nodal voltages is regarded being independent with load powers, differentiation of (A9.13a) yields (A9.13b).

$$\Delta G_{ii} + j\Delta B_{ii} = \left(P_{l,i} - jQ_{l,i}\right)/V_{ti}^2 \qquad \text{(A9.13a)}$$

$$\frac{\partial\left(\Delta G_{ii} + j\Delta B_{ii}\right)}{\partial V_{(.)i}} = \frac{-2V_{(.)i}}{V_{ti}^4}\left(P_{l,i} - jQ_{l,i}\right) \qquad \text{A9.13b)}$$

If the deviation of nodal voltages is risen from the variation of nodal powers, the equivalent admittances should be expressed by nodal injected currents as

$$\Delta G_{ii} + j\Delta B_{ii} = -\frac{I_{Ri} + jI_{Ji}}{V_{Ri} + jV_{Ji}} \qquad \text{(A9.14)}$$

and the injected currents are determined by nodal voltage equation $\boldsymbol{I} = \boldsymbol{YV}$. Therefore,

$$\frac{\partial \Delta G_{ii}}{\partial V_{(.)j}} = \frac{-1}{V_{ti}^2}\left[C_0\left(2V_{(.)j}\Delta G_{ii} + I_{(.)J}\right) + V_{Ri}\frac{\partial I_{Ri}}{\partial V_{(.)j}} + V_{Ji}\frac{\partial I_{Ji}}{\partial V_{(.)j}} \right],$$

$$\frac{\partial \Delta B_{ii}}{\partial V_{Rj}} = \frac{-1}{V_{ti}^2}\left[C_0\left(2V_{Ri}\Delta B_{ii} + I_{Ji}\right) + V_{Ri}\frac{\partial I_{Ji}}{\partial V_{Rj}} - V_{Ji}\frac{\partial I_{Ri}}{\partial V_{Rj}} \right],$$

$$\frac{\partial \Delta B_{ii}}{\partial V_{Jj}} = \frac{-1}{V_{ti}^2}\left[C_0\left(2V_{Ji}\Delta B_{ii} - I_{Ri}\right) + V_{Ri}\frac{\partial I_{Ji}}{\partial V_{Jj}} - V_{Ji}\frac{\partial I_{Ri}}{\partial V_{Jj}} \right] \qquad \text{(A9.15)}$$

A9.3 Derivatives to nodal voltages (V_j, δ_{Vj})

When nodal voltages in polar coordinates are defined as $V_j \angle \delta_{Vj}$, the derivatives of any element M_i in and $\boldsymbol{M_1}$ or $\boldsymbol{M_2}$ of (2.23) can be obtained from $V_{Rj} = V_j \cos\delta_{Vj}$ and $V_{Jj} = V_j \cos\delta_{Vj}$ as

$$\frac{\partial M_i}{\partial V_j} = \frac{\partial M_i}{\partial V_{Rj}}\cos\delta_{vj} + \frac{\partial M_i}{\partial V_{Jj}}\sin\delta_{vj},$$

$$\frac{\partial M_i}{\partial \delta_{vj}} = -\frac{\partial M_i}{\partial V_{Rj}}V_j \sin\delta_{vj} + \frac{\partial M_i}{\partial V_{Jj}}V_j \cos\delta_{vj} \qquad \text{(A9.16)}$$

A9.4 Derivatives of K to nodal injected power ($P_j + Q_j$)

Jacobian matrix $\boldsymbol{J}$ used in load flow calculation determines the linearized relationship between nodal powers and nodal voltages. $\partial V_{Ri}/\partial P_j$, $\partial V_{Ri}/\partial Q_j$, $\partial V_{Ji}/\partial P_j$ and $\partial V_{Ji}/\partial Q_j$ are the elements of $\boldsymbol{J}^{-1}$. Therefore, the derivatives of any element M_i in and $\boldsymbol{M_1}$ or $\boldsymbol{M_2}$ of (16) to nodal powers will be expressed as:

$$\frac{\partial M_i}{\partial P_j} = \sum_k \left(\frac{\partial M_i}{\partial V_{Rk}}\frac{\partial V_{Rk}}{\partial P_j} + \frac{\partial M_i}{\partial V_{Jk}}\frac{\partial V_{Jk}}{\partial P_j} \right)$$

$$\frac{\partial M_i}{\partial Q_j} = \sum_i \left(\frac{\partial M_i}{\partial V_{Rk}}\frac{\partial V_{Rk}}{\partial Q_j} + \frac{\partial M_i}{\partial V_{Jk}}\frac{\partial V_{Jk}}{\partial Q_j} \right) \qquad \text{(A9.17)}$$

A9.5 Derivatives of K to line admittance ($y_{mn} = g_{mn} + jb_{mn}$)

Change of a line admittance y_{mn} will affects admittance matrix $\boldsymbol{Y}$ and the initial system operating condition described by nodal voltages and injected currents. Derivative of $\boldsymbol{K}$ with respect to b_{mn} has the same form as that to g_{mn}. Only the latter is discussed.

The derivatives of $\boldsymbol{Y}_{GG}'$ to g_{mn} will be obtained from $\partial \boldsymbol{Y}/\partial g_{mn}$ which is constructed as: "1" on the sits of (m,m) and (n,n), "−1" on the sits of (m,n) and (n,m), "0" on other sites. The derivative of $\boldsymbol{Y}_{GG}'$ with respect to g_{mn} is:

$$\begin{aligned}\frac{\partial \boldsymbol{Y}_{GG}'}{\partial g_{mn}} = \frac{\partial \boldsymbol{Y}_{GG}}{\partial g_{mn}} - \frac{\partial \boldsymbol{Y}_{GL}}{\partial g_{mn}}(\boldsymbol{Y}_{LL}')^{-1}\boldsymbol{Y}_{LG} \\ +\boldsymbol{Y}_{GL}(\boldsymbol{Y}_{LL}')^{-1}\frac{\partial \boldsymbol{Y}_{LL}'}{\partial g_{mn}}(\boldsymbol{Y}_{LL}')^{-1}\boldsymbol{Y}_{LG} \\ -\boldsymbol{Y}_{GL}(\boldsymbol{Y}_{LL}')^{-1}\frac{\partial \boldsymbol{Y}_{LG}}{\partial g_{mn}}\end{aligned} \tag{A9.18}$$

However, due to $\boldsymbol{I} = \boldsymbol{YV}$, (A9.6) will becomes (in vector form)

$$\frac{\partial \boldsymbol{I}}{\partial g_{mn}} = \boldsymbol{Y}\frac{\partial \boldsymbol{V}}{\partial g_{mn}} + \frac{\partial \boldsymbol{Y}}{\partial g_{mn}}\boldsymbol{V} \tag{A9.19}$$

From (A9.7) to (A9.11), if $\partial M_i/\partial \boldsymbol{V}$ is regarded as a linear function of $\partial \boldsymbol{I}/\partial \boldsymbol{V}$ denoted as $f(.)$, the derivatives of M_i will be represented in vector form as

$$\frac{\partial M_i}{\partial g_{mn}} = f\left(\frac{\partial \boldsymbol{I}}{\partial \boldsymbol{V}}\right)\frac{\partial \boldsymbol{V}}{\partial g_{mn}} + f\left(\frac{\partial \boldsymbol{Y}}{\partial g_{mn}}\boldsymbol{V}\right) \tag{A9.20}$$

$\partial \boldsymbol{V}/\partial g_{mn}$ can be solved from (A9.21) which is obtained by differentiating the nodal power equation.

$$\frac{\partial V_i}{\partial g_{mn}}I_i^* + \sum_j\left(V_i\frac{\partial Y_{ij}^*}{\partial g_{mn}}V_j^* + V_iY_{ij}^*\frac{\partial V_j^*}{\partial g_{mn}}\right) = 0,\ i = 1,2,3,\ldots \tag{A9.21}$$

APPENDIX 10

VALIDITY OF THE PMT PROGRAM

Validation of the PMT algorithms is divided into two stages. The first stage (three steps) is to compare the results with the well-known Heffron Phillips (HP) model [6].

(a) Machine modeling is first checked by using a new single machine infinite bus model established in Appendix 16.

(b) The multimachine network described by (2.5) is checked against HP using a 2-machine 2-node system in which one machine (reference) has very large inertia and the output voltages ΔV_d and ΔV_q are made zero.

(c) This network equation (2.5) is once more checked by a large N-machine system in which two identical machines are connected to an arbitrary bus via identical reactance X_e (e.g. generator transformer reactance).

The above has confirmed the validity of the 3rd-order machine model together with the network equation (2.5) because *all* the eigenvalues obtained in HP analysis reappear in *all* the above cases irrespective the complexity of EXC/GOV representations, although some more eigenvalues come out in (b) and (c) because of more than one machine. The next stage is to check the network equation (2.7) (with any component) with the validated network equation (2.5) (with machines only):

(d) by treating an arbitrary transmission line (eventually eliminated in (2.5)) as a line component in (2.7),

(e) by treating a capacitor as an SVC component without feedback/control,

(f) with the existence of both multi-SVC and multi-line components.

The validity of the network equation (2.7) is also confirmed because eigenvalues obtained in *all* these computer runs are identical to the original (i.e. without SVC/line component). Note that the shunt SVC component (connected to one node) and the series line component (connected between two nodes) reflect the different ways of modular system connection.

APPENDIX 11

DATA OF 7-MACHINE SYSTEM

Bus number	Generation		Load	
	MW	MVar	MW	MVar
1	678.38	−186.07	125.00	−40.00
2	290.00	−58.67	260.00	−40.00
3	147.02	−29.70	80.00	0.0
4	229.85	63.92	100.00	−10.00
5	190.09	7.27	60.00	0.0
6	130.05	0.49	70.00	−10.00
7	150.05	−19.51	100.00	0.0
8	0.0	0.0	150.00	−40.00
9	0.0	0.0	50.00	0.0
10	0.0	0.0	120.00	0.0
11	0.0	0.0	20.00	0.0
12	0.0	0.0	60.00	−30.00
13	0.0	0.0	80.00	0.0
14	0.0	0.0	60.00	0.0
15	0.0	0.0	160.00	0.0
16	0.0	0.0	70.00	10.00
17	0.0	0.0	70.00	0.0
18	0.0	0.0	90.00	0.0
19	0.0	0.0	140.00	0.0

Table A11.1 Busbar data of the 7-machine system

Line number	From (Bus i)	To (Bus j)	*R*	*X*	*B*/2
1	1	8	0.00042	0.00674	0.07915
2	8	9	0.00006	0.00577	0.42992
3	8	10	0.00416	0.07560	0.01381
4	8	11	0.0	0.08979	0.01117
5	9	2	0.00123	0.03045	0.12917
6	9	10	0.00297	0.04278	0.12860
7	9	11	0.00200	0.04227	0.04017
8	3	10	0.00019	0.00138	0.02560
9	10	11	0.00075	0.00470	0.02332
10	10	12	0.00234	0.02326	0.03418
11	10	13	0.03658	0.04443	0.03382
12	11	12	0.00202	0.02184	0.03535
13	11	13	0.01195	0.05117	0.03924
14	14	4	0.0	0.06673	0.03861
15	4	15	0.00400	0.22582	0.03236
16	15	5	0.03504	0.20399	0.03227
17	15	19	0.00853	0.17754	0.03227
18	5	16	0.02324	0.11083	0.05505
19	16	17	0.01478	0.15114	0.05485
20	16	6	0.04827	0.11328	0.02341
21	16	19	0.00430	0.20123	0.02341
22	17	6	0.02507	0.12436	0.02337
23	17	18	0.00425	0.10385	0.13635
24	7	18	0.03643	0.11877	0.13695
25	18	19	0.00564	0.18352	0.13373
26	14	19	0.01200	0.22499	0.04167
27	12	4	0.02027	0.20269	0.05505
28	13	14	0.01596	0.15963	0.05485

Table A11.2 Circuit data of the 7-machine system

(Note: The impedance *R* & *X*, and the susceptance *B* are in per unit on 100MVA base)

Machine	Rating (MW)	R_a	X_d	X_q	X_d'	X_q'	X_d''	X_q''	T_{do}'	T_{qo}'	T_{do}''	T_{qo}''	M	Generator R	Transformer X
A_1	2 x 350	0.0	0.50	0.45	0.07	0.28	0.050	0.060	7.20	2.90	0.02	0.28	29.0	0.0	0.03808
A_2	2 x 200	0.0012	0.78	0.75	0.10	0.36	0.074	0.090	6.00	1.00	0.15	9.10	18.2	0.001822	0.09777
A_3	2 x 200	0.0012	0.78	0.75	0.10	0.36	0.074	0.090	6.00	1.00	0.15	9.10	18.2	0.001822	0.09777
B_1	3 x 100	0.0020	1.27	1.21	0.17	0.47	0.140	0.127	6.90	0.60	0.02	0.11	13.0	0.005503	0.13415
B_2	2 x 100	0.0020	1.50	1.10	0.22	0.47	0.140	0.127	4.30	0.60	0.02	0.11	10.4	0.005040	0.11040
B_3	4 x 80	0.0035	1.00	0.68	0.38	0.01	0.130	0.131	6.45	1.00	0.05	0.05	9.6	0.005533	0.14200
B_4	2 x 60	0.0048	2.93	1.86	0.32	1.86	0.200	0.200	9.55	0.05	0.05	0.05	8.4	0.006915	0.13905

Table A11.3 Machine Parameters

Note: For every machine,

1. Parameters are assumed identical within a group and those of a single set are shown,

2. Inertia constant M and the pu impedances are on 100MVA base,

3. Station load (with power factors 0.8) is 6% of machine MW output, and

4. Terminal voltage is normally kept at 1 pu.

Machine	In	Out	b	T_b	a	T_a	Label
A_1	1	2	−1.000	0.0	1.000	0.010	EXC
	2	3	50.000	0.0	1.000	0.030	GAIN
	3	4	1.000	0.500	1.000	0.050	PHAD
	4	5	20.000	0.400	1.000	3.000	FOR
	5	6	1.000	0.400	1.000	0.200	FB1
	6	4	−0.100	0.0	1.000	0.001	FB2
	5	7	0.100	0.0	0.0	0.0	KG
	7	8	0.400	2.880	1.000	2.880	REG
	65	64	−87.500	0.0	0.0	0.0	GOV
	64	61	1.000	0.0	1.000	0.990	KG/TG
A_2	1	2	−1.000	0.0	1.000	0.010	EXC
	2	3	50.000	0.0	1.000	0.010	GAIN
	3	4	1.000	0.500	1.000	0.050	PHAD
	4	5	20.000	1.000	1.000	3.000	FOR
	5	6	1.000	0.300	1.000	0.200	FB1
	6	4	−0.200	0.0	1.000	0.001	FB2
	5	7	0.100	0.0	0.0	0.0	KG
	7	8	0.400	2.400	1.000	2.400	REG
	65	64	−50.000	0.0	0.0	0.0	GOV
	64	61	1.000	0.0	1.000	0.990	KG/TG
A_3	1	2	−1.000	0.0	1.000	0.010	EXC
	2	3	50.000	0.0	1.000	0.010	GAIN
	3	4	1.000	0.500	1.000	0.050	PHAD
	4	5	20.000	1.000	1.000	3.000	FOR
	5	6	1.000	0.300	1.000	0.200	FB1
	6	4	−0.200	0.0	1.000	0.001	FB2
	5	7	0.100	0.0	0.0	0.0	KG
	7	8	0.400	2.400	1.000	2.400	REG
	65	64	−50.000	0.0	0.0	0.0	GOV
	64	61	1.000	0.0	1.000	0.990	KG/TG

Table A11.4a Transfer block data of EXC, GOV and PSS of 'A' machines
(Note: Defaulted node numbers of some variables:
1=ΔV_t, 8=ΔE_{fd}, 61=ΔP_m, 65=$\Delta\Omega$)

Machine	In	Out	b	T_b	a	T_a	Label
B_1	1	2	−1.000	0.0	1.000	0.010	EXC
	2	3	20.000	0.0	1.000	0.200	GAIN
	3	4	1.000	0.500	1.000	0.100	PHAD
	4	5	20.000	1.000	1.000	0.500	FOR
	5	6	1.000	0.400	1.000	0.200	FB1
	6	4	−0.200	0.0	1.000	0.001	FB2
	5	7	0.100	0.0	0.0	0.0	KG
	7	8	0.400	2.760	1.000	2.760	REG
	65	64	−25.000	0.0	0.0	0.0	GOV
	64	61	1.000	0.0	1.000	0.990	KG/TG
B_2	1	2	−1.000	0.0	1.000	0.010	EXC
	2	3	1.000	0.0	1.000	0.300	GA/TA
	3	8	20.000	0.0	1.000	0.040	GO/TO
	8	3	0.0	−0.050	1.000	1.000	KF/TF
	65	64	−25.000	0.0	0.0	0.0	GOV
	64	61	1.000	0.0	1.000	0.600	KG/TG
B_3	1	2	−1.000	0.0	1.000	0.010	EXC
	2	3	1.000	0.0	1.000	0.300	GA/TA
	3	8	20.000	0.0	1.000	0.040	GO/TO
	8	3	0.0	−0.050	1.000	1.000	KF/TF
	65	64	−20.000	0.0	0.0	0.0	GOV
	64	61	1.000	0.0	1.000	0.600	KG/TG
B_4	1	2	−1.000	0.0	1.000	0.010	EXC
	2	8	1.000	0.0	1.000	0.300	GA/TA
	3	8	20.000	0.0	1.000	0.040	GO/TO
	8	3	0.0	−0.050	1.000	1.000	KF/TF
	65	64	−15.000	0.0	0.0	0.0	GOV
	64	61	1.000	0.0	1.000	0.600	KG/TG

Table A11.4b Transfer block data of EXC, and GOV of 'B' machines
(Note: Defaulted node numbers of some variables:
1=ΔV_t, 8=ΔE_{fd}, 61=ΔP_m, 65=$\Delta\Omega$)

In	Out	b	T_b	a	T_a	Label
1	5	1.000	0.0	0.0	0.0	K2
2	5	0.003	0.0	0.0	0.0	K1
5	6	−3.000	0.000	1.000	0.2500	FILT
6	7	2.100	0.021	0.000	0.010	REG
7	8	3.000	0.000	1.000	0.0046	LINEA
8	3	1.000	−0.0015	1.000	0.001	SCR

Table A11.5 Transfer block data of voltage regulator of SVC
(Note: Defaulted node numbers of some variables:
1 = ΔV_{SVC}, 2 = ΔI_{SVC} and 3 = ΔB_L)

APPENDIX 12

MODAL ANALYSIS

In order to eliminate the cross-coupling between the state variables, consider a new state vector Z related to the original state vector X by the transformation:

$$X = PZ \tag{A12.1}$$

where $P = [U_1, U_2, \ldots]$, U_J = right eigenvector (A12.2)

By putting (A12.1) into (2.20) and (2.21), the state equations can be written as (A12.3) and (A12.4).

$$\dot{Z} = \Lambda Z + QBR + QE\dot{R} \tag{A12.3}$$

$$Y = CPZ + DR \tag{A12.4}$$

where $\Lambda = QZP$ = diagonal matrix of eignevalues.

$$Q = P^{-1} = [V_1, V_2 \ldots]^T, \qquad V_J = \text{left eigenvector}$$

Matrix $[QB + QE\Lambda]$ is referred to as mode controllability matrix and the matrix CP as the mode observability matrix

The mode shape associated with λ_J can be determined easily from CU_J which is the jth column of CP and its magnitude it the observability index (i.e. OI = $|CU_J|$).

The magnitude of jth row of the matrix $[QB + QE\Lambda]$, i.e. $|V_J^T(B + \lambda_J E)|$, is defined as the controllability index (CI) associated with λ_J. In case of input R applied to a block of Fig. 2.11b with $T_b = 0$, matrix $E = 0$. (e.g. the input ΔB_L in Fig. 4.2).

The residue index can be obtained from OI*CI = $|CU_J| * |V_J^T(B + \lambda_J E)|$

APPENDIX 13

PROPERTIES OF TIME CONSTANT SENSITIVITY (FOR LEAD CIRCUIT)

Let the complex eigenvalues of mode j be $\lambda_J = \alpha_J \pm j\omega_J$ and $[1 + pT]$ be the transfer function of a sample lead circuit. Then the circuit gain G and phase shift θ for this mode are given by (dropping the subscripts J for λ_J, α_J and ω_J)

$$1 + pT \equiv 1 + \lambda T \equiv G\angle\theta \tag{A13.1}$$

where $$G^2 = (1+\alpha T)^2 + \omega^2 T^2 \tag{A13.2a}$$

and $$\tan\theta = \omega T/(1+\alpha T) \tag{A13.2b}$$

Differentiating α with respect to T

$$\frac{\partial\alpha}{\partial T} = \frac{\partial\alpha}{\partial G}\frac{\partial G}{\partial T} + \frac{\partial\alpha}{\partial\theta}\frac{\partial\theta}{\partial T} \tag{A13.3}$$

the RRSC S_{JT} with respect to T obtained from sensitivity analysis can be written

$$S_{JT} = \frac{\partial\alpha}{\partial T/T} = \frac{\partial\alpha}{\partial G/G}\frac{\partial G/G}{\partial T/T} + \frac{\partial\alpha}{\partial\theta}\frac{\partial\theta}{\partial T/T} \tag{4.14}$$

where $$\frac{\partial G/G}{\partial T/T} = \frac{\alpha T + \alpha^2 T^2 + \omega^2 T^2}{(1+\alpha T)^2 + \omega^2 T^2} = g \tag{A13.4a}$$

and $$\frac{\partial\theta}{\partial T/T} = \frac{\omega T}{(1+\alpha T)^2 + \omega^2 T^2} = f \tag{A13.4b}$$

can be directly evaluated; (4.14) has two unknowns: $\partial\alpha/(\partial G/G)$ and $\partial\alpha/\partial\theta$.

For n lead circuits in cascade, there are n S_{JT}'s with respect to their corresponding T's (e.g. S_{JT} = –0.0025, –0.0680 and –0.0967, ... with respect to T = 0.01, 0.2, 4.0, ... for the interarea mode $\lambda = -0.19 \pm j3.91$). Thus, substituting in (4.14), the g and f values for any two T's (to give an arbitrary set of 2 equations with 2 unknowns), it is found that the

solutions for $\partial\alpha/(\partial G/G)$ (= –0.0093) and $\partial\alpha/\partial\theta$ (= –0.0656) are independent of the choice of T's. Moreover, for a cascade circuit with a transfer function $G_d{*}G_a\angle\theta_a{*}G_b\angle\theta_b$..., the 'RRSCs' with respect to the G_d gain constant (S_{JG}) and with respect to the gains of the first-order circuits are always equal, so that

$$S_{JG} = \frac{\partial\alpha}{\partial G/G} \qquad \text{for } G = G_a,\ G_b,\ \ldots. \tag{A13.5}$$

However g and f will vary with T according to (A13.4), and, assuming $\omega >> \alpha$, can be approximated by

$$g \approx \frac{\omega^2T^2}{1+\omega^2T^2} \tag{A13.6a}$$

and

$$f \approx \frac{\omega T}{1+\omega^2T^2} \tag{A13.6b}$$

Since $g(\omega T) + g(1/(\omega T)) = 1$ and $f(\omega T) = f(1/(\omega T))$, g and f are positive-value functions, appearing 'symmetric' about $T = 1/\omega$ as shown in Fig. 4.5a. In the actual study the exact (A13.4) are employed without simplification to obtain the sensitivity plots.

For a simple lead circuit with transfer function (TF) changed from $G_a\angle\theta_a$ to $G_a(1+\varepsilon)\angle(\theta_a+\Delta\theta_a)$ due to a positive ΔT change (where $\varepsilon = \Delta G_a/G_a$), the variations of ε and $\Delta\theta_a$ are of interest in the sensitivity synthesis. To simplify treatment, a complementary lag circuit with TF = $G_a^{-1}\angle-\theta_a$ is artificially added so that the overall TF becomes $G\angle\theta = (1+\varepsilon)\angle\Delta\theta_a$. Referring to the Bode plots (G and θ) in Fig. 4.5b and 4.5c, ε (= $\Delta G/G = \Delta G$ since $G = 1$ nominally) and $\Delta\theta_a$(= $\Delta\theta$) can then be singled out for plotting. Here, the synthesis is based on the condition that $T_1 = T_2$ (i.e. for unity circuit gain G) and ΔG is preferentially used (instead of $\Delta G/G$) for convenience in this case as a mean to depict the circuit gain variations in the Bode plots. In Fig. 4.5, the T and ω axes are both in logarithmic scale.

Noting that $g = (\partial G/G)/(\partial T/T) \approx \varepsilon/(\Delta T/T)$ and $f = \partial\theta/(\Delta T/T) \approx \Delta\theta_a/(\Delta T/T)$, the g and f plots in Fig. 4.5a (for a particular ω and with varying T) may also be derived from the G and θ plots (for a particular T and with varying ω) respectively. For example, the points m and n in Fig. 4.5a can be obtained by m' and n' in Fig. 4.5b and 4.5c.

Since $\Delta\alpha = S_{JT}\Delta T/T = S_{JG}\Delta G_a/G_a + (\partial\alpha/\partial\theta)\Delta\theta_a$, whenever S_{JG} or $\partial\alpha/\partial\theta$ is negative (positive), G_a or θ_a has to increase (decrease) to increase damping if considered separately. Although both G_a and θ_a increase with T, the degree of variation is dependent on the relative T and $1/\omega_J$ values as shown in the Bode plots in Fig. 4.5b and 4.5c (where $\Delta G_a/G_a = \Delta G$ and $\Delta\theta_a = \Delta\theta$). Note that at this mode frequency ω_J, $\Delta G > \Delta\theta$ if $T > 1/\omega_J$ (Fig. 4.5b), $\Delta G = \Delta\theta$ if $T = 1/\omega_J$ (Fig. 4.5c), and at different mode frequencies, $\Delta G_S > \Delta G_J$ if $\omega_S > \omega_J$ (Fig. 4.5c).

Considerations for a lag circuit are exactly complementary to the above treatment and are not separately elaborated.

APPENDIX 14

GAIN SYNTHESIS OF A CASCADE CIRCUIT

For a SVC damping controller with single lead/lag stage having a transfer function $G_d[1 + \lambda(T+\Delta T)]/[1+\lambda T]$, the overall gain will be G_dG_a and the two parameter are G_d and T. (G_d is the gain constant of the controller and G_a is the stage gain).

Suppose the SVC instability occurs at an overall controller gain of 3 p.u. (i.e. $G_cG_{aS} = 3$), the corresponding G_d will be $G_d = G_c = 3/G_{aS}$. (G_{aS} is G_a at ω_S.) For a 9.5 dB gain margin, the normal operating gain G_o is one third of G_c, resulting $G_o = 1/G_{aS}$. Referring to Fig 4.5c with a lead compensation (i.e. $\Delta T > 0$), the stage gain G_{aS} is *increased* by, say $\Delta G_S = 0.008$, and the on-site tuning requires G_o *decreased* by the same amount, as shown in Table A14.1. Because the interarea mode is affected by overall gain G_o*G_{aI} and G_{aI} is increased by, say $\Delta G_I = 0.003$, the overall change is $\Delta G_I - \Delta G_S = -0.005$. ($G_{aI}$ is G_a at ω_I.) With similar reasoning, a lag circuit (with $\Delta T < 0$) will increase the controller gain at ω_I by $\Delta G_I - \Delta G_S = (-0.003) - (-0.008) = 0.005$ instead, by using the difference between the transient gain reductions (since lag) at the two mode frequencies.

The above explanation on transient gain change is based on adjustment on lead time constant T_1 at $T_1 = T_2$ for convenience. The tendency is also valid for adjustment on lag time constant T_2 or for $T_1 \neq T_2$.

Gain	G_{aS}	$G_c = 3/G_{aS}$	$G_o = 1/G_{aS}$	G_{aI}	G_oG_{aI}
$\Delta T = 0$	1	3	1	1	1
$\Delta T > 0$	1.008	2.976	0.992	1.003	0.995
$\Delta T < 0$	0.992	3.024	1.008	0.997	1.005

Table A14.1 Controller gain synthesis of $G_d[1 + \lambda(T+\Delta T)]/[1+\lambda T]$ for different ΔT

APPENDIX 15

PHASE OF THE GEP(s)

In order to compute the phase shift of *GEP(s)*, the state ($\Delta\Omega$) in the block diagram (Fig. 6.1) should be disconnected or the inertia of the machine has to assume very large values to make the generator $\Delta\Omega/\Delta\delta$ constant. Otherwise, any change in ΔPe ($\Delta Pe_o+\Delta Pe_p$) will cause a change in $\Delta\Omega/\Delta\delta$ and affect ΔPe itself. In practice, the measured transfer function ($\Delta Pe/\Delta Epss$) cannot equal *GEP(s)* because it is impossible to hold $\Delta\Omega$ constant. As an alternative, the phase shift of *GEP(s)* can be approximated by the angle difference between the voltage reference ΔV_{ref} and the terminal voltage (ΔV_t) as shown in Fig. A15.1 [13].

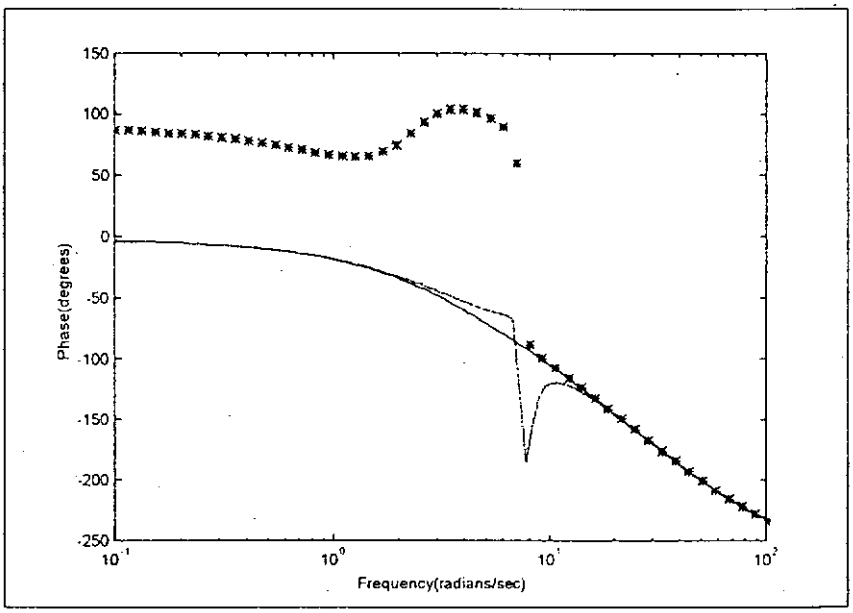

Fig. A15.1 Phase characteristics of *GEP(s)*-(solid line), $\Delta Pe/\Delta Epss$ -(star line) and $\Delta V_t/\Delta V_{ref}$-(dashed line)

APPENDIX 16

SINGLE MACHINE INFINITE BUS MODEL

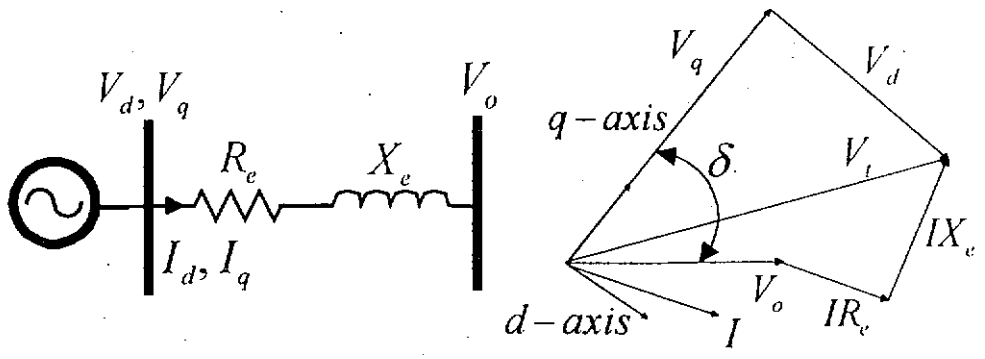

Fig. A16.1 System configuration and Phasor diagram

From Fig. A16.1, using the infinite bus as reference, the machine terminal voltage equations are:

$$V_q = I_d X_e + I_q R_e + V_o \cos\delta \tag{A16.1}$$

$$V_d = -I_q X_e + I_d R_e + V_o \sin\delta \tag{A16.2}$$

and for small perturbation, take the form:

$$\Delta I_d = \frac{1}{X_e^2 + R_e^2}[X_e \Delta V_q + R_e \Delta V_d + V_o(X_e \sin\delta - R_e \cos\delta)\Delta\delta] \tag{A16.3}$$

$$\Delta I_q = \frac{1}{X_e^2 + R_e^2}[R_e \Delta V_q - X_e \Delta V_d + V_o(R_e \sin\delta + X_e \cos\delta)\Delta\delta] \tag{A16.4}$$

Thus, machine modules of any order (e.g. Fig. 2.3, Fig. A2.1, Fig. A2.2 or Fig. A2.3) can be easily connected to the network module (Fig. A16.2) as they have the same five connection, namely, ΔV_d, ΔV_q, ΔI_d, ΔI_q and $\Delta\delta$.

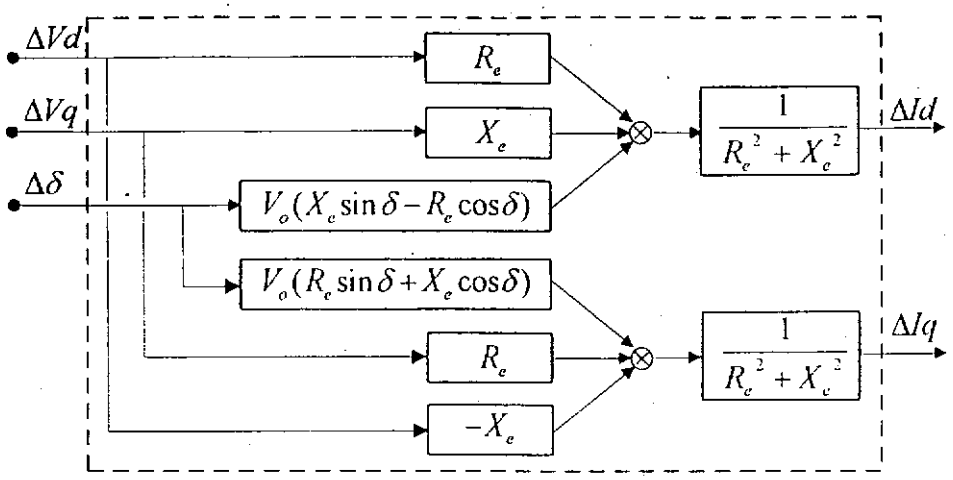

Fig. A16.2 Network model for single machine infinite bus

APPENDIX 17

SYSTEM DATA OF SINGLE AND TWO MACHINE SYSTEMS FOR H_∞ PSS DESIGN

A17.1 Single machine case (1000MVA base)

Rated power = 800 MW, Rated power factor = 0.8,

$R_a = 0$	$X_d = 1.95$	$X_d' = 0.3$	$X_d'' = 0.2$	$X_q = 1.9$
$X_q' = 0.45$	$X_q'' = 0.2$	$T_{do}' = 7.4$	$T_{do}'' = 0.03$	$T_{qo}' = 0.4$
$T_{qo}'' = 0.07$	$M = 7.6$	$R_e = 0$	$K_a = 50$	$T_a = 0.03$
$K_g = -20$	T_g=0.5			

A17.2 Two machine case (100MVA base)

Machine G1:

$R_a = 0$	$X_d = 0.362$	$X_q = 0.352$	$X_d' = 0.06$	$X_d'' = 0.0434$	$X_q' = 0.122$
$X_q'' = 0.0434$	$T_{do}' = 7.8$	$T_{do}'' = 0.022$	$T_{qo}' = 0.9$	$T_{qo}'' = 0.074$	$Hg = 17.65$
$D = -1$	$K_a = 212$	$T_a = 0.01$	$K_g = -100$	T_g=0.2	

Machine G2:

$R_a = 0$	$X_d = 0.557$	$X_q = 0.5$	$X_d' = 0.11$	$X_d'' = 0.08$	$X_q' = 0.34$
$X_q'' = 0.08$	$T_{do}' = 6$	$T_{do}'' = 0.014$	$T_{qo}' = 1$	$T_{qo}'' = 0.15$	$H_g = 9.8$
$D = -2$	$K_a = 212$	$T_a = 0.01$	$K_g = -100$	$T_g = 0.2$	

Transmission line and capacitor data

$R_l = 0.038$	$X_l = 0.0406$	$B/2 = 0.46$	$C_1 = -1.5$	$C_2 = -2.5$